5-2014

Use of Semi-Analytical Solutions to Examine Parameter Sensitivity and the Role of Spatially Variable Stream Hydraulics in Transient Storage Modeling

Noah M. Schmadel
Utah State University

USE OF SEMI-ANALYTICAL SOLUTIONS TO EXAMINE PARAMETER SENSITIVITY AND THE ROLE OF SPATIALLY VARIABLE STREAM HYDRAULICS IN TRANSIENT STORAGE MODELING

by

Noah M. Schmadel

A dissertation submitted in partial fulfillment
of the requirements for the degree

of

DOCTOR OF PHILOSOPHY

in

Civil and Environmental Engineering

Approved:

Bethany T. Neilson Major Professor	David K. Stevens Committee Member
Justin E. Heavilin Committee Member	Joseph M. Wheaton Committee Member
L.E. Anders Wörman Committee Member	Mark R. McLellan Vice President for Research and Dean of the School of Graduate Studies

UTAH STATE UNIVERSITY
Logan, Utah

2014

ABSTRACT

Use of Semi-Analytical Solutions to Examine Parameter Sensitivity and the Role of Spatially Variable Stream Hydraulics in Transient Storage Modeling

by

Noah M. Schmadel, Doctor of Philosophy

Utah State University, 2014

Major Professor: Dr. Bethany T. Neilson
Department: Civil and Environmental Engineering

Interpreting water quality and ecological implications in stream systems depends on accurate predictions of the fate and transport of solute and heat. Applying a representative solute and heat transport model that incorporates the influences of surface and hyporheic transient storage requires knowledge of individual, dominant processes over different spatial scales. However, estimating parameters that represent those dominant processes and determining appropriate residence time distributions are common challenges due to the inherent heterogeneity of characteristics within streams. Recent progress has been made to better represent residence times by scaling parameters with field-based geometric and hydraulic measurements. Despite this advancement, it is still unclear what spatial detail of observations is necessary and how best to represent that detail in reach scale model applications. This dissertation addresses some of these gaps in stream research by developing semi-analytical solutions to existing two-zone solute and

temperature transient storage models. For the solute transport component, closed form solutions to the temporal moments were derived as functions of model parameters and, therefore, used to directly examine the sensitivity of transient storage parameters. It was found that identifying parameters representing storage volume is critical to support accurate solute predictions. Beyond examining storage parameters, these semi-analytical solutions were used with high-resolution channel width information to determine the role of spatially variable hydraulics in one-dimensional model applications. For solute and temperature predictions, reach segment lengths within the model representation needed to capture the spatial correlation structure in observations to represent the hydraulic variability. Specific to temperature modeling, individual components of the model, such as the boundary condition and surface flux, were isolated. With an understanding of the boundary condition contribution to the temperature prediction, the component representing surface flux was found most sensitive to spatially variable hydraulics. Hydraulic conditions that translated into higher residence times had the largest effect on predictions. Through the use of these semi-analytical solutions, this dissertation provides a foundation to ultimately better represent stream systems with transient storage models and improve solute and temperature predictions over long reach scales.

(166 pages)

PUBLIC ABSTRACT

Use of Semi-Analytical Solutions to Examine Parameter Sensitivity and the Role of Spatially Variable Stream Hydraulics in Transient Storage Modeling

by

Noah M. Schmadel, Doctor of Philosophy

Utah State University, 2014

Major Professor: Dr. Bethany T. Neilson
Department: Civil and Environmental Engineering

Anticipating how stream water quality will respond to change, such as increased pollution or water diversions, requires knowledge of the main mechanisms controlling water and chemical constituent movement and a reasonable representation of those mechanisms. By deriving mathematical models to represent a stream system and collecting supporting field-based measurements, water quality response can be predicted. However, because each stream is unique and the movement of water and constituents is spatially and temporally complex, assessing whether the stream is appropriately represented and whether predictions are trustworthy is still a challenge within the scientific and management communities.

Building on decades of stream research, this dissertation provides a step towards better representing some of the complexities found within streams and rivers to better predict water quality responses over long stream distances. First, a method is presented to

assess which mechanisms are considered most important in chemical constituent predictions. Next, the number of measurements necessary to represent the general complexities of water, mass, and heat movement in streams was determined. The advancements developed in this dissertation provide a foundation to more efficiently and accurately inform water resource management.

(166 pages)

ACKNOWLEDGMENTS

First and foremost, I express my heartfelt thanks to my advisor, Dr. Bethany Neilson. Throughout the seven short years that I have been part of your group, you have strived to make me a better professional and person despite my constant hardheadedness. Thank you for taking a chance on me. Although I may be moving on to greener pastures, the way you care about others, mentor, and view (and contribute to) the world makes it impossible to leave cheerfully. I do, however, look forward to the prospect of more fun and painful days collaborating in the field. You have taught me (other than basically everything I know) that when we do well, we *all* do well.

Immense thanks to my committee for investing and believing in me. Dr. David Stevens, your vast knowledge and countless skills are a source of inspiration. You are one of the best teachers I have ever had! Thank you for always taking the time to listen, critique, and help. Every time that I stopped by your office fumbling, you dropped everything to help. Dr. Justin Heavilin, thank you. That is all. Seriously, I would not have finished without you! From the derivations to the coding to the talks to the papers, you have had my back every step of the way. You are so good at what you do and are such a great person that I have secretly idolized you (and Dr. Laurie McNeill). Dr. Anders Wörman, thank you for getting me to Sweden, your constant help, and being an all-out pleasure to work with. While you know more about engineering and hydrology than most on this planet, you are a sincere and unassuming person. I look forward to future collaboration. Dr. Joseph Wheaton, although I did not seek your help as much as I would have liked to, thank you for the advice and support. At every stage of the program, you provided thoughtful feedback and encouragement.

Dr. Mac McKee, thank you for making it possible for me to come to Utah State. When I showed interest in working under Beth, you told her, “If there is a student interested in coming here, we will make it happen.” Dr. Laurie McNeill, thank you for all the advice, encouragement, kindness, and lessons. I am grateful I got to see you work. Joan McLean, thank you for getting me to Utah State and always providing help.

Thanks to those for help with field and laboratory work, countless discussions, and making work fun. Andrew Hobson, I miss our discussions, working together in the field, and you reaffirming my love of engineering. Thank you for making sure I did not give up. Cami Snow, every day spent in the office and field with you was pure enjoyment. Tyler King, you are so nice, positive, and helpful, it is really annoying. You simply make everything better. Mark Winkelaar, thank you for the many discussions, help with data, and the lessons of how to properly and elegantly shred. Joakim Riml, thank you for making my trip to Sweden smooth and for all the help since. I look forward to more discussions and collaboration.

Thanks to my family and friends for making any of my success possible. My dear mother, any goodness in me comes from you. Thank you for always encouraging me to learn and wonder. I am thankful each day for the magical childhood you gave me. My father, thank you for teaching me to be ethical and honest. I once asked you, “When others take advantage of you, why don’t you take advantage of them too?” You replied, “Son, there are some things I am unwilling to change about myself for personal gain.” I carry that lesson with me every day. Thank you for enduring with me, Elizabeth. Your love, support, and laughter make anything possible and everything enjoyable.

Noah M. Schmadel

CONTENTS

LIST OF TABLES

LIST OF FIGURES

CHAPTER 1

INTRODUCTION

Hydrologic research of the past half century has identified many of the physical drivers of solute and heat transport and the associated connections to ecology and biogeochemical processes. Applying and continuing this research is critical to protect and manage water resources. Specific to stream systems, a conceptual understanding of the mechanisms driving and influencing solute and heat transport currently exists. This understanding includes the role of channel properties (e.g., streambed permeability and geomorphic features) and hydraulic characteristics (e.g., stream depth and velocity) and their effect on solute retention and residence times. These retention processes, often collectively referred to as transient storage, hinder or slow the migration of flowing waters and are of great importance because they often control biogeochemical transformations, ecology, and water quality [e.g., *Boano et al*., 2014]. Typically, transient storage research is focused on the fate and transport of solutes. However, determining solute fate and ecological implications requires simultaneous consideration of solute and heat transport [e.g., *Hester and Doyle*, 2011; *Williams and Boorman*, 2012].

Building on novel interpretations of dye tracers attempting to describe transient storage processes (originally referred to as "dead zones" by *Hays* [1966]), the transient storage model (TSM) formulation was developed based on the concept that streams continually exchange water with sediments rather than function as pipes [*Bencala and Walters*, 1983]. Although transient storage is widely recognized as consisting of complex pathways occurring over various spatial and temporal scales [e.g., *Buffington and Tonina*, 2009; *Stonedahl et al*., 2010], TSM formulations are typically one-dimensional

representations of the governing transport processes. These simplifications can provide a reasonable representation of transport processes and are often necessary to predict solute concentrations or stream temperature over long reach scales (on the order of hundreds of meters to kilometers). However, a more accurate representation of a stream (e.g., two or three-dimensional modeling approaches) may be important for certain modeling objectives (e.g., capturing the influence of smaller scale geomorphic features on transient storage to asses ecological connections) [*Tonina and Buffington*, 2009]. Furthermore, while transient storage can be generally attributed to surface and subsurface transport processes, applications of TSMs still commonly represent all exchange flowpaths with a single, lumped process [e.g., *Kelleher et al.*, 2013; *Runkel*, 1998; *Schmid et al.*, 2010]. This lumped representation is often referred to as the one-zone TSM. This one-zone approach may provide a limited interpretation of processes related to reactive transport due to inaccurate representation of residence time distributions and the inability to capture surface and subsurface specific responses [e.g., *Runkel*, 2007; *Stewart et al.*, 2011]. Therefore, to more realistically represent storage residence times, this single zone has been separated in the development of two-zone TSMs. A second storage zone has been added to represent varying hyporheic (i.e., subsurface) timescales [*Choi et al.*, 2000; *Harvey et al.*, 2005] or to independently account for surface transient storage (STS) and hyporheic transient storage (HTS) [*Briggs et al*., 2009; *Neilson et al*., 2010a, 2010b]. STS is generally defined as slower moving, recirculating stream water relative to main stream flow and HTS is defined as the adjacent alluvial aquifer continuously exchanging with stream water. A two-zone approach is required at times because STS and HTS rates of exchange between the stream can be an order of magnitude different [*Briggs et al.*, 2010]

and the temperatures between these zones differ greatly [*Bingham et al.*, 2012; *Neilson et al.*, 2009].

The spatial variability of transient storage may also be an important consideration in the model representation because the heterogeneity of STS and HTS is influenced by differing stream hydraulics [e.g., *O'Connor et al.*, 2010; *Stonedahl et al.*, 2012]. Within TSM formulations, spatial variability is represented by discretizing the reach of interest into unique, one-dimensional segments and hydraulics are often represented by segment-wise average width, depth, and velocity [e.g., *Schmid et al*., 2010]. However, to more accurately represent to complex spatial variability of velocities in surface waters, a two or three-dimensional hydrodynamic model would be necessary. Although increased model complexity may be necessary for specific cases, the required data increase significantly and are typically impractical to gather at large spatial scales. While the goal of TSM applications is to represent dominant processes in model predictions, the one-zone formulation is often preferred with a uniform representation of hydraulics due to minimal data requirements and fewer parameters needing calibration.

Formulations of the TSM are most commonly solved using numerical techniques to simulate solute or heat transport [e.g., *Cardenas et al.*, 2014; *Gooseff et al.*, 2005a; *Neilson et al.*, 2010b; *Runkel and Chapra*, 1993; *Runkel*, 1998]. Although numerical techniques are the preferred method under certain conditions (e.g., time varying flows), analytical solution techniques can be useful for a better understanding of how the variables, parameters, and components of the model capture the overall behavior of a system being modeled [e.g., *De Smedt*, 2006; *Kazezyılmaz-Alhan*, 2008; *Schmid*, 2004; *Wörman*, 1998]. For example, analytical techniques have been used to isolate the

influence of the initial and boundary conditions, which provides a better understanding of the mechanisms represented in a prediction [*Heavilin and Neilson*, 2012]. Another benefit to analytical techniques is that closed form solutions to the temporal moments can be produced. These moment solutions provide statistical characteristics of the model that are functions of model parameters. Therefore, these solutions allow for the direct comparison of different models of similar formulations [e.g., *Wörman*, 2000] or estimation of parameter sensitivity based solely on possible ranges [e.g., *Gupta and Cvetkovic*, 2000; *Valocchi*, 1990]. More recently, analytical techniques have been found useful for incorporating the effects of spatially explicit parameters in the model representation while avoiding numerical pitfalls such as instability or truncation error [*Riml and Wörman*, 2011]. Despite their recognized value in these cases, semi-analytical solutions are absent for both solute and heat two-zone TSM formulations.

Parameters of TSM formulations are often inversely calibrated using solute tracer techniques and aggregated over a study reach in lieu of a detailed spatial representation [e.g., *Stream Solute Workshop*, 1990]. Although these inverse techniques are popular due to the ability to reproduce observations [e.g., *Runkel*, 2007; *Schmid et al.*, 2010], inversely estimated parameters may provide indirect physical meaning concerning transport processes [e.g., *Marion et al.*, 2003; *Ward et al.*, 2010]. This uncertainty can result in inconclusive interpretations of transient storage residence times [e.g., *Gooseff et al.*, 2007; *Harvey and Bencala*, 1993; *Wondzell and Swanson*, 1999]. *Kelleher et al*. [2013] recognized that transient storage parameters are typically not identifiable due to parameter interactions related to stream characteristics (e.g., flow and channel geometry). They emphasize that sensitivity analyses are needed, but usually overlooked, to assess

whether parameters representing transient storage are identifiable. Furthermore, *Kelleher et al*. [2013] found that it is possible to better isolate the sensitivity of parameters by constraining some with hydraulic information (e.g., width and depth). Parameter sensitivity analyses have been performed frequently on one-zone formulations [e.g., *Gooseff et al.*, 2005b; *Wagner and Harvey*, 1997], but analyses on two-zone formulations are limited. Therefore, there is still a need to determine whether these two storage processes are represented well in a prediction or whether this more complicated model is warranted under different conditions of transient storage residence times.

Because meaningful parameter estimation is a persistent challenge in transient storage modeling, especially when considering a second transient storage zone, there have been many recent attempts to use field-based measurements to reduce parameter uncertainty [e.g., *Bandaragoda and Neilson*, 2011; *Jackson et al.*, 2012; *O'Connor et al.*, 2010; *Stonedahl et al.*, 2012]. In particular, *Jackson et al*. [2012] and *O'Connor et al*. [2010] used spatial measurements of width, depth, and velocity and related them to hydraulics to scale transient storage parameters. Although these measurements may provide a more realistic representation of transport processes, approaches are lacking to understand the spatial detail necessary to support one-dimensional solute and heat transport modeling at reach scales. By building on previous work, there is opportunity to develop these needed approaches by applying semi-analytical solutions to isolate components of the model [*Heavilin and Neilson*, 2012] and incorporate high-resolution spatial information [e.g., *Riml and Wörman*, 2011] extracted from imagery [e.g., *Bingham et al.*, 2012].

This dissertation addresses some of these gaps in stream research. Semi-analytical solutions to two-zone solute and heat TSM formulations are provided and associated approaches are developed to better understand parameter sensitivity and the role of spatially variable hydraulics in reach scale predictions. In this dissertation, spatially variable hydraulics are defined by segment-wise channel widths that are used to determine mean depths and velocities used in the one-dimensional model representation. Through these solutions, the sensitivity of transient storage parameters representing two zones are examined under varying conditions of STS and HTS residence times (Chapter 2). This provides information as to whether STS and HTS processes are represented well in the solute prediction and, therefore, if this more complicated formulation is warranted. Because detailed hydraulic information may provide a better representation of transient storage residence times, the role of spatially variable hydraulics in solute (Chapter 3) and temperature (Chapter 4) predictions is assessed.

CHAPTER 2[1]

EXAMINING THE SENSITIVITY OF TRANSIENT STORAGE PARAMETERS WITH CLOSED FORM TEMPORAL MOMENT SOLUTIONS

Abstract

To better understand the influence of model parameter estimates on solute transport predictions, we present closed form solutions to the first temporal moment and second through fourth central moments. These were derived from a Laplace-domain solution to a one-dimensional, two-zone transient storage stream transport model that reflects surface transient storage (STS) and hyporheic transient storage (HTS) processes in the parameterization. A fuzzy number sensitivity analysis method was then used to quantify the relative influence of STS and HTS parameters on the moment solutions. To illustrate the utility of such solutions combined with a sensitivity analysis, we present results for conditions when STS or HTS processes are comparable or dominant. These results indicate that parameters representing the sizes of STS and HTS zones are the most sensitive in two-zone transient storage modeling and illustrate that this approach can provide information regarding when a two-zone representation of STS and HTS is warranted.

Introduction

The migration of solutes in streams is affected by transient storage processes, ultimately increasing solute residence time. Transient storage has been widely recognized as having complex pathways that are generally attributed to either surface or subsurface

[1] Coauthored by Noah M. Schmadel, Justin E. Heavilin, Bethany T. Neilson, and Anders Wörman

transport processes [e.g., *Bencala and Walters*, 1983; *Bencala et al.*, 2011]. While residence times and mechanisms vary, the dominant storage processes are commonly characterized with "lumped" parameters of one-zone transient storage model (TSM) formulations [e.g., *Runkel*, 1998; *Schmid et al.*, 2010]. One-zone TSMs have been found to capture the influences of dominant storage processes for most stream conditions [*Choi et al.*, 2000]; however, such formulations provide a limited representation of influences on reactive solute transport due to differing temperatures, solute concentrations, and residence times [e.g., *Runkel et al.*, 1996; *Runkel*, 2002].

The formulation of a TSM with two storage zones addresses some of the limitations of a one-zone TSM by representing varying hyporheic (i.e., subsurface) and surface transient storage timescales [*Harvey et al.*, 2005]. Furthermore, some two-zone formulations have been used to capture the influences of surface transient storage (STS) and hyporheic transient storage (HTS) specific reactions [*Stewart et al.*, 2011] and heat transport mechanisms [*Neilson et al*., 2010a, 2010b]. The most common two-zone model formulations include the two-storage zone [2-SZ; *Briggs et al.*, 2009; *Choi et al.*, 2000; *Harvey et al.*, 2005] and two-zone temperature and solute [TZTS; *Neilson et al*., 2010a, 2010b] models. With any similarity in timescales, *Choi et al*. [2000] discussed the difficulty of attributing specific storage zones to either STS or HTS through inverse modeling with stream solute tracers. *Briggs et al*. [2009] and *Harvey et al*. [2005] addressed this challenge by independently collecting data from storage zones to support interpretations of inversely estimated parameters specifically associated with STS or HTS. Their approaches, identical to *Choi et al*. [2000], applied the 2-SZ model that uses cross-sectional areas to describe storage zones. *Neilson et al*. [2010a, 2010b] further

constrained the physical layout of storage zones with widths and depths (necessary for heat transport) to specifically reflect STS and HTS in the TZTS model. Although the increased model complexity within two-zone models may be necessary for specific cases, the tradeoffs associated with a greater number of parameters and the corresponding influence on model predictions must be considered.

Analytical and semi-analytical solutions have been found useful in gaining insight into how the variables, parameters, and components of a stream transport model capture the overall behavior of a system being modeled [*Heavilin and Neilson*, 2012; *Wörman*, 1998]. Although the one-zone TSM has typically been solved numerically [OTIS-P; *Runkel*, 1998], semi-analytical solutions have been derived from integral transforms [*De Smedt*, 2006; *Kazezyılmaz-Alhan*, 2008; *Schmid*, 2003]. Integral transforms, particularly the Laplace transform, result in solutions that provide a moment generating function used to derive closed form temporal moment solutions [*Aris*, 1958]. Temporal moments centered about the mean, hereafter referred to as central moments, have been used to gain insight into the statistical characteristics of a solute residence time probability density function (PDF), compare different models of similar formulations [*Wörman*, 2000; *Wörman et al.*, 2002], and link hydrological conditions (e.g., advection and dispersion) with variable stream flow [*Ward et al.*, 2013]. Furthermore, they have been used to investigate the sensitivity of model parameters without model simulations [e.g., *Gupta and Cvetkovic*, 2000; *Valocchi*, 1990].

The objective of this chapter is to illustrate the utility of closed form central moment solutions to two-zone TSMs explicitly representing STS and HTS. We combined these solutions with a fuzzy number sensitivity analysis method and established the

relative influence of individual parameters on moment solutions. We applied this approach to cases where STS or HTS processes are dominant or comparable to illustrate the utility of such solutions when determining if a two-zone representation of STS and HTS is warranted.

Model and Solutions

The formulation of the TZTS model [*Neilson et al*., 2010a, 2010b] and parameter calibration techniques using solute and temperature observations together [*Bandaragoda and Neilson*, 2011] have demonstrated promising instream solute and temperature predictions. Assuming flow is steady, the conservative governing transport equations of the solute component of the TZTS model can be written as [*Neilson et al.*, 2010b]

$$\frac{\partial C}{\partial t} = D\frac{\partial^2 C}{\partial x^2} - \frac{Q}{YB_{tot}(1-\beta)}\frac{\partial C}{\partial x} + \frac{\alpha_{STS}Y_{STS}}{Y(1-\beta)\beta B_{tot}^{\ 2}}(C_{STS} - C) + \frac{\alpha_{HTS}}{Y_{HTS}Y}(C_{HTS} - C), \qquad (2\text{-}1)$$

$$\frac{dC_{STS}}{dt} = \frac{\alpha_{STS}}{(\beta B_{tot})^2}(C - C_{STS}), \qquad (2\text{-}2)$$

$$\frac{dC_{HTS}}{dt} = \frac{\alpha_{HTS}}{Y_{HTS}^{\ 2}}(C - C_{HTS}), \qquad (2\text{-}3)$$

where equation (2-1) represents main channel (MC) transport; C is the zonal solute concentration (M L^{-3}); the subscripts STS and HTS represent surface transient storage and hyporheic transient storage, respectively; Q is the volumetric flow rate of the MC (L^3 T^{-1}); α_{STS} is the exchange rate coefficient between the MC and the STS zone (L^2 T^{-1}); α_{HTS} is the exchange rate coefficient between the MC and HTS zone (L^2 T^{-1}); Y, Y_{STS}, and Y_{HTS} are the MC, STS, and HTS depths (L), respectively; B_{tot} is the total channel width (L); β is the STS fraction of the total channel width; $B = B_{tot}(1-\beta)$ is the MC width (L);

$B_{STS} = \beta B_{tot}$ is the STS zone width (L); x is the longitudinal distance (L); and t is time (T). Note that B_{STS} and Y_{HTS} represent the exchange lengths of the STS and HTS zones, respectively.

Initial concentrations are assumed zero,

$$C(x, t=0) = C_{STS}(x, t=0) = C_{HTS}(x, t=0) = 0\,, \tag{2-4}$$

the upper boundary condition is treated as a Dirichlet type (similar to *Schmid* [2003]), and solutions are bounded,

$$C(x=0, t) = g(t) \text{ and } C(x \to \infty, t) = 0, \tag{2-5}$$

where $g(t)$ represents a time-dependent inflow solute breakthrough curve. Taking the Laplace transform (time variable transformed) of equations (2-1)-(2-3) and the boundary condition, and applying the initial conditions yields the solutions in s,

$$\overline{C} = \overline{g}(s) \exp\left[\frac{x}{2D}\left(U - \sqrt{U^2 + 4D\psi(s)}\right)\right], \tag{2-6}$$

$$\overline{C}_{STS} = \frac{\kappa_3}{(s + \kappa_3)}\overline{C}\,, \tag{2-7}$$

$$\overline{C}_{HTS} = \frac{\kappa_4}{(s + \kappa_4)}\overline{C}\,, \tag{2-8}$$

where $\psi(s) = \left(s + \kappa_1 + \kappa_2 - \frac{\kappa_1\kappa_3}{(s+\kappa_3)} - \frac{\kappa_2\kappa_4}{(s+\kappa_4)}\right)$, $\kappa_1 = \frac{\alpha_{STS} Y_{STS}}{YBB_{STS}}$, $\kappa_2 = \frac{\alpha_{HTS}}{Y_{HTS} Y}$, $\kappa_3 = \frac{\alpha_{STS}}{B_{STS}^{\,2}}$, and $\kappa_4 = \frac{\alpha_{HTS}}{Y_{HTS}^{\,2}}$. Here $\overline{C}(x,s) = \mathcal{L}\{C(x,t)\}$ is the zonal concentration in the Laplace domain, $\overline{g}(s) = \mathcal{L}\{g(t)\}$, s is the Laplace variable, and $U = Q/(BY)$ is the mean velocity of the MC (L T^{-1}). The full derivation of these solutions, solutions to the 2-SZ model, and a conceptual illustration of the TZTS and 2-SZ models (Figure A-1) are provided in

Appendix A. Equations (2-6)-(2-8) were numerically inverted into the original state space using the *Hollenbeck* [1998] function based on the *De Hoog et al.* [1982] algorithm and compared to numerical approximations for validation.

The Laplace-domain solutions (equations (2-6)-(2-8)) were normalized by the zeroth temporal moment, $\overline{C}(x,s)/\overline{g}(s=0)=\overline{c}(x,s)$, so that $\int_o^\infty c(x,t)dt=1$ where $\mathcal{L}^{-1}\{\overline{c}(x,s)\}=c(x,t)$ is the solute residence time PDF. The higher order derivatives of normalized equations (2-6)-(2-8) evaluated at $s = 0$ yielded the closed form solutions to the first temporal moment and the second through fourth central moments (also referred to as moment solutions) (Table 2-1). The first temporal moment represents the mean residence time, μ_t, of $c(x,t)$. The second central moment describes the variance, σ_t^2, about the mean from an Eulerian perspective [e.g., *Wörman*, 2000]. The third, S_t, and fourth, K_t, central moments are related to the statistical definitions of skewness and kurtosis, respectively. Note that the MC moment solutions contain two types of terms: those originating from the boundary condition (denoted by ($x = 0$)) and those from the exponential function (Table 2-1 and see Appendix A for the full derivations).

Fuzzy Number Sensitivity Analysis

Although there are a wide variety of sensitivity analysis methods available to investigate the impact of uncertain model parameters on model outputs (e.g., see *Tang et al*. [2007]), we use a fuzzy number sensitivity analysis because fuzzy numbers provide a versatile way to represent parameter distributions with limited prior knowledge. Using the moment solutions (Table 2-1), we employed triangular fuzzy numbers spanning

Table 2-1. Closed form solutions to the first temporal moment (mean) and the second (variance) through fourth central moments of the zonal solute residence time probability density functions. These solutions were derived from equations (2-6)-(2-8) normalized by the zeroth temporal moment, $\bar{g}(s=0)$.

Moment	Zone	
	Main channel	STS and HTS
Mean (T)	$\mu_t = \mu_t(x=0) + \frac{x}{U}\Psi$ where $\Psi = 1 + \frac{Y_{STS}B_{STS}}{YB} + \frac{Y_{HTS}}{Y}$	$\mu_{t,STS} = \mu_t + \frac{B_{STS}^{\ 2}}{\alpha_{STS}}$ $\mu_{t,HTS} = \mu_t + \frac{Y_{HTS}^{\ 2}}{\alpha_{HTS}}$
Variance (T^2)	$\sigma_t^2 = \sigma_t^2(x=0) + 2\frac{x}{U}\left(\Theta + \frac{D}{U^2}\Psi^2\right)$ where $\Theta = \frac{Y_{STS}B_{STS}^{\ 3}}{YB\alpha_{STS}} + \frac{Y_{HTS}^{\ 3}}{Y\alpha_{HTS}}$	$\sigma_{t,STS}^2 = \sigma_t^2 + \frac{B_{STS}^{\ 4}}{\alpha_{STS}^{\ 2}}$ $\sigma_{t,HTS}^2 = \sigma_t^2 + \frac{Y_{HTS}^{\ 4}}{\alpha_{HTS}^{\ 2}}$
Third central moment (T^3)	$S_t = S_t(x=0) + 6\frac{x}{U}\left(\Phi + \frac{2D}{U^2}\Theta\Psi + \frac{2D^2}{U^4}\Psi^3\right)$ where $\Phi = \frac{Y_{STS}B_{STS}^{\ 5}}{YB\alpha_{STS}^{\ 2}} + \frac{Y_{HTS}^{\ 5}}{Y\alpha_{HTS}^{\ 2}}$	$S_{t,STS} = S_t + 2\frac{B_{STS}^{\ 6}}{\alpha_{STS}^{\ 3}}$ $S_{t,HTS} = S_t + 2\frac{Y_{HTS}^{\ 6}}{\alpha_{HTS}^{\ 3}}$
Fourth central moment (T^4)	$K_t = K_t(x=0) + 2\frac{x}{U}\left(6\sigma_t^{\ 2}(x=0)\Theta + 6\sigma_t^{\ 2}(x=0)\frac{D}{U^2}\Psi^2\right) + \frac{x}{U}\left(24\Omega + \frac{24D\Theta^2 + 48D\Phi\Psi}{U^2} + \frac{144D^2}{U^4}\Theta\Psi^2 + \frac{120D^3}{U^6}\Psi^4\right) + \frac{x^2}{U^2}\left(12\Theta^2 + \frac{24D}{U^2}\Theta\Psi^2 + \frac{12D^2}{U^4}\Psi^4\right)$ where $\Omega = \frac{Y_{STS}B_{STS}^{\ 7}}{YB\alpha_{STS}^{\ 3}} + \frac{Y_{HTS}^{\ 7}}{Y\alpha_{HTS}^{\ 3}}$	$K_{t,STS} = K_t + 6\frac{B_{STS}^{\ 4}}{\alpha_{STS}^{\ 2}}\sigma_t^{\ 2} + 9\frac{B_{STS}^{\ 8}}{\alpha_{STS}^{\ 4}}$ $K_{t,HTS} = K_t + 6\frac{Y_{HTS}^{\ 4}}{\alpha_{HTS}^{\ 2}}\sigma_t^{\ 2} + 9\frac{Y_{HTS}^{\ 8}}{\alpha_{HTS}^{\ 4}}$

ranges of TZTS model storage parameter values (see Figure B-2 in Appendix B for an example of these fuzzy numbers). The general transformation method, proposed by *Hanss* [2002] and further explained in *Hanss* [2005], was then used to implement these

fuzzy numbers and identify the relative influence (i.e., sensitivity) of each storage parameter on the moment solutions. In short, use of this method consisted of: (1) generation of possible parameter combinations by sampling within the triangular fuzzy numbers to represent uncertainty in parameters, (2) evaluation of the moment solutions for each combination to construct resulting fuzzy numbers for the moments to represent uncertainty in solutions, and finally (3) evaluation of the relative influence of each parameter on the moment solutions by essentially normalizing each parameter fuzzy number by the resulting moment fuzzy numbers. In the end, with only ranges of parameter values and a central tendency assumption, this approach provided an understanding of the influence of each storage parameter on moment solutions on a cumulative scale of 0-100%. This analysis was repeated on the solute residence time PDF, $c(x,t)$, to form an overall comparison to influences on the moment solutions.

Application Example of Moment Solutions

In this application example, B, Y, and D are held constant because these can be set through direct measurements [e.g., *O'Connor et al*., 2010] and often dominate model sensitivity if treated as calibration parameters [e.g., *Kelleher et al*., 2013]. By setting these, we investigate how the sensitivities of STS and HTS parameters change under varying storage conditions. To define storage conditions, *Choi et al*. [2000] established residence time criteria where the two storage zone processes fall under *additive* (Case I), *competitive* (Case II), or *dominant* (Case III) conditions. Under Case I, lumped storage parameters of a one-zone TSM represent two storage processes well because individual exchange fluxes and storage capacities of each zone are comparable. Under Case II, two

storage processes are not characterized well by a one-zone TSM because exchange fluxes and storage capacities between each zone are not comparable. Parameters representing both zones are key to understanding solute transport under these competitive conditions. Under Case III, a one-zone TSM is sufficient because transient storage is primarily driven by both the exchange flux and storage capacity of a single zone.

These three cases are defined with an understanding of timescales through dimensionless ratios of residence times (R_t) and exchange fluxes (R_q) between the two storage zones. Specifically, *Choi et al.* [2000] observed that parameter combinations resulting in a $R_t < 5$ implied Case I conditions and $R_t > 5$ implied either Case II or Case III conditions. Within *Choi et al.* [2000], however, there is no distinction between STS and HTS.

To illustrate the utility of the closed form moment solutions combined with a sensitivity analysis, we first established working parameter ranges to represent storage conditions where (1) the influences of STS and HTS are comparable (Case I) or when (2) one storage zone (either STS or HTS) dominates transient storage (Case III). This was completed through Latin hypercube sampling within the overall parameter ranges presented in *Choi et al.* [2000] (see Appendix B for details). R_t and R_q were then calculated for each parameter set to identify those representing Case I and III conditions. These ratios, however, were calculated differently depending on relative STS or HTS dominance. When the STS residence time (t_{STS}) is larger than the HTS residence time (t_{HTS}) and the HTS exchange flux (q_{HTS}) is larger than the STS exchange flux (q_{STS}), the residence time ratio was calculated by

$$R_{t_{STS}} = \frac{t_{STS}}{t_{HTS}} = \frac{B_{STS}Y_{STS}}{Y_{HTS}B}\frac{q_{HTS}}{q_{STS}} = \frac{B_{STS}Y_{STS}}{Y_{HTS}B}R_{q_{STS}}, \tag{2-9}$$

facilitated by the substitutions $q_{STS} = \alpha_{STS} \frac{Y_{STS}}{B_{STS}}$ and $q_{HTS} = \alpha_{HTS} \frac{B}{Y_{HTS}}$. Here $B_{STS}Y_{STS}$ and $Y_{HTS}B$ represent the storage capacities for the STS and HTS zones, respectively, and $R_{q_{STS}}$ is the associated exchange flux ratio. When $t_{HTS} > t_{STS}$, the residence time ratio is defined as $R_{t_{HTS}}$, which is the inverse of equation (2-9), and the exchange flux ratio is defined as $R_{q_{HTS}}$. When considering both STS and HTS, Case I occurs when $R_{t_{STS}} < 5$ and $t_{HTS} \leq t_{STS}$ or $R_{t_{HTS}} < 5$ and $t_{HTS} > t_{STS}$. Case III is present when nearly all transient storage is driven by a small exchange flux and a large storage capacity in a single zone (i.e., when $t_{HTS} \leq t_{STS}$, $q_{STS} << q_{HTS}$, $Y_{HTS}B << B_{STS}Y_{STS}$, and $R_{t_{STS}} >> 5$ or when $t_{HTS} > t_{STS}$, $q_{STS} >> q_{HTS}$, $Y_{HTS}B >> B_{STS}Y_{STS}$, and $R_{t_{HTS}} >> 5$).

The utility of moment solutions becomes apparent when looking at examples of Case I and III. Each storage parameter (α_{STS},α_{HTS}, Y_{STS}, Y_{HTS}, and B_{STS}) was treated as a triangular fuzzy number and the remaining parameters were set to values presented in *Choi et al*. [2000] (Q = 0.08 m^3 s^{-1}, D = 0.4 m^2 s^{-1}, x = 150 m) and *Wagner and Harvey* [1997] (B = 2 m and Y = 0.5 m). See Appendix B for details. For both of these Case I and III examples, the combined influence of α_{STS} and α_{HTS} is only ~20-35% on σ_t^2, S_t, and K_t (Figure 2-1). This indicates that mean residence time (μ_t in Table 2-1) is influenced solely by the parameters representing storage zone sizes (B_{STS}, Y_{STS}, and Y_{HTS}) and the exchange lengths (B_{STS} and Y_{HTS}) account for a majority of the influence on σ_t^2, S_t, and K_t. Specifically for the additive case examples, the individual influences of α_{STS} and α_{HTS} on $c(x,t)$, σ_t^2, S_t, and K_t are nearly the same. Furthermore, the influences of B_{STS} and Y_{HTS} on $c(x,t)$, σ_t^2, S_t, and K_t are nearly equal (Figures 2-1A and 2-1C). For the dominant case

examples, Y_{HTS} (~70%) has the greatest influence when $t_{HTS} > t_{STS}$ (Figure 2-1B) and B_{STS} (~55%) has the greatest influence when $t_{HTS} \leq t_{STS}$ (Figure 2-1D) on σ_t^2, S_t, and K_t. As would be expected, the key parameters and relative importance of each within the context of model simulations (i.e., $c(x,t)$) differ from that of individual moments. However, the first two moments together generally provide much of the sensitivity information contained within the model results.

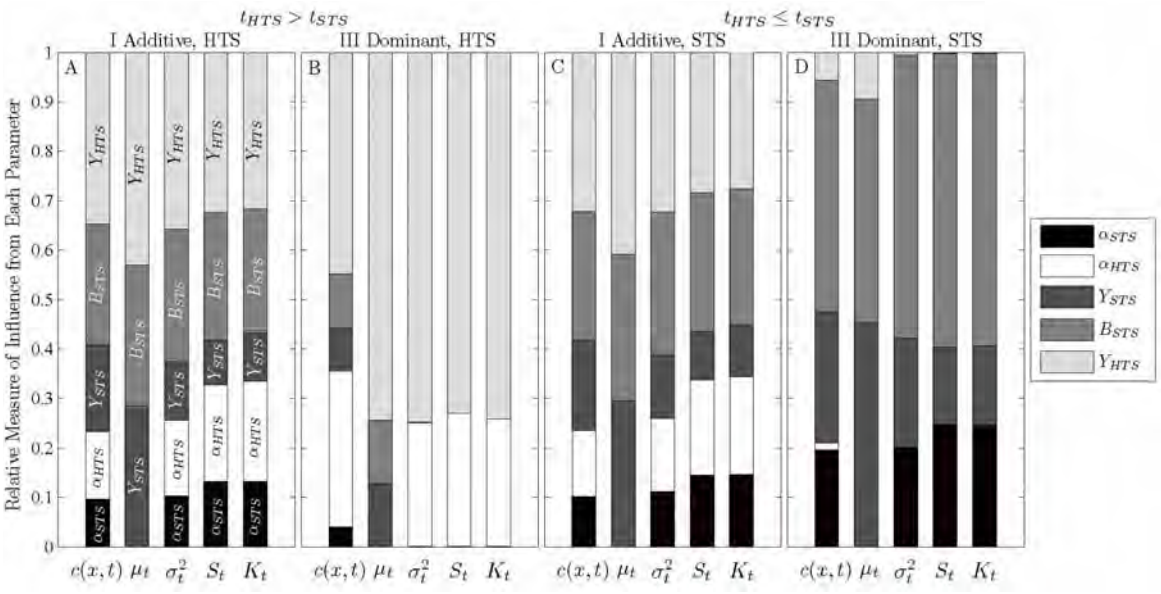

Figure 2-1. A fuzzy number sensitivity analysis to estimate the relative influence of each TZTS model storage parameter on the solute residence probability density function ($c(x,t)$) and the moment solutions (mean (μ_t), variance (σ_t^2), third central moment (S_t), and fourth central moment (K_t)). These results illustrate *additive* (Case I) and *dominant* (Case III) storage conditions for when HTS residence time is greater than STS residence time ($t_{HTS} > t_{STS}$) and when STS residence time is greater than HTS ($t_{HTS} \leq t_{STS}$). When $t_{HTS} > t_{STS}$ for the additive case (A), each parameter has a notable influence on $c(x,t)$, σ_t^2, S_t, and K_t. When $t_{HTS} \leq t_{STS}$ for the additive case (C), the results are nearly identical because storage timescales are comparable. For the dominant cases, there are fewer parameters significantly influencing the moments. The HTS exchange coefficient, α_{HTS}, has a relative influence of less than 30% and the exchange length, Y_{HTS}, has more than 70% influence on σ_t^2, S_t, and K_t when $t_{HTS} > t_{STS}$ (B). Conversely, when $t_{HTS} \leq t_{STS}$ (D), α_{STS} has a relative influence of less than 30% while the exchange length, B_{STS}, has an influence of nearly 60%.

The parameter sensitivity results on the moment solutions allow for clear identification of either additive (Case I) or dominant (Case III) conditions, which are where two storage zones may be sufficiently represented by one lumped zone. Focusing on α_{STS} and α_{HTS}, for example, the influences are nearly equal for Case I (Figures 2-1A and 2-1C), but the influence of only one is present for Case III (Figures 2-1B and 2-1D). Consequently, any results that fall in between Case I and III imply competitive conditions (Case II) where a two-zone TSM approach would be warranted. See Appendix B for information regarding the sensitivity of 2-SZ model storage parameters.

Discussion

Detail regarding the mathematical representation of transport processes can be inferred from the Laplace-domain solutions (equations (2-6)-(2-8)) and the closed form moment solutions (Table 2-1). The MC solute transport is an exponential decay of the boundary condition (equation (2-6)), the STS concentration is represented as the MC concentration influenced by α_{STS} and B_{STS} (equations (2-7)), and the HTS concentration is represented as the MC concentration influenced by α_{HTS} and Y_{HTS} (equation (2-8)). Although these semi-analytical solutions in the Laplace domain require numerical inversion to the original state space to represent solute concentrations, equations (2-6)-(2-8) themselves provide moment generating functions. From these solutions, we derived closed form moment solutions to describe the transport solution in the original state space without numerical inversion. The moment solutions directly show that μ_t is influenced only by the storage parameters Y_{STS}, B_{STS}, and Y_{HTS} while σ_t^2, S_t, and K_t are additionally influenced by α_{STS} and α_{HTS} (Table 2-1). An advantage to using the moment solutions

combined with a sensitivity analysis is that the influence of parameters can be evaluated from parameter ranges without requiring model simulations.

Fuzzy numbers provide a versatile way to investigate the impact of uncertain parameters without detailed knowledge of parameters (e.g., parameter probability density functions) or satisfying traditional assumptions (e.g., normally distributed model error) associated with probabilistic or statistical approaches [*Hanss and Turrin*, 2010]. Although there are a wide variety of sensitivity analysis methods (e.g., differential and variance-based [*Tang et al.*, 2007]), each has advantages and disadvantages. For example, differential methods are widely used because of their simplicity, but these vary one parameter at a time and do not account for parameter interactions [e.g., *Wagner and Harvey*, 1997]. Variance-based methods are a more robust multivariate approach that can account for these parameter interactions, but can be computationally intensive and constrained by statistical assumptions [*Tang et al*., 2007]. Although the general transformation method used within this fuzzy number sensitivity analysis does not explicitly isolate parameter interactions, it is a less computationally intensive multivariate approach than variance-based methods. It also retains simplicity in the interpretation because the relative influence of each parameter is provided on a cumulative scale which allows for a direct comparison of parameter influences under different storage conditions (Figure 2-1).

In our moment solution application example, parameter influences in terms of STS and HTS widths and depths revealed that the storage exchange lengths (B_{STS} and Y_{HTS}) account for the majority of influence from storage capacity (Figure 2-1). Conversely, for the 2-SZ model formulation, the cross-sectional areas represent the

storage capacity (see Figure B-3 in Appendix B). Both results highlight the importance of appropriately representing storage sizes and how parameterization can alter interpretation of key storage processes. Under the additive conditions (Case I), the relative influences of the STS and HTS exchange coefficients (α_{STS} and α_{HTS}) and exchange lengths (B_{STS} and Y_{HTS}) are nearly the same (i.e., the influences of $\alpha_{STS} \approx \alpha_{HTS}$ and $B_{STS} \approx Y_{HTS}$) (Figures 2-1A and 2-1C). These results are not surprising because the storage timescales are comparable. The dominant conditions (Case III) are clearly distinguishable from the additive conditions based solely on either STS or HTS parameters dominantly influencing results (Figures 2-1B and 2-1D). Note that the overall parameter influences on $c(x,t)$ are not consistent with the influences on μ_t, σ_t^2, S_t, or K_t. This result confirms that a combination of moments is necessary to represent parameter influence on model predictions. However, similar to *Leube et al*. [2012], the first two moments (μ_t and σ_t^2) generally represent the majority of the influence on the model. Higher order moment solutions are likely more important to consider if they are used to estimate transient storage parameters [e.g., *Schmid*, 2003].

Finally, this application provided an example of how to use this approach to identify when the use of a one-zone TSM is sufficient or when use of a two-zone TSM is warranted. Additive (Case I) or dominant (Case III) conditions can rely on a one-zone TSM approach. However, situations where there is no apparent dominance of one zone or the contributions of each zone are not identical (i.e., the influences of STS parameters are not equal to the influences of HTS parameters), a two-zone TSM approach would be necessary. When appropriate, one-zone TSMs are preferable due to fewer parameters to calibrate and their wide use in past decades allowing for comparison between a variety of

stream systems [e.g., *Cheong and Seo*, 2003; *Harvey and Wagner*, 2000]. However, considering the relative importance of STS and HTS may be necessary when modeling reactive solute [*Stewart et al*., 2011] and heat transport [*Neilson et al*., 2010a, 2010b] and, therefore, would require a two-zone TSM approach.

Conclusions

The moment solutions combined with a fuzzy number sensitivity analysis provide an efficient approach to determine the relative influence of each storage parameter on the model output. From the application example, we found that parameters representing storage sizes (e.g., B_{STS} or Y_{HTS}) consistently had the largest influences. While higher order moments may be important to support storage parameter estimation techniques, only the first two moments representing mean residence time and variance were necessary to represent dominant parameter influence on a solute prediction. This approach can also help determine when use of a two-zone transient storage model is warranted.

CHAPTER 3[2]

THE INFLUENCE OF SPATIALLY VARIABLE STREAM HYDRAULICS ON REACH SCALE SOLUTE TRANSPORT MODELING

Abstract

Within the context of reach scale transient storage modeling, there is limited understanding of how best to establish reach segment lengths that represent the effects of spatially variable hydraulic and geomorphic channel properties. In this chapter, we progress this understanding through the use of channel property distributions derived from high-resolution imagery that are fundamental for hydraulic routing. We vary the resolution of reach segments used in the model representation and investigate the minimum number necessary to capture spatially variable influences on downstream predictions of solute residence time probability density functions while sufficiently representing the observed channel property distributions. We also test if the corresponding statistical moments of the predictions provide comparable results and, therefore, a method for establishing appropriate reach segment lengths. We find that the predictions and the moment estimates begin to represent the majority of the variability at reach segment lengths coinciding with distances where observed channel properties are spatially correlated. With this approach, reach scales where the channel properties no longer significantly change predictions can be established, which provides a foundation for more focused transient storage modeling efforts.

[2] Coauthored by Noah M. Schmadel, Bethany T. Neilson, Justin E. Heavilin, David K. Stevens, and Anders Wörman

Introduction

Pioneering studies of transient storage modeling considered the spatial variability of hydraulic and geomorphic channel properties important [e.g., *Bencala and Walters*, 1983]. Despite this recognition, successive approaches tended to aggregate inversely estimated channel properties over a study reach in lieu of a detailed spatial representation [e.g., *Stream Solute Workshop*, 1990]. The success of this simplified approach to reproduce solute observations led to many similar applications over past decades [e.g., *Neilson et al.*, 2010b; *Runkel*, 2007; *Schmid et al.*, 2010]. However, because inversely estimated parameters provide indirect physical meaning concerning transport processes [e.g., *Marion et al.*, 2003; *Ward et al.*, 2010], a uniform representation of channel properties can result in inconclusive interpretations of transient storage residence times [e.g., *Gooseff et al.*, 2007; *Harvey and Bencala*, 1993; *Wondzell and Swanson*, 1999]. It is understood that a more realistic representation of transient storage processes may require a spatial understanding of channel properties [*Jackson et al.*, 2012; *O'Connor et al.*, 2010], but approaches are lacking to establish the necessary level of detail in transient storage modeling.

While retrieval of any physical information from inversely estimated model parameters depends on reach length selection [*Harvey et al.*, 1996; *Wagner and Harvey*, 1997], reducing the number of parameters through measurements can provide a better understanding of key processes [e.g., *Loheide and Gorelick*, 2006]. Direct measurements of channel properties related to stream hydraulics (e.g., channel width, depth, and velocity) [*Jackson et al.*, 2012; *O'Connor et al.*, 2010; *Stonedahl et al.*, 2012] and detailed subsurface mapping from near-surface tracer tests [*Toran et al.*, 2013; *Ward et*

al., 2012] have shown that transient storage processes are linked with spatially variable channel properties. Despite the promise of these recent efforts, measuring or extrapolating over longer reach scales is difficult because storage processes are persistently heterogeneous [*Wondzell and Gooseff*, 2013]. Nonetheless, a better representation of transient storage processes at a reach scale may be possible through a more realistic spatial understanding of channel properties. As higher spatial resolution information becomes available through remote sensing [e.g., *Bingham et al.*, 2012], there is opportunity to investigate the influence of some spatially variable channel properties on reach scale predictions of solute transport and determine the level of spatial detail beyond which no new information is gained.

The objective of this chapter is to determine the number of reach segments and corresponding lengths necessary to capture the effects of spatially variable channel properties related to the stream hydraulics in transient storage modeling. Using remotely sensed data from a 6.96-km study reach, we derive the high-resolution distribution of channel widths and corresponding distributions of depth, velocity, and the dispersion coefficient based on hydraulic principles of open-channel flow. Hereafter we refer to the channel width, depth, velocity, and dispersion estimates as channel properties. With this site specific information, we vary the resolution of reach segments and investigate the minimum number necessary by comparing segment-averaged distributions to the observed distributions of channel properties and by comparing reach scale solute predictions made with different resolutions of reach segments in the model representation. Furthermore, we compare statistical moments of the predictions to test if results are similar. To investigate a possible pattern between spatial variability and reach

segment lengths where the effects are captured, we repeat these comparisons using subsets of data from 1-km sections of the original study reach.

Methods

Channel Property Estimates Derived From Observations

We build on previous work that produced a clipped raster of observed water temperatures (banks, vegetation, and sandbars excluded) from remotely sensed, high-resolution three-band and thermal infrared imagery to establish a study reach distribution of total channel width (B_{tot}) estimates. This imagery was collected from an aerial platform over the Virgin River, located in southwestern Utah, on June 22, 2007. Using this clipped raster (0.7 m pixel resolution) from *Bingham et al*. [2012] (Figure 3-1A), we delineated B_{tot} every 5 meters over a 6.96-km study reach to arrive at $B_{tot}(x)$. Here x is the streamwise distance from 0 m (upper reach limit) to 6.96-km (downstream reach limit). This delineation consisted of setting transects (assumed perpendicular to main stream flow) along a centerline bisecting the clipped raster. Each transect was clipped to the outline of the raster that represents the edge of water (see Figure 3-1B for example). Mean stream depth ($Y(x)$), mean stream velocity ($U(x)$), and the longitudinal dispersion coefficient ($D(x)$) were estimated from the $B_{tot}(x)$ estimates using hydraulic principles and relationships (i.e., momentum, continuity, Manning's equation, and *Fischer's* [1975] empirical relationship for $D(x)$). Flow (Q) and mean streambed slope (S_o) were assumed constant over the study reach. See Appendix C for details.

The study reach is a desert river system with sand to gravel substrate and a reach-averaged S_o of 0.0039 m m^{-1}. The influence of groundwater is assumed negligible based

on previous work [*Bandaragoda and Neilson*, 2011; *Bingham et al.*, 2012; *Herbert*, 1995; *Neilson et al.*, 2010a, 2010b]. Q measured at the upper reach limit during this period was ~1.06 m^3 s^{-1}, but can range from 0.5-25 m^3 s^{-1} during typical seasonal variations. Q is assumed to be steady based on continuous water levels recorded at the upper reach limit. A Rhodamine WT tracer was instantaneously injected at the upper reach limit and measured 6.47 km downstream. This indicated mean residence time was ~6 hours through this section, which was used to estimate a mean velocity and reach-averaged Manning's roughness coefficient of 0.06.

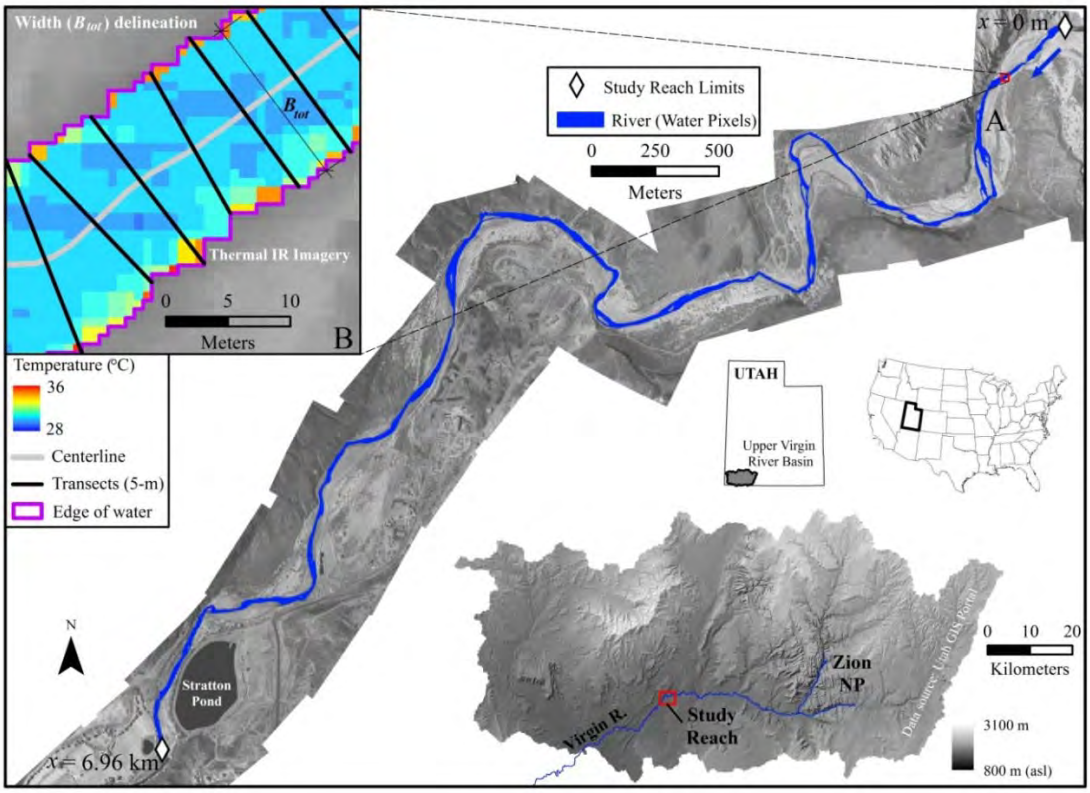

Figure 3-1. Virgin River study reach located in southwestern Utah. (A) The clipped raster of only water temperature pixels from *Bingham et al*. [2012] used to delineate total channel width ($B_{tot}(x)$ in m) every 5 streamwise meters. These water temperatures are the result of thermal infrared imagery (0.7 m pixel resolution) collected from an aerial platform. (B) Starting with a centerline bisecting this clipped raster, transects (assumed perpendicular to main stream flow) were set every 5 meters and clipped by the outline of the raster that represents the edge of water. These resulting transect lengths provide representative $B_{tot}(x)$ estimates.

Study Reach Segmentation

In an effort to determine the necessary number of reach segments (k), we divided the total study reach length (X) into segments of equal length (Δx). The value of k was varied from 1, 2, …, N where N is the maximum possible number of reach segments and $\Delta x_k = X/k$ (for this study, $X/N = 5$ m). From the different segmentations ($k = 1, 2, \ldots, N$), corresponding vectors of observed widths ($\mathbf{B}_{tot,ki}$) were extracted where i is the segment index (Figure 3-2). From each reach segment specific vector, corresponding width distributions ($f(\mathbf{B}_{tot,ki})$) were established and the expected values (i.e., segment-wise averages) were estimated as

$$E[\mathbf{B}_{tot,ki}] = \int_0^\infty \mathbf{B}_{tot,ki} f(\mathbf{B}_{tot,ki}) d\mathbf{B}_{tot,ki} , \tag{3-1}$$

where $E[\ldots]$ denotes the expected value and $f(\mathbf{B}_{tot,ki})$ is the nonparametric probability density function (PDF) of $\mathbf{B}_{tot,ki}$ (see Table 3-1 and Figure 3-2 for summary of relevant notation). A kernel density estimator (normal kernel and 0.1 m bandwidth) was used to estimate each reach segment specific PDF. Unique values of $E[\mathbf{Y}_{ki}]$, $E[\mathbf{U}_{ki}]$, and $E[\mathbf{D}_{ki}]$ were then estimated with this same procedure where $\mathbf{Y}_{ki}$, $\mathbf{U}_{ki}$, and $\mathbf{D}_{ki}$ are the resulting vectors of depth, velocity, and dispersion estimates within the ith reach segment. In the end, this study reach segmentation procedure produced varying values of $E[\mathbf{B}_{tot,ki}]$, $E[\mathbf{Y}_{ki}]$, $E[\mathbf{U}_{ki}]$, and $E[\mathbf{D}_{ki}]$ at Δx_k for $k = 1, 2, \ldots, N$.

To understand the importance of Δx_k on the spatial correlation of $E[\mathbf{B}_{tot,ki}]$ and how this segment-wise averaged value influences interpretation of results, a semivariogram was constructed of the study reach $B_{tot}(x)$ estimates. This consisted of quantifying the squared differences of pairs of $B_{tot}(x)$ corresponding to different separation distances (referred to as lag distance). These squared differences produced the

Table 3-1. Summary of notation relevant to the study reach segmentation.

Notation	Description
$\mathbf{B}_{tot,ki}$	Reach segment vector of total channel width estimates (m)
$f(\mathbf{B}_{tot,ki})$	Probability density function of $\mathbf{B}_{tot,ki}$
k	Number of reach segments, varies from 1, 2, …, N
i	Reach segment index
N	Maximum number of reach segments
$E[\ldots]$	Expected value (segment-wise average) (m)
Δx_k	Reach segment length for each k, X/k (m)
X	Total study reach length (m)

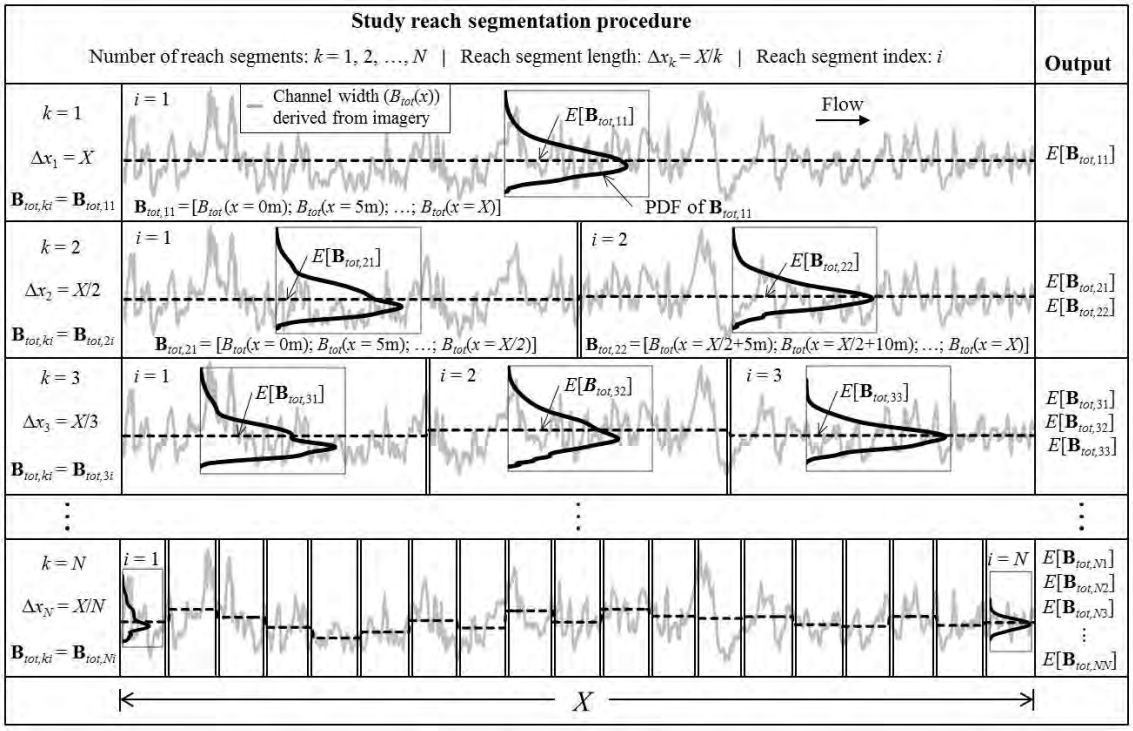

Figure 3-2. Illustration of the study reach segmentation procedure used over different resolutions of segmentations to find the necessary number of segments. The study reach is divided into $k = 1, 2, \ldots, N$ reach segments of equal length ($\Delta x_k = X/k$) where N is the maximum possible number of reach segments and X is the total length of the study reach. The total channel width estimates ($B_{tot}(x)$) derived from the imagery correspond to streamwise distances (x). In this case, $x = 0$ m to $x = X$ at 5-m intervals and $X/N = 5$ m. For each k, $\mathrm{B}_{tot,ki}$ is a vector of width estimates that fall within the ith reach segment. The expected value (denoted by $E[\ldots]$) of $\mathrm{B}_{tot,ki}$ is estimated from the corresponding probability density function (PDF). This procedure was repeated using the mean depth ($Y(x)$), mean velocity ($U(x)$), and longitudinal dispersion coefficient ($D(x)$) estimates to produce varying $k = 1, 2, \ldots, N$ values of $E[\mathrm{Y}_{ki}]$, $E[\mathrm{U}_{ki}]$, and $E[\mathrm{D}_{ki}]$ where Y_{ki}, U_{ki}, and D_{ki} are the respective vectors of estimates within the ith reach segment.

semivariance in $B_{tot}(x)$ at each lag distance. If spatial correlation is present, the semivariance of $B_{tot}(x)$ will approach the overall variance in $B_{tot}(x)$ as lag distance increases. If correlation is not present, the semivariance will be similar to the overall variance at every lag distance.

Comparison of Channel Property Distributions

We compared distributions of segment-averaged channel properties to their observed distributions to investigate the minimum number of reach segments necessary to represent the observed distributions. We hypothesize that this minimum number will provide some sense of the reach segment lengths necessary to capture the spatial variability in channel properties. Specifically, we compared distributions of $E[\mathbf{B}_{tot,ki}]$, $E[\mathbf{Y}_{ki}]$, $E[\mathbf{U}_{ki}]$, and $E[\mathbf{D}_{ki}]$ for segmentation varying from $k = 1, 2, \ldots, N$ to distributions of $B_{tot}(x)$, $Y(x)$, $U(x)$, and $D(x)$ derived from the observations over the entire study reach.

The Kolmogorov-Smirnov (K-S) test was applied to compare nonparametric cumulative distribution functions (CDF) of $E[\mathbf{B}_{tot,ki}]$, $E[\mathbf{Y}_{ki}]$, $E[\mathbf{U}_{ki}]$, and $E[\mathbf{D}_{ki}]$ (referred to as the k-distributions) to CDFs of $B_{tot}(x)$, $Y(x)$, $U(x)$, and $D(x)$ (referred to as the reference distributions). In this test, the resulting K-S statistic provides the maximum difference between each corresponding k-distribution and reference distribution (where $0 <$ K-S statistic < 1). The p-value was also quantified to provide the probability that this K-S statistic is equal to or larger than all possible differences between the two distributions. A relatively high K-S statistic accompanied by a low p-value indicates that the reference distribution is not sufficiently represented. If the p-value approaches unity and the K-S statistic approaches zero, the two distributions are considered statistically the same.

Comparison of Solute Predictions

We compared solute predictions made with increasing reach segmentation ($k > 1$) to the prediction made with the reach-averaged values ($k = 1$) and investigated the minimum number of reach segments required to capture the effects of spatially variable channel properties. Using the values of $E[\mathbf{B}_{tot,ki}]$, $E[\mathbf{Y}_{ki}]$, $E[\mathbf{U}_{ki}]$, and $E[\mathbf{D}_{ki}]$, we make reach scale predictions of solute residence time PDFs for segmentation varying from $k = 1, 2, \ldots, N$ using a two-zone transient storage model.

Governing Equations and Solution

We use the solute component of the two-zone temperature and solute (TZTS) transient storage model because the physical layout is constrained by widths and depths in the parameterization. Assuming flow is steady, exchange with storage zones is instantaneous, and the active stream channel and storage zones are rectangular, the governing equations are [*Neilson et al.*, 2010b]

$$\frac{\partial C}{\partial t} = D\frac{\partial^2 C}{\partial x^2} - \frac{Q}{YB_{tot}(1-\beta)}\frac{\partial C}{\partial x} + \frac{\alpha_{STS}Y_{STS}}{Y(1-\beta)\beta B_{tot}{}^2}(C_{STS} - C) + \frac{\alpha_{HTS}}{Y_{HTS}Y}(C_{HTS} - C), \quad (3\text{-}2)$$

$$\frac{dC_{STS}}{dt} = \frac{\alpha_{STS}}{(\beta B_{tot})^2}(C - C_{STS}), \quad (3\text{-}3)$$

$$\frac{dC_{HTS}}{dt} = \frac{\alpha_{HTS}}{Y_{HTS}{}^2}(C - C_{HTS}), \quad (3\text{-}4)$$

where equation (3-2) represents solute transport in the main portion of the stream (hereafter referred to as the main channel (MC)); $C(x,t)$ is the solute concentration (mg m^{-3}); the subscripts STS and HTS represent surface transient storage and hyporheic transient storage, respectively; α_{STS} is the exchange rate coefficient between the MC and the STS zone (m^2 s^{-1}); α_{HTS} is the exchange rate coefficient between the MC and the HTS

zone (m^2 s^{-1}); Y_{STS} and Y_{HTS} are the STS and HTS mean depths (m), respectively; β is the STS fraction of the total channel width; and t is time (s).

Assuming initial and boundary conditions are

$$C(x,0) = C_{STS}(x,0) = C_{HTS}(x,0) = 0,$$

$$C(0,t) = g(t), \text{ and } C(\infty,t) = 0, \tag{3-5}$$

where $g(t)$ represents a time-dependent (Dirichlet type) inflow solute breakthrough curve, the resulting Laplace-domain solution to the MC (equation (3-2)) is

$$\overline{C} = \overline{g}(s)\exp\left[\frac{x}{2D}\left(U - \sqrt{U^2 + 4D\psi(s)}\right)\right], \tag{3-6}$$

where $\psi(s) = \left(s + \kappa_1 + \kappa_2 - \frac{\kappa_1\kappa_3}{(s+\kappa_3)} - \frac{\kappa_2\kappa_4}{(s+\kappa_4)}\right)$, $\kappa_1 = \frac{\alpha_{STS}Y_{STS}}{Y(1-\beta)\beta B_{tot}^{\ 2}}$, $\kappa_2 = \frac{\alpha_{HTS}}{Y_{HTS}Y}$,

$\kappa_3 = \frac{\alpha_{STS}}{(\beta B_{tot})^2}$, and $\kappa_4 = \frac{\alpha_{HTS}}{Y_{HTS}^{\ 2}}$. Here $\overline{C}(x,s) = \mathcal{L}\{C(x,t)\}$ is the solute concentration in the Laplace domain, s is the Laplace variable, and $\overline{g}(s) = \mathcal{L}\{g(t)\}$. Because we are only looking at the influence of spatially variable channel properties, we set α_{STS}, α_{HTS}, Y_{STS}, Y_{HTS}, and β to values within the narrowed bounds presented in *Bandaragoda and Neilson* [2011] and held these constant over the entire study reach. Note that the STS and HTS widths are βB_{tot} and $B_{tot}(1-\beta)$, respectively, and, therefore, change throughout the study reach.

Convolution of Reach Segment Specific Solutions

From the Laplace-domain solution in equation (3-6), the predicted reach scale solute breakthrough curves for segmentation varying from $k = 1, 2, \ldots, N$ were obtained through a convolution of reach segment specific Laplace-domain solutions,

$$\mathcal{L}\{C_k(x=X,t)\} = \overline{C}_k(x=X,s) = \overline{g}(s)\cdot\overline{c}_{k1}(\Delta x_k,s)\cdot\overline{c}_{k2}(\Delta x_k,s)\cdot\ldots\cdot\overline{c}_{ki}(\Delta x_k,s), \quad (3\text{-}7)$$

where

$$\overline{c}_{ki}(\Delta x_k,s) = \frac{\overline{C}_{ki}(\Delta x_k,s)}{\overline{g}(s)}, \quad (3\text{-}8)$$

and $\mathcal{L}^{-1}\{\overline{c}_{ki}(\Delta x_k,s)\} = c_{ki}(\Delta x_k,t)$ is the solute residence time PDF of the *i*th of *k* reach segment. *Riml and Wörman* [2011] state that this convolution is valid for study reaches with large Péclet numbers (i.e., $(XU)/D >> 1$) to assume one-way advective communication between reach segments. Meeting this condition ensures that mass is conserved and the upstream reach segment solution can be used as the boundary condition for the next downstream reach segment solution.

For the purpose of expressing predicted breakthrough curves as solute residence time PDFs, equation (3-7) was normalized by the zeroth temporal moment. To arrive at the *k*th solute residence time PDF prediction, $\overline{c}_k(X,s)$ was inverted into the original state space using the *Hollenbeck* [1998] function based on the *De Hoog et al*. [1982] algorithm. The root mean square error (RMSE) was used to assess the change between predictions for $k > 1$ and $k = 1$. The rate of change in RMSE with respect to a change in *k* determined the value of *k* necessary for convergence in the predictions (i.e., where further segmentation no longer significantly influences the predictions).

Comparison of Statistical Moments

Similar to investigating the effects of reach segmentation on solute residence time PDF predictions, the effects on statistical moments were also investigated to determine if these provide a measure for establishing reach segment lengths. Because the Laplace-

domain solution in equation (3-6) provides a moment generating function [*Aris*, 1958], we accomplished this through closed form temporal moment solutions.

Temporal moments centered about the mean (hereafter referred to as central moments) describe statistical characteristics of a solute residence time PDF at a spatial position. The first temporal moment represents the mean solute residence time (μ_t) and the second central moment represents the variance (σ_t^2) about the mean from an Eulerian perspective [e.g., *Wörman*, 2000]. The third central moment (S_t) is related to the formal statistical definition of skewness. We derived closed form moment solutions weighted by spatial variability factors that represent the variation of spatially variable channel properties from their reach-averaged values. Using similar derivation techniques developed by *Riml and Wörman* [2011], the mean residence time of $c_k(X,t)$ for segmentation varying from $k = 1, 2, \ldots, N$ is $\langle \mu_t \rangle_k$ (s) where $\langle ... \rangle$ denotes the study reach-averaged value for each k. Subsequently, the variance about the mean is $\langle \sigma_t^2 \rangle_k$ (s^2) and the third central moment is $\langle S_t \rangle_k$ (s^3). See Appendix D for the closed form moment solutions and spatial variability factors.

These moment solutions weighted by spatial variability factors allow the influence of spatially variable channel properties on solute transport solutions to be evaluated without completing model simulations. This influence is expressed as the percent change of the mean, variance, and third central moment estimates for $k > 1$ from the corresponding estimates for $k = 1$. The rate of percent change in the moment estimate with respect to a change in k determines the k where increased reach segmentation no longer significantly changes the estimate.

Repeat of Comparisons Using Different Channel Property Distributions

To investigate a possible pattern between spatial variability and reach segment lengths where the effects on solute predictions are captured, we repeated each comparison (comparison of distributions, solute predictions, and statistical moments) using subsets of data from the study reach. These subsets are width estimates derived from the imagery that fall within 1-km sections of the original study reach. These data were used to create different distributions of channel properties; depth, velocity, and the dispersion coefficient were calculated using the same constant Q and S_o. The 1-km sections were treated as individual reaches with unique, observed distributions. Semivariograms of width estimates from each 1-km section were constructed to understand the influence of spatial correlation on the interpretation of results. To further illustrate the importance of a more realistic representation of channel properties and spatial correlation within streams, we again repeated each comparison (and semivariogram construction) using randomly generated width estimates. These estimates follow an assumed lognormal distribution with a similar expected value and variance as observed over the entire study reach (Appendix E for details).

Results

Channel Property Estimates Derived From Observations

The $B_{tot}(x)$ estimates derived every 5 m from the imagery range from 3-42 m with a study reach expected value ($k = 1$) of 16.8 m (Figure 3-3A). The semivariance of $B_{tot}(x)$ indicates that width estimates are spatially correlated at distances up to ~150 m (gray shading in Figure 3-3B); thus, $B_{tot}(x)$ estimates greater than 150 m apart are considered

spatially independent. From the $B_{tot}(x)$ estimates, $Y(x)$ ranges from 0.11-0.55 m with an expected value of 0.21 m, $U(x)$ ranges from 0.23-0.71 m s^{-1} with an expected value of 0.34 m s^{-1}, and $D(x)$ ranges from 0.5-137 m^2 s^{-1} with an expected value of 24.4 m^2 s^{-1}.

Comparison of Channel Property Distributions

The differences between nonparametric cumulative *k*-distributions of $E[\mathbf{B}_{tot,ki}]$ and the reference distribution of $B_{tot}(x)$ decrease as *k* increases (Figure 3-4). For example, when $k = 10$, the *k*-distribution clearly does not represent the reference distribution (Figure 3-4A); however, by increasing the number of reach segments to $k = 50$, the corresponding *k*-distribution more closely represents the reference distribution. The maximum differences (K-S statistic) for segmentation varying from $k = 1, 2, \ldots, N$ decrease as *k* increases (Figure 3-4B). As reach segment lengths begin to coincide with spatial correlation in width estimates ($\Delta x_k < 150$ m), the maximum difference begins to stabilize (vertical gray line in Figure 3-4B); although the *p*-value is relatively low at this point, it generally increases with further segmentation (black line in Figure 3-4C

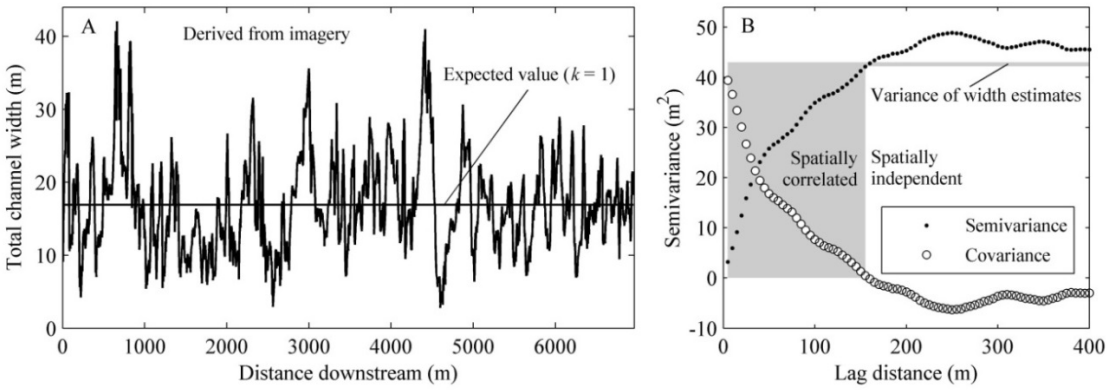

Figure 3-3. (A) Total channel width estimates ($B_{tot}(x)$) derived every 5 streamwise meters from the imagery (clipped raster) shown in Figure 3-1. The expected value of the width distribution for $k = 1$ is shown. (B) The semivariance, variance, and covariance of $B_{tot}(x)$ at different separation distances (lag distance) indicate that $B_{tot}(x)$ estimates are spatially correlated at distances up to 150 m, which is shown by the gray shading. $B_{tot}(x)$ estimates greater than 150 m apart are considered spatially independent.

represents the moving average of 10 consecutive values). Here, only the K-S test results of $E[\mathbf{B}_{tot,ki}]$ relative to $B_{tot}(x)$ are shown because reference distributions of $Y(x)$, $U(x)$, $D(x)$ were represented similarly.

Comparison of Solute Predictions

The solute residence time PDF predictions for $k > 1$ clearly differ from the prediction for $k = 1$ (Figure 3-5). A majority of the change in the solute response appears to occur for $50 \geq k > 1$ (light gray band in Figure 3-5A which represents all predictions from $k = 2$ to $k = 50$). When $k > 50$ (approximate to $\Delta x_k < 150$ m), the responses begin to converge to the solution representing the effects of spatially variable channel properties and essentially begin to lay on top of each other with further segmentation (dark gray band in Figure 3-5A which represents predictions from $k = 51$ to $k = 400$). The resolution at which the influence of segmentation stabilizes becomes apparent through the RMSE estimates that compare predictions when $k > 1$ to the prediction where $k = 1$ (Figure 3-5B). The RMSE begins to level off abruptly for $\Delta x_k < 150$ m where reach segment lengths coincide with the distances where $B_{tot}(x)$ estimates are spatially correlated (vertical gray line in Figure 3-5B). The rate of change in the RMSE with respect to a change in k further indicates that the prediction begins to converge at $\Delta x_k < 150$ m (Figure 3-5C). Note that the Péclet number for $k = 1$ is ~100, indicating that the convolution approach is appropriate for the conditions of this study reach.

Comparison of Statistical Moments

The $\langle \mu_t \rangle_k$, $\langle \sigma_t^2 \rangle_k$, and $\langle S_t \rangle_k$ estimates for $k > 1$ diverge from the respective estimates for $k = 1$ (Figure 3-6). Similar to the solute prediction results, the percent

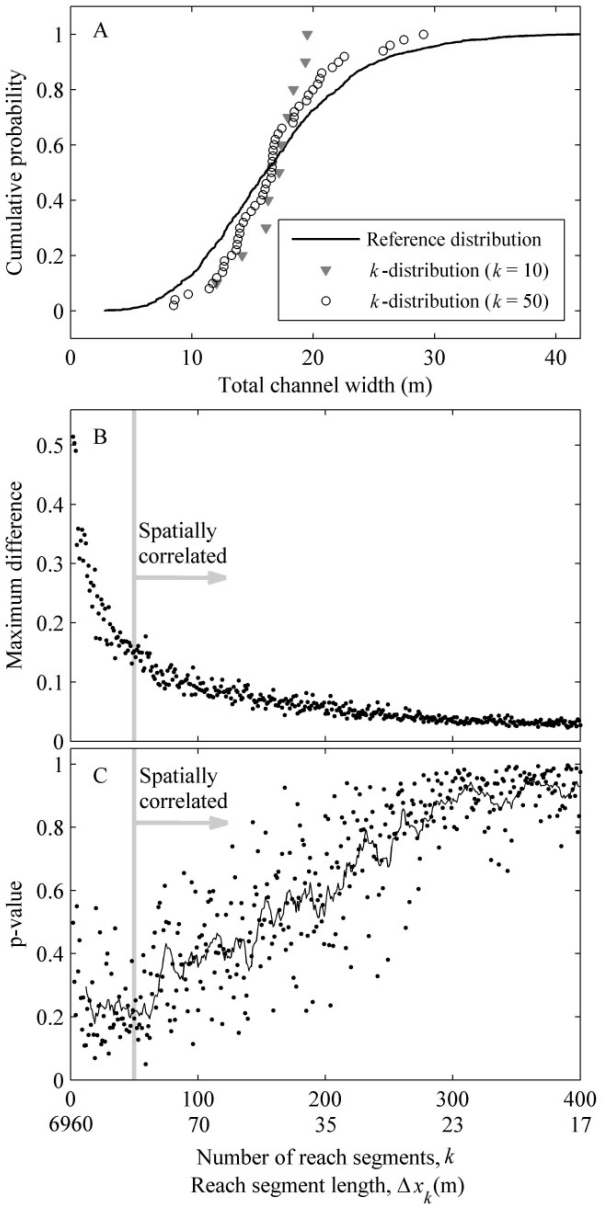

Figure 3-4. (A) Example nonparametric cumulative distribution functions (CDF) of segment-average widths ($E[B_{tot,ki}]$) for $k = 10$ and $k = 50$ reach segments (k-distribution) relative to the reference distribution of observed width estimates ($B_{tot}(x)$). (B) The resulting Kolmogorov-Smirnov (K-S) statistic (maximum difference) for varying $k = 1, 2, \ldots, N$ reach segments. The vertical gray line corresponds to the reach segment lengths (Δx_k) equivalent to the lag distances where $B_{tot}(x)$ estimates are considered spatially correlated (see Figure 3-3B). (C) The accompanying p-value that represents the probability that the maximum difference is equal to or larger than all possible differences between the k-distribution and the reference distribution. The p-value steadily increases with further segmentation at Δx_k coinciding with spatial correlation (vertical gray line). The black line is the moving average of 10 consecutive values, which is included to illustrate the increasing trend. If the p-value approaches unity and the maximum difference approaches zero, the k-distribution and the reference distribution are considered statistically the same.

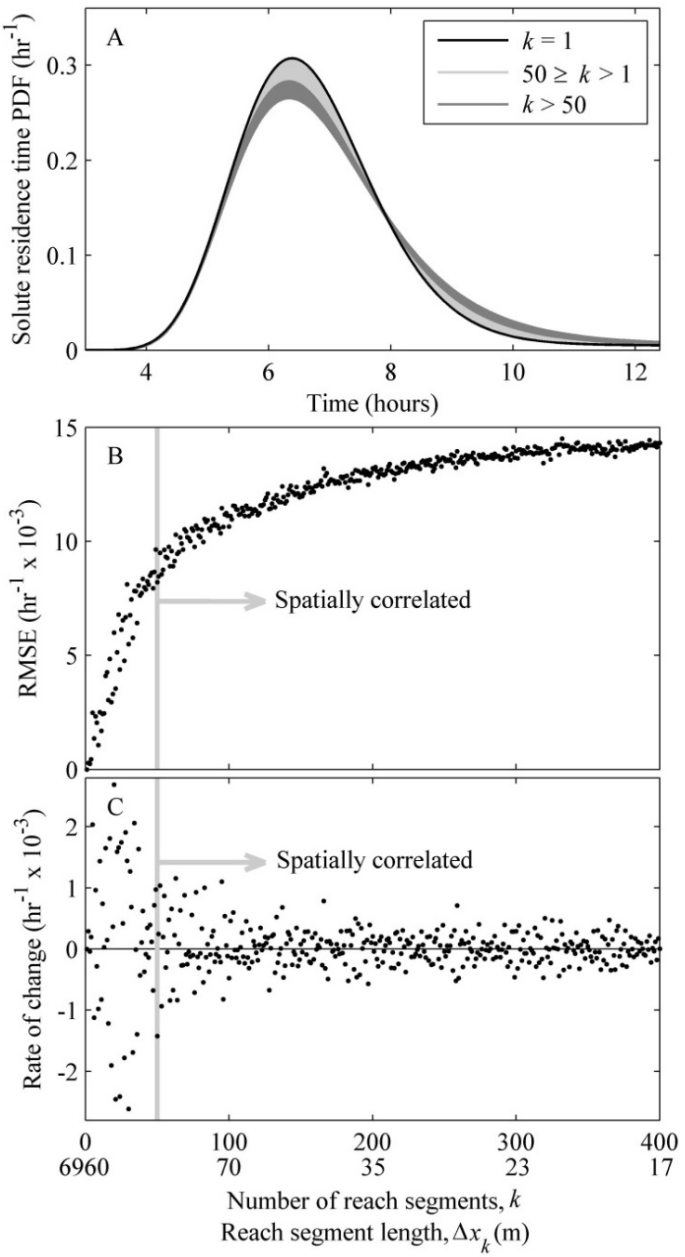

Figure 3-5. (A) Solute residence time probability density function (PDF) predictions at the downstream reach limit ($c_k(X,t)$) for varying $k = 1, 2, \ldots, N$ reach segments. Shown in black is the prediction for $k = 1$ where channel properties are uniform. Predictions for $50 \geq k > 1$ are shown in light gray. Shown in dark gray are the predictions for $k > 50$ which begin to converge or lay on top of each other with further segmentation. (B) The root mean square error (RMSE) as a measure of change of the predictions for $k > 1$ from the prediction for $k = 1$. The RMSE appears to flatten out asymptotically as k increases. The vertical gray line corresponds to the reach segment lengths (Δx_k) equivalent to the lag distances where total channel width ($B_{tot}(x)$) estimates are considered spatially correlated (see Figure 3-3B). (C) The rate of change in RMSE with respect to a change in k indicates that change in the prediction begins to diminish at reach scales equivalent to spatial correlation in $B_{tot}(x)$ estimates shown by the vertical gray line.

change in moment estimates begins to level off abruptly at reach segment lengths coinciding with spatial correlation in $B_{tot}(x)$ estimates (vertical gray lines in Figures 3-6A, 3-6B, and 3-6C). All moment estimates increase with further segmentation and a majority of the possible percent change occurs at reach segment lengths coinciding with spatial correlation. The rate of percent change of $\langle \mu_t \rangle_k$, $\langle \sigma_t^2 \rangle_k$, and $\langle S_t \rangle_k$ with respect to a change in k indicates that the influence of further reach segmentation on moment estimates begins to diminish at $\Delta x_k < 150$ m (vertical gray lines in Figures 3-6D, 3-6E, and 3-6F).

Repeat of Comparisons Using Different Channel Property Distributions

For illustrative purposes, we show an example of width estimates derived from imagery that fall within three, unique 1-km sections of the original study reach (Reaches 1, 2, and 3 in Figure 3-7A). Each unique reach has similar expected values for $k = 1$, but different CDFs (Figure 3-7B) and variance of width estimates (Figure 3-7C). The semivariance of each reach indicates that the width estimates are spatially correlated at distances up to 170 m, 90 m, and 40 m for Reaches 1, 2, and 3, respectively (vertical gray and black lines in Figure 3-7C). By repeating the comparisons presented earlier using width estimates within these 1-km sections, we exposed a pattern between the spatial variability in channel properties and reach segment lengths where the effects on solute predictions are captured. The influence of spatial variability on a solute prediction (shown here by the variance of the solute residence time PDF) begins to stabilize at reach segment lengths consistently coinciding with spatial correlation in the observed widths (vertical gray and black lines in Figure 3-7D). From this example, increased variability in width estimates results in increased magnitude of change in the prediction. However,

fewer reach segments are necessary to represent that variability because there is an increase in the distances where spatial correlation persists. The K-S test results for comparing distributions for each reach are not shown because similar results occurred.

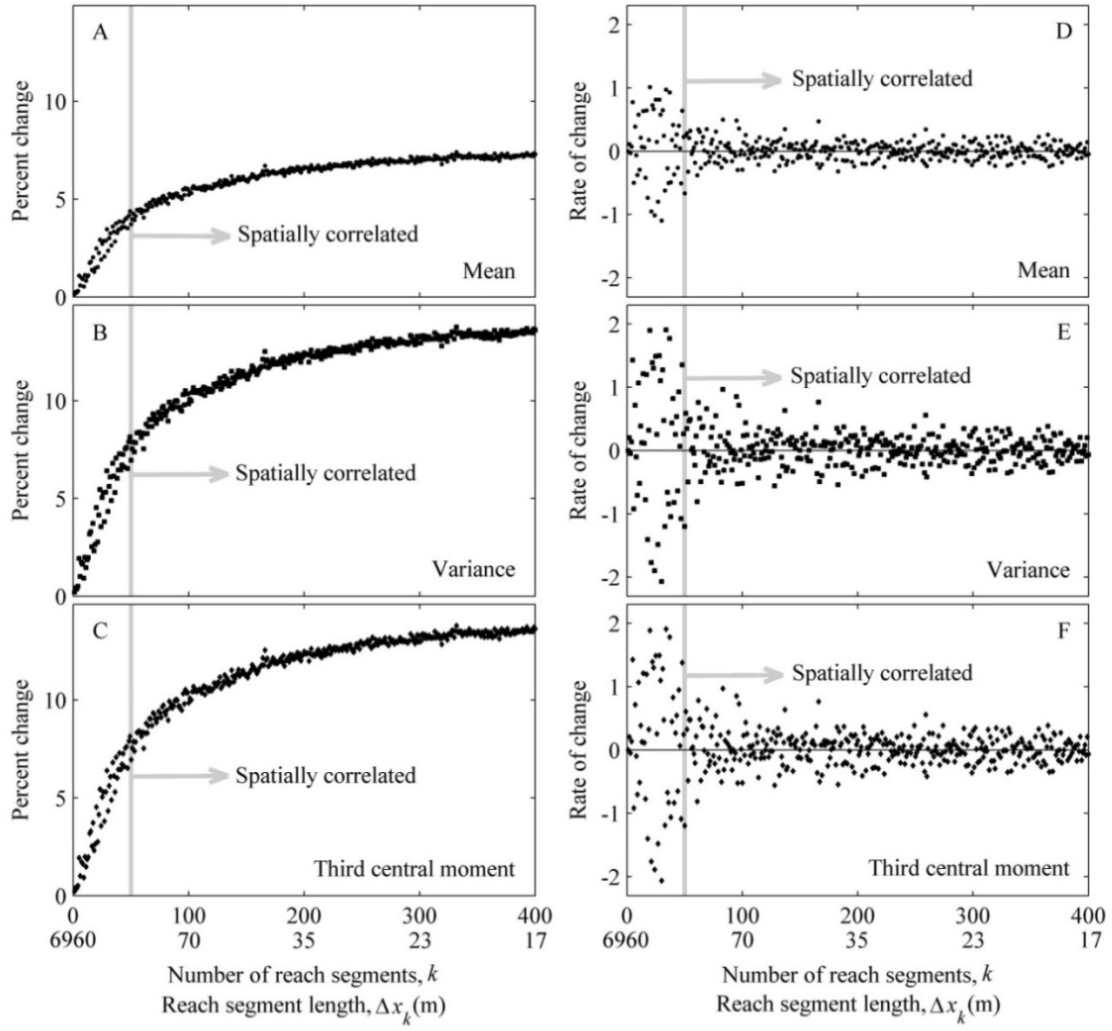

Figure 3-6. The percent change of the (A) mean, $\langle \mu_t \rangle_k$, (B) variance, $\langle \sigma_t^2 \rangle_k$, and (C) third central moment, $\langle S_t \rangle_k$, estimates for more than one reach segment ($k > 1$) relative to the estimates for $k = 1$. These percent changes increase asymptotically as k increases. The vertical gray lines correspond to the reach segment lengths (Δx_k) equivalent to the lag distances where total channel width ($B_{tot}(x)$) estimates are considered spatially correlated (see Figure 3-3B). The rate of percent change with respect to a change in k of (D) $\langle \mu_t \rangle_k$, (E) $\langle \sigma_t^2 \rangle_k$, and (F) $\langle S_t \rangle_k$ indicates that the change in moment estimates due to increased reach segmentation begins to diminish at reach scales equivalent to spatial correlation in $B_{tot}(x)$ estimates, which is shown by the vertical gray lines.

The randomly generated width estimates are not spatially correlated at any distance because the semivariance is similar to the overall variance at every lag distance (see Figure E-1 in Appendix E). The repeated K-S test results (comparison of distributions) using randomized width estimates are drastically different from the observed counterpart. It takes roughly an order of magnitude more reach segments to represent the reference distribution (see Figure E-2 in Appendix E). Repeating the comparison of solute predictions using randomized width estimates indicates that the solution does not begin to converge at any number of reach segments. The solute residence time PDF prediction continues to change with increased segmentation until the full dataset is incorporated into the solution (see Figure E-3 in Appendix E). Repeating the statistical moment comparison produced similar results where the change in moment estimates does not stabilize or converge to a solution that represents the effects of spatial variability (see Figure E-4 in Appendix E).

Discussion

The Influence of Spatially Variable Channel Properties

Channel properties controlling stream hydraulics are fundamental to transient storage modeling [e.g., *O'Connor et al.*, 2010; *Runkel*, 2007]. Because these properties are spatially variable [*Bencala and Walters*, 1983], finding appropriate reach segmentation scales is necessary to capture the influence of this variability in solute predictions. Ultimately, adequately capturing the spatial variability in channel properties may be critical in representing key transport processes. In this chapter, an approach is provided to determine reach scales necessary to capture the effects of spatially variable

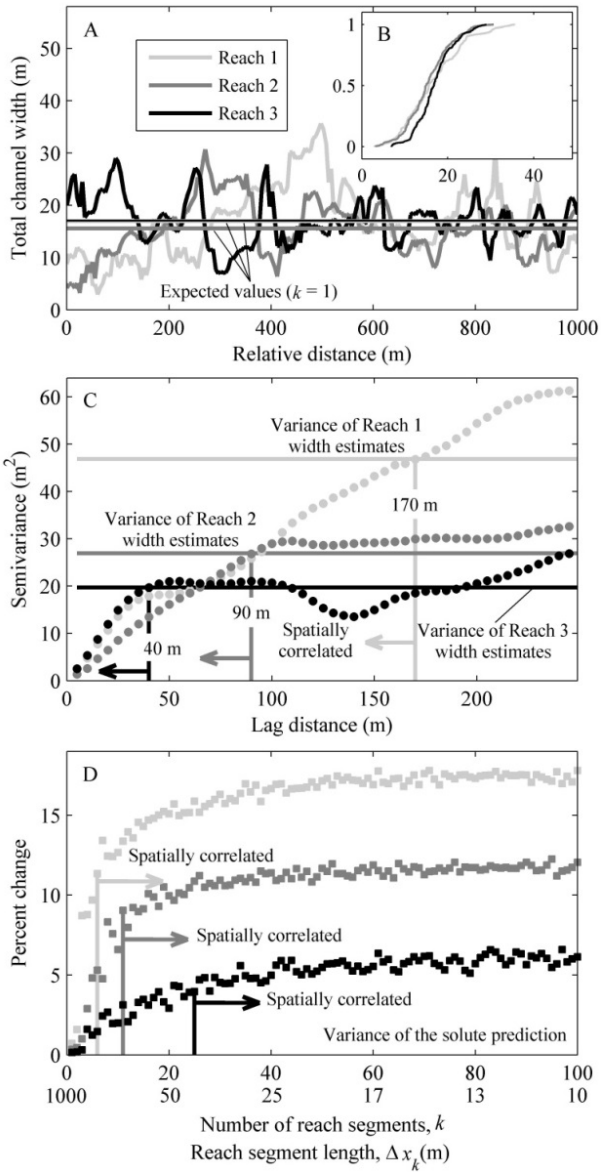

Figure 3-7. (A) Example width estimates derived every 5 meters from the imagery shown in Figure 3-1 of three 1-km sections of the original study reach. These 1-km sections are treated as individual, unique reaches designated by Reaches 1, 2, and 3. The expected value of each corresponding width distribution is shown (for k = 1). (B) The cumulative distribution functions for each reach (same scales as Figure 3-4A). (C) The semivariance and variance of Reach 1, 2, and 3 width estimates at different separation distances (lag distance) indicate that width estimates are spatially correlated at distances unique for each reach (170, 90, and 40 m, respectively), which is shown by the vertical gray and black lines. The colors correspond to A. From this example, increased variance of width estimates results in increased distances where estimates are spatially correlated. Consequently, if distances are increased where spatial correlation persists, fewer reach segments are required to represent that variability. (D) Percent change of the variance (second central moment) of the solute residence time probability density function predictions for Reaches 1, 2, and 3. The colors correspond to A. The vertical gray and black lines again correspond to spatial correlation in width estimates.

channel properties related to stream hydraulics in transient storage modeling. By varying the resolution of segments representing a continuous study reach, we found that distances where width estimates were spatially correlated (Figures 3-3B and 3-7C) consistently coincided with the reach segment lengths where change in the solute residence time PDF prediction began to diminish (Figures 3-5, 3-6, and 3-7). Based on this study, a majority of the effects of variability on a solute prediction can be anticipated if reach segmentation captures spatial correlation. Only a coarse representation of the observed distribution of channel properties was required by the reach segments to capture spatial correlation and a majority of the variability (Figure 3-4). At this point, the maximum difference also began to stabilize and the *p*-value increased steadily with further segmentation. This suggests that the level of variability will dictate the influence on a solute prediction and appropriate reach segment lengths. We found that increased spatial variability (represented by variance of width estimates) resulted in increased magnitude of change in the solute residence time PDF prediction (Figure 3-7). However, fewer reach segments were necessary to capture that increased variability because the influence of spatial correlation persisted over longer distances. Although we exposed a pattern between spatial correlation in observations and effects on solute predictions, it is still unclear if this correlation structure will always correspond to the reach segmentation that captures the influences of spatial variability. This study does illustrate that high spatial resolution data are necessary to apply this approach and to determine appropriate reach segmentation. As remote sensing has made such data more accessible [e.g., *Bingham et al.*, 2012], incorporating spatial information into solute predictions is feasible.

Previous Approaches

Two common modeling approaches developed to address spatially variable model parameters are a convolution of individual, reach segment specific residence time PDFs [*Riml and Wörman*, 2011; *Saco and Kumar*, 2002] and stochastic analyses that apply probabilistic descriptions of parameter variability [*Li and Zhou*, 1997; *Stewardson and McMahon*, 2002]. The convolution approach requires supporting data to adequately capture the effects of parameter variability. Most have not had such data to determine if this requirement is met and, therefore, have inferred the effects of parameter variability [*Riml and Wörman*, 2011; *Saco and Kumar*, 2002]. With the use of high-resolution data to support the convolution approach applied here, we found that when reach segments are no longer considered spatially independent, a majority of the effects of spatial variability were captured (Figure 3-5). Furthermore, we found that, similar to *Saco and Kumar* [2002], the representation of hydraulic parameter distributions influenced the variance in the final downstream solute response. Specifically, variance increased as more spatial detail was incorporated into the model, but began to stabilize at reach scales coinciding with spatial correlation (Figures 3-6B and 3-6E).

If supporting data are limited, stochastic analyses can be used to estimate the influence on solute predictions by inferring the variance in the parameter distributions [*Li and Zhou*, 1997]. However, parameter values are assumed random to infinitely small spatial scales. Based on this study, if channel properties are assumed spatially random, the solute prediction does not converge at any reach segment length (see Figures E-3 and E-4 in Appendix E). Because we see convergence in a prediction coinciding with spatial correlation, assuming a distribution based on an average and variance does not represent

the spatial variability of a stream system or provide an understanding of the amount of information necessary to represent that variability. While approaches are needed to capture the influences of spatial variability in solute predictions, there is a need to better understand the link between incorporating more spatial information and variance producing mechanisms in modeling applications.

Implications to Better Represent Transport Processes

Commonly, parameters representing both channel properties and transient storage processes are considered uniform and are estimated inversely through stream tracer experiments [e.g., *Stream Solute Workshop*, 1990]. Although tracer techniques are often useful for inferring reach function, transient storage parameters are not identifiable due to strong parameter interactions related to stream characteristics [*Kelleher et al.*, 2013]. A decrease in the number of parameters and other uncertainty sources would allow for better transient storage parameter estimation. This chapter provides a fundamental step to set the number of reach segments where spatially variable channel properties related to stream hydraulics are captured.

The next steps require consideration of additional spatially variable stream characteristics controlling transient storage such as streambed permeability [e.g., *Salehin et al.*, 2004; *Ward et al.*, 2014] and geomorphic features [e.g., *Gomez et al.*, 2012; *Stonedahl et al.*, 2013; *Zarnetske et al.*, 2007]. However, methods for extracting the necessary spatial information from high resolution data are required to scale parameters given that prior efforts have shown that measurements of channel width, depth, and velocity scaled with transient storage parameters provided residence time predictions different than those estimated with inversely calibrated hydraulic parameters [*O'Connor*

et al., 2010]. With high resolution imagery, we show that only a coarse number of measurements is needed to represent spatial correlation unique to each reach and, therefore, the effects of spatially variable stream hydraulics on a solute prediction. Building on this approach, it is possible to extract more detailed information from imagery such as STS widths [*Bingham et al*., 2012], sinuosity, and geomorphic units (e.g., pool-riffle sequences). This additional spatial detail may allow for investigating methods to scale parameters over space and determine the associated effects on solute transport.

Regardless of the potential for more detailed spatial information and because transient storage processes are persistently heterogeneous [e.g., *Jackson et al.*, 2012; *Wondzell*, 2006], more work is needed to link spatially variable channel properties to transient storage parameters over longer reach and network scales. However, establishing this link will likely require an understanding of the spatial scales necessary to capture the significant effects of spatially variable main channel properties.

Conclusions

While other studies have inferred the effects of spatial variability on solute transport, this chapter illustrated the smallest reach scales necessary to capture the effects of this variability on predictions of solute residence time probability density functions. Starting with distributions of channel properties related to stream hydraulics (width, depth, velocity, and dispersion) derived from high-resolution imagery, we presented an approach to determine such scales. Based on a convolution of reach segment specific transient storage model solutions, changes in predictions began to diminish at segment

lengths equivalent to distances where channel properties were spatially correlated. Changes in the moment estimates also began to diminish at the same segment lengths where channel properties were spatially correlated. The moment estimates revealed that the incorporation of greater spatial detail produced variance in the prediction. From the distributions derived from observations, reach segments needed to capture only a majority of the actual spatial variability in channel properties to reflect the significant effects on predictions. While increased variability in observations had a greater influence on a prediction, fewer reach segments were necessary to represent that variability because spatial correlation persisted over longer distances. It is currently unclear if data structure and spatial correlation will always correspond to the same reach scales necessary for transient storage modeling. However, this study showed that a majority of the effects of spatial variability on a solute transport prediction can be anticipated if spatial correlation is captured by reach segments. More work is also needed to link increased spatial detail to variance producing mechanisms. This study highlights the need for high spatial resolution data to apply this approach and determine the influence of spatial variability on solute transport modeling. An increased spatial understanding of channel properties and proper representation of these influences may allow for more focused efforts to identify other model parameters and thus provide a better understanding of key transport processes.

CHAPTER 4[3]

THE INFLUENCE OF SPATIALLY VARIABLE STREAM HYDRAULICS ON REACH SCALE TEMPERATURE MODELING

Abstract

While a myriad of processes control water temperature, the most significant in streams without notable shading or groundwater inputs are surface heat fluxes at the air-water interface. These fluxes are particularly sensitive to parameters representing the water surface area to volume ratio. Channel geometry dictates this ratio; however, it is currently unclear how spatial variability in stream hydraulics influences temperature predictions or how contribution of the boundary condition influences interpretation of processes most sensitive to this variability. To investigate these influences, we used high-resolution spatial observations collected over a 25-km reach within a Laplace-domain solution to a two-zone temperature transient storage model. We found that for the study reach and flow condition, changes in the surface area to volume ratio did not consistently coincide with changes in stream temperature. However, notable changes in cumulative mean residence time corresponded with changes in the temperature extremes throughout the study reach. The surface fluxes were clearly the most sensitive to spatial variability when the effects of the boundary condition were absent. Consistent with solute transport, reach segment lengths that include the spatial correlation in observations are necessary to capture the spatial influences of hydraulics on temperature predictions.

[3] Coauthored by Noah M. Schmadel, Bethany T. Neilson, and Justin E. Heavilin

Introduction

Stream temperature impacts biogeochemical transformations, dissolved oxygen content, and metabolic rates. Therefore, forecasting water quality and ecological health depends on accurate predictions of stream temperature. Stream temperature is controlled by the energy and hydrologic fluxes at the air-water and water-streambed interfaces [e.g., *Hannah et al.*, 2004, 2008; *Webb and Zhang*, 1997]. Common among all streams, these fluxes are driven by gradients caused by (1) meteorological conditions (e.g., solar radiation and air temperature) and (2) hydraulic (e.g., stream width, depth, and velocity) and geomorphic (e.g., streambed permeability and material) channel properties [e.g., *Caissie*, 2006]. In streams that do not have large groundwater inputs, tributaries, or notable shading, stream temperature is most sensitive to surface heat fluxes at the air-water interface [e.g., *Johnson*, 2004; *Kelleher et al.*, 2012; *Mosley*, 1983]. While there are numerous studies that investigate the relationship between meteorological conditions (e.g., air temperature) and stream temperature [e.g., *Caissie et al.*, 2001; *Stefan and Preud'homme*, 1993], few have focused on how the spatial variability in stream hydraulics influences surface heat fluxes and stream temperature. Past studies have, however, suggested that the contribution of surface heat fluxes to stream temperature is strongly sensitive to the hydraulic channel properties. In particular, the wetted surface area (based on width) of the air-water interface has been found proportional to the total energy available to heat stream water [*Edinger et al.*, 1968; *Link et al.*, 2013]. Furthermore, the amplitude of stream temperature typically increases with a decrease in depth (i.e., increase in the ratio between the air-water interface surface area and water volume) [*Gu et al.*, 1998]. Conversely, increased velocity has been shown to dampen

stream temperature amplitude due to decreased residence time in the channel [*Arscott et al.*, 2001; *Gu and Li*, 2002]. Although there is compelling evidence that hydraulic channel properties are important controls, their role in dictating stream temperature is still ambiguous because there is little understanding regarding the influence of spatial variability in those properties. Without this understanding, the corresponding influence of a changing surface area and, therefore, surface heat fluxes, is poorly understood.

In past efforts to predict stream temperature deterministically, model complexity has varied from accounting only for individual surface heat fluxes [SNTEMP; *Theurer et al.*, 1984] to including the effects of bed conduction and transient storage [TZTS; *Neilson et al*., 2010a, 2010b]. The goal is to represent important heat transfer and transport processes; however, by increasing model complexity, data requirements to estimate or calibrate parameters is also increased [e.g., *Bandaragoda and Neilson*, 2011]. Beyond parameter estimation, additional challenges include assessing whether a prediction represents processes accurately and evaluating the relative contributions of initial or boundary conditions on that prediction. Particularly in the context of temperature modeling, these challenges may be significant given that contribution of the uppermost reach boundary condition can persist over long reach scales (on the order of kilometers) [*Heavilin and Neilson*, 2012]. However, it is still unclear whether contributions of the initial and boundary conditions in the prediction will mute the interpretation of the role of heat fluxes at the air-water and water-streambed interfaces. Furthermore, assessing which processes are most sensitive to spatial variability may also be difficult if the contributions of heat fluxes are not realistically represented. While the influence of spatially variable

channel properties has been considered for solute transport (see Chapter 3), there is a similar need for consideration of this influence in the context of temperature predictions.

In this chapter, we set out to determine the role of spatially variable hydraulics in context of stream temperature modeling. This spatial variability is represented by channel width data assessed from high-resolution imagery that is used to determine mean depths and velocities. Determining this role requires consideration of initial condition, boundary condition, and surface heat flux contributions throughout the reach being modeled. We present a semi-analytical solution to a heat transport model to isolate these contributions. We apply a convolution of this solution to incorporate spatial detail. Using this convolution technique, we determine how best to represent spatial variability by varying the number of segments representing the study reach and investigating the minimum number and, therefore, the segment lengths necessary to capture this variability.

Methods

Temperature Model and Solutions

To investigate the influence of spatially variable hydraulics on stream temperature predictions, we develop a semi-analytical solution to a two-zone transient storage temperature model. This solution, unlike numerical techniques, allows us to look at both the influence of spatial variability and the individual contributions of the initial conditions, boundary condition, and surface heat flux terms throughout the study reach.

Governing Equations

Because stream temperature predictions are sensitive to the surface area to volume ratio, we use the temperature component of the two-zone temperature and solute

(TZTS) transient storage model that is physically constrained by widths and depths in the parameterization [*Neilson et al*., 2010a, 2010b]. While this formulation allows for more realistic model representation of fluxes at the air-water and water-streambed interfaces, it also allows for the direct incorporation of observed spatially variable hydraulic channel properties. Assuming flow is steady, exchange with storage zones is instantaneous, and the active stream channel and storage zones are rectangular, the governing equations are [*Neilson et al.*, 2010a]

$$\frac{\partial T}{\partial t} = D\frac{\partial^2 T}{\partial x^2} - \frac{Q}{YB_{tot}(1-\beta)}\frac{\partial T}{\partial x} + \frac{\alpha_{STS}Y_{STS}}{Y(1-\beta)\beta B_{tot}{}^2}(T_{STS} - T) + \frac{\alpha_{HTS}}{Y_{HTS}Y}(T_{HTS} - T) + \frac{\alpha_{sed}}{Y_{HTS}Y}\left(\frac{\rho_{sed}C_{p,sed}}{\rho C_p}\right)(T_{HTS} - T) + h(t,T), \quad (4\text{-}1)$$

$$\frac{dT_{STS}}{dt} = \frac{\alpha_{STS}}{(\beta B_{tot})^2}(T - T_{STS}) + \frac{\alpha_{sed}}{Y_{HTS}Y_{STS}}\left(\frac{\rho_{sed}C_{p,sed}}{\rho C_p}\right)(T_{STS,sed} - T_{STS}) + h_{STS}(t, T_{STS}), \quad (4\text{-}2)$$

$$\frac{dT_{HTS}}{dt} = \frac{\alpha_{HTS}}{Y_{HTS}{}^2}\left(\frac{\rho C_p}{\rho_{sed}C_{p,sed}}\right)(T - T_{HTS}) + \frac{\alpha_{sed}}{Y_{HTS}{}^2}(T - T_{HTS}) + \frac{\alpha_{sed}}{Y_{HTS}Y_{gr}}(T_{gr} - T_{HTS}), \quad (4\text{-}3)$$

$$\frac{dT_{STS,sed}}{dt} = \frac{\alpha_{sed}}{Y_{HTS}{}^2}(T_{STS} - T_{STS,sed}) + \frac{\alpha_{sed}}{Y_{HTS}Y_{gr}}(T_{gr} - T_{STS,sed}), \quad (4\text{-}4)$$

where equation (4-1) represents heat transport in the main portion of the stream (hereafter referred to as the main channel (MC)); the subscripts STS, HTS, sed, STS,sed, and gr represent surface transient storage, hyporheic transient storage, sediments below the MC, sediments below the STS zone, and the deeper ground layer, respectively; T is the water temperature (°C); Q is the volumetric flow rate ($m^3\ d^{-1}$); Y is the volume depth (m); B_{tot} is the total channel width (m); β is the STS width fraction of B_{tot}; D is the longitudinal dispersion coefficient ($m^2\ d^{-1}$); α_{STS} and α_{HTS} are the exchange rate coefficients between

the MC and the STS and HTS zones, respectively (m^2 d^{-1}); α_{sed} is the thermal diffusivity coefficient of the streambed (m^2 d^{-1}); ρ and ρ_{sed} are the densities of water and streambed material, respectively (kg m^{-3}); C_p and $C_{p,sed}$ are the heat capacities of water and streambed material, respectively (cal kg^{-1} $°C^{-1}$); x is distance (m); t is time (d); and $h(t, T)$ is the surface heat flux term (°C d^{-1}) (see *Neilson et al*. [2010a] for more details). The surface heat flux term more specifically acts as a forcing function on the temperature model,

$$h(t,T) = \frac{A_S}{V\rho C_p} J_{atm} = \frac{A_S}{V\rho C_p}\left[J_{sn} + J_{an} - \left(J_{br} + J_c + J_e\right)\right], \tag{4-5}$$

where A_S is the stream water surface area at the air-water interface (m^2), V is the water volume (m^3), and J_{atm} is the total surface heat flux energy available to warm or cool stream water (cal m^{-2} d^{-1}) due to net solar shortwave radiation (J_{sn}), net atmospheric longwave radiation (J_{an}), longwave back radiation from the water (J_{br}), conduction and convection (J_c), and evaporation and condensation (J_e) (see *Chapra* [1997] and Appendix F for formulations). Furthermore, J_{atm} is a function of T and measured meteorological conditions of J_{sn}, air temperature, relative humidity, and wind speed. Note that because the channel is assumed rectangular, the surface area to volume ratio that scales the influence of J_{atm} on water temperature is $A_S/V = 1/Y$.

Solutions

Building on previous work that only looked at MC heat transport processes [*Heavilin and Neilson*, 2012], we derived a Laplace-domain solution to equation (4-1) to isolate components that individually represent transport of the initial and boundary conditions, ground conduction, and surface heat fluxes. Using the Laplace transform to

solve equation (4-1) required the surface heat flux term (equation (4-5)) to be linearized. J_{br} and J_e are nonlinear with regard to water temperature and were linearized through a Taylor series expansion about the initial temperature, T_0. The linearized equation (4-5) simplifies to

$$h(t,T) \approx \frac{\phi(t)}{Y} T + \frac{\theta(t)}{Y}, \tag{4-6}$$

where $\phi(t)$ (m d^{-1}) varies only upon wind speed and $\theta(t)$ (°C m d^{-1}) varies upon wind speed, air temperature, relative humidity, and net solar shortwave radiation (see Appendix F for details regarding this linearization and for the expressions of $\phi(t)$ and $\theta(t)$). *Heavilin and Neilson* [2012] found that removing nonlinearities from the surface heat flux term did not significantly impact predictions and that assuming a constant wind speed was appropriate for the meteorological conditions used in this three day study period. Therefore, a constant wind speed is assumed for a less complicated solution technique.

Assuming initial and boundary conditions are

$$T(x,0) = T_0,$$

$$T_{STS}(x,0) = T_{STS,0},$$

$$T_{HTS}(x,0) = T_{HTS,0},$$

$$T_{STS,sed}(x,0) = T_{STS,sed,0}, \text{ and}$$

$$T(0,t) = T_{in}(t), \tag{4-7}$$

the resulting Laplace-domain solution to stream temperature (equation (4-1)), separated into terms that represent contributions of the boundary condition, surface fluxes, ground conduction, and initial conditions, is

$$\begin{aligned}
\overline{T}(x,s) = & \mathcal{L}\{T_{in}(t)\} f(x,s) && \textit{Boundary condition} \\
& + \mathcal{L}\{\theta(t)\}\left[\frac{1-f(x,s)}{\psi(s)Y}\right] \\
& + \mathcal{L}\{\theta_{STS}(t)\}\left[\frac{\kappa_1 - \kappa_1 f(x,s)}{\psi(s)\gamma_{STS}(s)Y_{STS}}\right] && \textit{Surface fluxes} \\
& + \mathcal{L}\{T_{gr}(t)\}\left[\frac{\gamma_{gr}(s) - \gamma_{gr}(s)\cdot f(x,s)}{\psi(s)}\right] && \textit{Ground conduction} \\
& + T_o\left[\frac{1-f(x,s)}{\psi(s)}\right] \\
& + T_{STS,o}\left[\frac{\kappa_1 - \kappa_1 f(x,s)}{\psi(s)\gamma_{STS}(s)}\right] \\
& + T_{HTS,o}\left[\frac{(\kappa_2 + \varepsilon\kappa_5) - (\kappa_2 + \varepsilon\kappa_5) f(x,s)}{\psi(s)\gamma_{HTS}(s)}\right] && \textit{Initial conditions} \\
& + T_{STS,sed,o}\left[\frac{\varepsilon\kappa_1\kappa_6 - \varepsilon\kappa_1\kappa_6\cdot f(x,s)}{\psi(s)\gamma_{STS}(s)\gamma_{STS,sed}(s)}\right], && (4\text{-}8)
\end{aligned}$$

where s is the Laplace variable, $f(x,s) = \exp\left(\frac{x}{2D}\left(U - \sqrt{U^2 + 4D\psi(s)}\right)\right)$,

$$\psi(s) = \left(s - \frac{\phi}{Y} + \kappa_1 + \kappa_2 + \varepsilon\kappa_5 - \frac{\kappa_1\kappa_3}{\gamma_{STS}(s)} - \frac{\kappa_2\kappa_4}{\varepsilon\gamma_{HTS}(s)} - \frac{\kappa_2\kappa_7}{\gamma_{HTS}(s)} - \frac{\kappa_4\kappa_5}{\gamma_{HTS}(s)} - \frac{\varepsilon\kappa_5\kappa_7}{\gamma_{HTS}(s)}\right),$$

$$U = \frac{Q}{B_{tot}(1-\beta)Y},\ \varepsilon = \frac{\rho_{sed}C_{p,sed}}{\rho C_p},\ \gamma_{STS}(s) = \left(s - \frac{\phi_{STS}}{Y_{STS}} + \kappa_3 + \varepsilon\kappa_6 - \frac{\varepsilon\kappa_6\kappa_7}{\gamma_{STS,sed}(s)}\right),$$

$$\gamma_{HTS}(s) = \left(s + \frac{\kappa_4}{\varepsilon} + \kappa_7 + \kappa_8\right),\ \gamma_{STS,sed}(s) = \left(s + \kappa_7 + \kappa_8\right),$$

$$\gamma_{gr}(s) = \left(\frac{\varepsilon\kappa_1\kappa_6\kappa_8}{\gamma_{STS}(s)\gamma_{STS,sed}(s)} + \frac{\kappa_2\kappa_8 + \varepsilon\kappa_5\kappa_8}{\gamma_{HTS}(s)}\right),\ \kappa_1 = \frac{\alpha_{STS}Y_{STS}}{Y(1-\beta)\beta B_{tot}^{\ 2}},\ \kappa_2 = \frac{\alpha_{HTS}}{Y_{HTS}Y},$$

$$\kappa_3 = \frac{\alpha_{STS}}{(\beta B_{tot})^2},\ \kappa_4 = \frac{\alpha_{HTS}}{Y_{HTS}^{\ 2}},\ \kappa_5 = \frac{\alpha_{sed}}{Y_{HTS}Y},\ \kappa_6 = \frac{\alpha_{sed}}{Y_{HTS}Y_{STS}},\ \kappa_7 = \frac{\alpha_{sed}}{Y_{HTS}^{\ 2}},\ \text{and}\ \kappa_8 = \frac{\alpha_{sed}}{Y_{HTS}Y_{gr}}.$$

To incorporate spatially variable information into the prediction, we apply a convolution of the Laplace-domain solution (equation (4-8)),

$$
\begin{aligned}
\overline{T}(X,s) = {} & \mathcal{L}\{T_{in}(t)\}\prod_{i=1}^{k} f_i(\Delta x,s) \\
& + \mathcal{L}\{\theta(t)\}\left[\sum_{i=1}^{k-1}\left(\frac{1-f_i(\Delta x,s)}{\psi_i(s)Y_i}\prod_{j=i+1}^{k} f_j(\Delta x,s)\right)+\frac{1-f_k(\Delta x,s)}{\psi_k(s)Y_k}\right] \\
& + \mathcal{L}\{\theta_{STS}(t)\}\left[\sum_{i=1}^{k-1}\left(\frac{\kappa_{1,i}-\kappa_{1,i}f_i(\Delta x,s)}{\psi_i(s)\gamma_{STS,i}(s)Y_{STS,i}}\prod_{j=i+1}^{k} f_j(\Delta x,s)\right)+\frac{\kappa_{1,k}-\kappa_{1,k}f_k(\Delta x,s)}{\psi_k(s)\gamma_{STS,k}(s)Y_{STS,k}}\right] \\
& + \mathcal{L}\{T_{gr}(t)\}\left[\sum_{i=1}^{k-1}\left(\frac{\gamma_{gr,i}-\gamma_{gr,i}f_i(\Delta x,s)}{\psi_i(s)}\prod_{j=i+1}^{k} f_j(\Delta x,s)\right)+\frac{\gamma_{gr,k}-\gamma_{gr,k}f_k(\Delta x,s)}{\psi_k(s)}\right] \\
& + T_o\left[\sum_{i=1}^{k-1}\left(\frac{1-f_i(\Delta x,s)}{\psi_i(s)}\prod_{j=i+1}^{k} f_j(\Delta x,s)\right)+\frac{1-f_k(\Delta x,s)}{\psi_k(s)}\right] \\
& + T_{STS,o}\left[\sum_{i=1}^{k-1}\left(\frac{\kappa_{1,i}-\kappa_{1,i}f_i(\Delta x,s)}{\psi_i(s)\gamma_{STS,i}}\prod_{j=i+1}^{k} f_j(\Delta x,s)\right)+\frac{\kappa_{1,k}-\kappa_{1,k}f_k(\Delta x,s)}{\psi_k(s)\gamma_{STS,k}}\right] \\
& + T_{HTS,o}\left[\sum_{i=1}^{k-1}\left(\frac{(\kappa_{2,i}+\varepsilon\kappa_{5,i})-(\kappa_{2,i}+\varepsilon\kappa_{5,i})f_i(\Delta x,s)}{\psi_i(s)\gamma_{HTS,i}}\prod_{j=i+1}^{k} f_j(\Delta x,s)\right)\right. \\
& \qquad \left. + \frac{(\kappa_{2,k}+\varepsilon\kappa_{5,k})-(\kappa_{2,k}+\varepsilon\kappa_{5,k})f_k(\Delta x,s)}{\psi_k(s)\gamma_{HTS,k}}\right] \\
& + T_{STS,sed,o}\left[\sum_{i=1}^{k-1}\left(\frac{\varepsilon\kappa_{1,i}\kappa_{6,i}-\varepsilon\kappa_{1,i}\kappa_{6,i}f_i(\Delta x,s)}{\psi_i(s)\gamma_{STS,i}\gamma_{STS,sed,i}}\prod_{j=i+1}^{k} f_j(\Delta x,s)\right)\right. \\
& \qquad \left. + \frac{\varepsilon\kappa_{1,k}\kappa_{6,k}-\varepsilon\kappa_{1,k}\kappa_{6,k}f_k(\Delta x,s)}{\psi_k(s)\gamma_{STS,k}\gamma_{STS,sed,k}}\right]
\end{aligned}
\quad , \text{(4-9)}
$$

where k is the number of reach segments in the model representation (i.e., the number of spatial observations), i is the reach segment index, $\Delta x = X/k$ is the corresponding reach segment length (m), and X is the total reach length (m). In this convolution, the upstream reach segment solution is used as the boundary condition for the next downstream reach segment solution and so on. Ground temperature, T_{gr}, is assumed constant. To arrive at $T(X, t)$, we invert term-by-term into the original state space. See Appendix F for the full derivation and inversion techniques. Because these solutions (equations (4-8) and (4-9)) are a summation of individual terms, the prediction is referred to as total temperature.

Spatial Data and Model Application Example

Stream Hydraulics Estimated From Observations

High-resolution channel widths were estimated from remotely sensed imagery to investigate the influence of spatially variable hydraulics on a temperature prediction. We build on previous work that produced a clipped raster of only water temperatures (banks, vegetation, and sandbars excluded) [*Bingham et al*., 2012] and use techniques presented in Chapter 3 to estimate channel widths every 1 meter over a 25-km study reach (see Figure G-1 in Appendix G for example). The channel properties related to hydraulics were estimated from these widths ($B_{tot}(x)$) including depth ($Y(x)$) and velocity ($U(x)$) through the use of momentum and continuity, and dispersion ($D(x)$) using *Fischer's* [1975] empirical formula (see Appendix C for details). *Heavilin and Neilson* [2012] found that for this particular case study, the contribution of the boundary condition in temperature predictions persists over many kilometers; therefore, the study reach was expanded beyond the 7-km portion of the imagery used in Chapter 3 to the entire available dataset of 25 km. Because the contribution of the boundary condition may still be present past 25 km, we extended our spatial test domain by repeating the dataset from the beginning to keep the data structure consistent with the direction of flow. Although flow is not anticipated to remain constant over space and any variation will alter hydraulic channel properties (e.g., depth and velocity), we assume that channel widths will not significantly change with any anticipated change in flow (i.e., rectangular channel). To focus only on the influence of spatially variable hydraulics using spatial data representing natural channel structure, flow is assumed steady and constant over space. Furthermore, the transient storage parameters, α_{STS}, α_{HTS}, Y_{STS}, Y_{HTS}, β, and Y_{gr} were set to

values within the narrowed bounds presented in *Bandaragoda and Neilson* [2011] and held constant over the entire study reach. Thermal diffusivity, density, and heat capacity of the streambed material were set to the values presented in *Bingham et al*. [2012]. See Appendix G for these parameter values and other site description information (e.g., streambed slope and flow). Note that the STS and HTS widths are βB_{tot} and $B_{tot}(1-\beta)$, respectively, and, therefore, change relative to B_{tot} throughout the study reach.

Because data structure may be important for capturing spatial variability in the model representation, we estimated the spatial scale where width estimates are considered spatially correlated. Estimating this scale consisted of quantifying the squared differences of pairs of width estimates at different separation distances. This produced the semivariance at each separation distance. The spatial scale where width estimates are considered spatially correlated was determined by where the semivariance approaches the overall variance in width estimates (see Appendix G for details). The spatial correlation in width estimates was determined through the 25-km study reach.

Importance of a Representative Reach-Average

Before looking into the full effects of spatial variability on total stream temperature, we examined the sensitivity of the prediction to an appropriate representation of reach-averaged hydraulics. Regardless of whether spatial detail is necessary in the model representation, this sensitivity illustrates the importance of an accurate reach-average channel width estimate (and corresponding depth and velocity) to an accurate prediction. Typically, an average width value is based on a limited number of spot measurements from the field. To mimic this approach, we extracted all width values that fall within one standard deviation of the mean of the observed distribution. This

range was selected because trained judgment within a field setting would avoid extremely wide or narrow locations. The hydraulic channel property estimates associated with these extracted widths were used to make corresponding temperature predictions through the 25-km study reach. To provide information regarding the sensitivity of stream temperature to accurate reach-averaged hydraulic estimates, we computed the absolute differences between predictions using the minimum width and those from the other observed widths.

Influence of Spatially Variable Hydraulics on Temperature Predictions

Next, we look at the influence of spatially variable hydraulics to determine whether spatial detail is necessary or if reach averages are sufficient for an accurate temperature prediction. Stream temperature predictions were made using the 1-m spatially variable hydraulic information with equation (4-9) (hereafter referred to as the spatially variable prediction) and compared these to the baseline prediction that used the average hydraulics for the entire 25-km study reach. We also investigated the influence of spatially variable hydraulics on the boundary condition and channel surface flux terms. These influences were quantified by computing the absolute differences between the spatially variable and baseline predictions. To further investigate these influences over space, we computed the overall ranges of these absolute differences through the study reach for the last diel cycle of the three day study period. These ranges are measures of how the temperature extremes (i.e., the maximum and minimum temperature values) change due to spatially variable hydraulics. Use of the last portion of the simulation period excludes contributions from the initial condition terms because they have completely decayed by the third day.

Because the surface area to volume ratio scales the contribution of the surface heat flux to stream temperature in the solution (equations (4-8) and (4-9)), we also computed the difference between the spatially variable and baseline surface area to volume ratios. Residence times through the study reach are related to these ratios. Therefore, the differences between spatially variable and baseline cumulative mean residence times were estimated. The cumulative mean residence times, which reflect the influence of all of the upstream spatial detail, were approximated from the first temporal moment of a residence time distribution that represents the transport of a conservative solute through the reach (see Chapter 3 and Appendix F for details). These ratio and residence time differences further show how varying hydraulics might impact the stream temperature extremes.

Finally, we test whether the contribution of the boundary condition plays a role in the interpretation of which terms are most sensitive to spatial variability and, therefore, cause temperature changes. Because total temperature is the sum of all solution terms (equation (4-9)), we compare the range in temperature differences (spatially variable – baseline) to the corresponding range in the channel surface flux term differences through the study reach where the contribution of the boundary condition ranges from 0-100%.

Reach Segmentation Necessary to Capture Spatial Variability

With an understanding of the extreme influences of spatial variability (1-m hydraulic information) on temperature and some indications of when spatial detail is necessary over a reach-average, it is important to determine how best to reasonably represent that variability or approximate the reach-average. We vary the number of reach segments (k), and, therefore, the reach segment lengths (Δx) representing the continuous

study reach and predict temperature for each k using the convolution solution (equation (4-9)). Following the reach segmentation procedure from Chapter 3, the value of k was varied from 1, 2, …, N and divided the total study reach length (X) into segments of equal length for each k ($\Delta x_k = X/k$). Here, N is the maximum possible number of reach segments and $X/N = 1$ m for this study. For each segmentation ($k = 1, 2, \ldots, N$), segment-wise average widths were estimated from the corresponding 1-m values that fall within each reach segment. This was repeated for depth, velocity, and the dispersion coefficient. At each number of reach segments k, the absolute differences between the spatially variable and baseline predictions were computed again. However, in this case, the spatially variable predictions are made with increasing segmentation and the corresponding hydraulic estimates ($k > 1$). The baseline prediction is unchanged, but now denoted by $k = 1$. Similarly, we computed the range between the minimum and maximum temperature differences for the last diel cycle for each k. The minimum number of reach segments where these ranges no longer change with further segmentation should provide the reach segment lengths necessary to represent the effects of spatially variable hydraulics.

Results

Stream Hydraulics Estimated From Observations

The widths estimates, $B_{tot}(x)$, within the 25-km study reach are highly variable and range from 3-44 m with a reach average of 15.8 m (Figure 4-1A). The 500-m moving average of these estimates shows sections that undergo abrupt change and sections that are more uniform. The distances where widths are spatially correlated change through the reach, ranging from 30-800 m (Figure 4-1B). These values are the separation distances

between observed widths where the semivariance is similar to the corresponding overall variance in the width estimates, which both change through the reach (see Appendix G for details). For example, when the entire 25-km width dataset is considered, width estimates less than 800 m apart (separation distance) are spatially correlated. From the $B_{tot}(x)$ estimates, $Y(x)$ ranges from 0.11-0.40 m with a reach average of 0.21 m, $U(x)$ ranges from 0.21-0.59 m s^{-1} with a reach average of 0.35 m s^{-1}, and $D(x)$ ranges from 1.7-152 m^2 s^{-1} with a reach average of 22 m^2 s^{-1}.

Importance of a Representative Reach-Average

The predicted stream temperature at the end of the study reach (25 km) is clearly sensitive to the representation of reach-averaged hydraulics (gray shading in Figure 4-2A

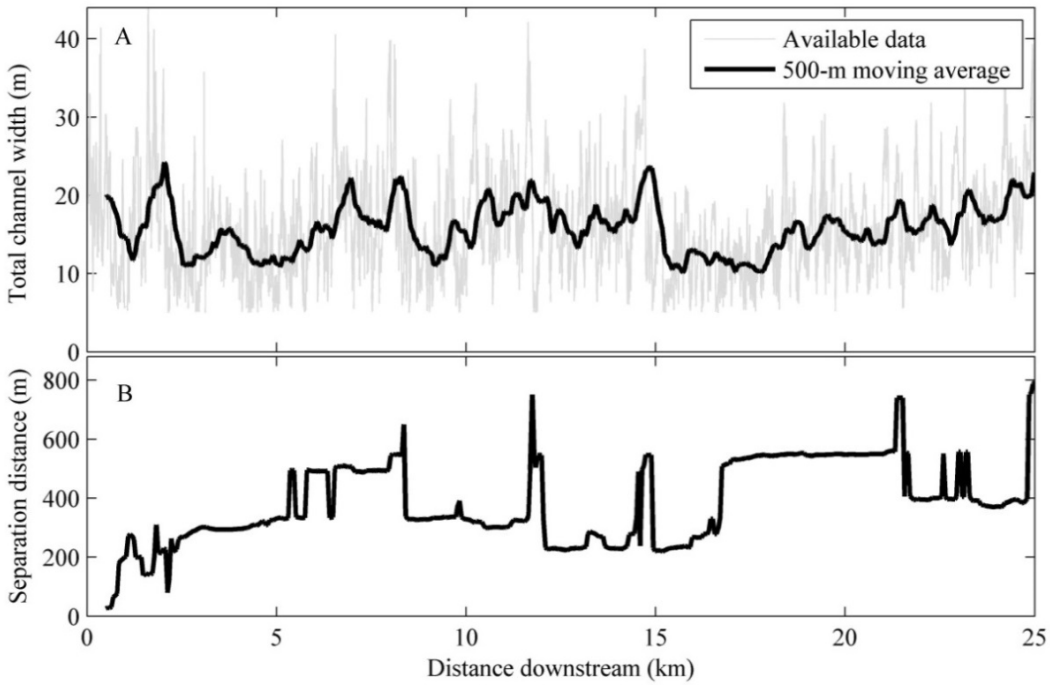

Figure 4-1. (A) Available channel width estimates observed every 1 meter from the thermal imagery covering 25 kilometers and the 500-m moving average to show the general width structure. (B) The separation distances relative to the boundary condition where observed widths are considered spatially correlated through the 25-km study reach. For example, if only the first 10 km of width observations are considered, these estimates are spatially correlated up to ~380 m apart (see Figure G-2 in Appendix G for details).

which represents the range of all predictions based on widths within one standard deviation of the observed width distribution mean). The absolute difference between the predictions can be larger than 4 ^{o}C (Figure 4-2B). This suggests that if a reach-average unrealistically represents a channel, the temperature extremes can be significantly overestimated or underestimated.

Influence of Spatially Variable Hydraulics on Temperature Predictions

The contribution of the boundary condition term persists past the available 25-km width dataset (Figure 4-3A). By repeating the dataset, the channel surface flux term

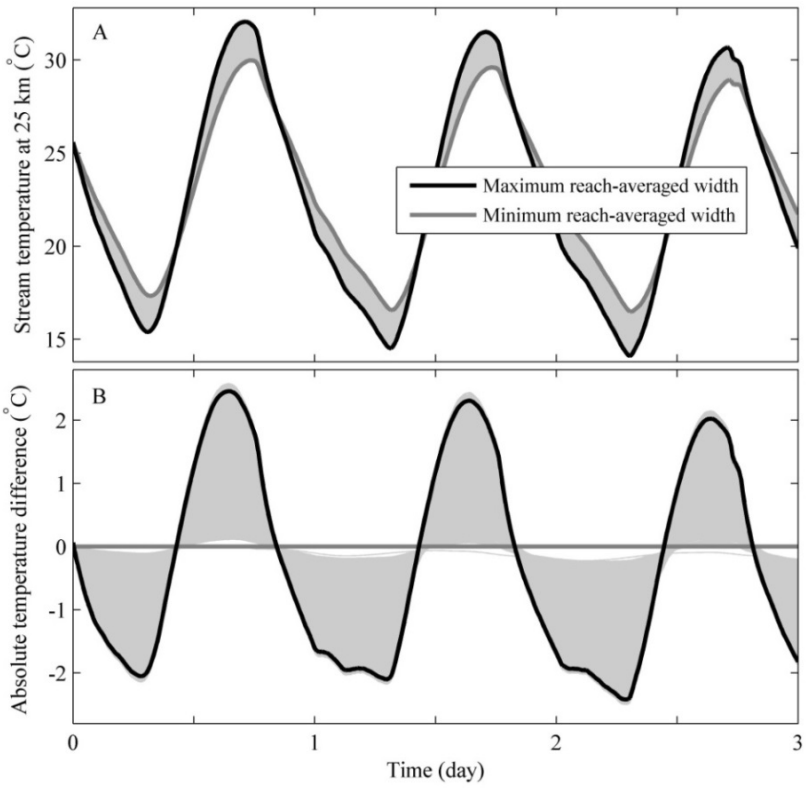

Figure 4-2. Channel width estimates (and the corresponding depth and velocity estimates) that fall within one standard deviation of the overall 25-km distribution were treated as possible reach-averaged values in each corresponding temperature prediction. (A) Stream temperature predictions based on these possible reach-averaged hydraulic channel properties. The gray shading represents all predictions using widths in between the minimum and maximum values. (B) The absolute differences between all temperature predictions and the prediction based on the minimum reach-averaged channel width.

eventually controls the majority of the total temperature prediction when the contribution of the boundary condition has fully decayed. At this point, the ground conduction and STS surface flux terms make up the remaining contributions (see Figure F-2 in Appendix F for these term and initial condition term contributions). Because these results are from the end of three day study period, the contributions of the initial condition terms have fully decayed over this amount of time. The spatially variable and baseline predictions had similar relative term contributions; therefore, these results are from the baseline prediction. Incorporating the 1-m spatially variable hydraulic information into the solution (equation (4-9)) did, however, change the total temperature extremes at 25 km (Figure 4-3B). The maximum temperature extreme increased by 1.0 °C (positive difference) and the minimum extreme decreased by 0.6 °C (negative difference) (Figure 4-3C). The channel surface flux term mostly increased and the boundary condition term decreased as a result of increasing spatial detail through segmentation.

The largest range of absolute temperature differences (spatially variable – baseline) was ~1.6 °C for the last diel cycle (Figure 4-3C), but is not consistent through the reach (Figure 4-4A). The lowest range is ~0.2 °C. However, for the hydraulic conditions of this reach, these ranges illustrate that the spatially variable prediction consistently has higher maxima and lower minima temperatures than the baseline prediction. An increase in each 1-m reach segment surface area to volume ratio generally coincides with a larger range of temperature differences; however, a decrease or increase in this ratio does not consistently relate to the range of differences (Figure 4-4B). The cumulative mean residence time integrates the influences of conditions upstream of a point in the study reach. Therefore, an average increase in residence times (positive

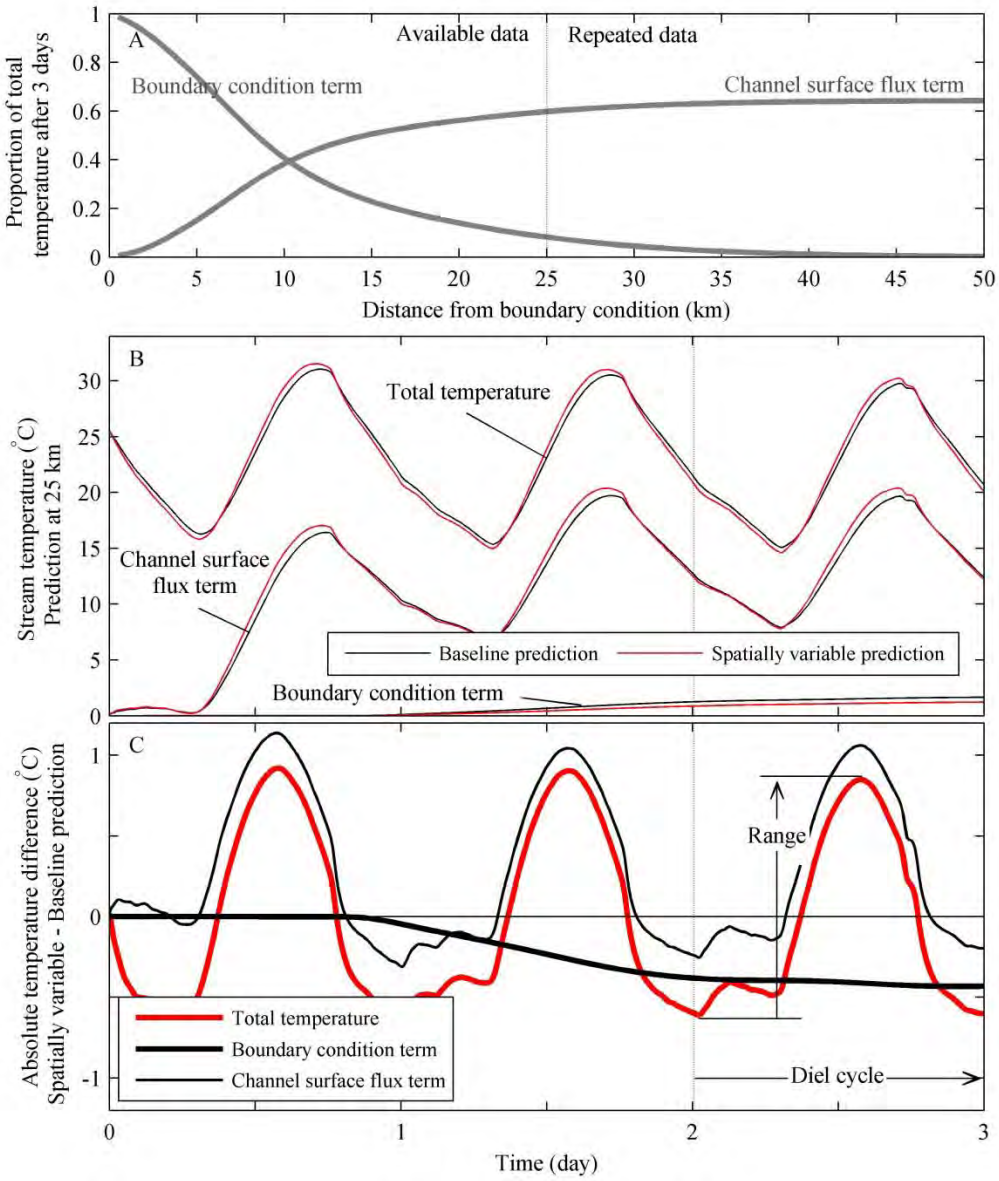

Figure 4-3. (A) The proportional contribution of the boundary condition and channel surface flux terms in equation (4-8) to the total temperature prediction at the end of three days over space. Because spatially variable hydraulic information did not substantially alter these contributions, we show the contributions estimated from the baseline (reach-averaged) prediction. See Figure F-2 in Appendix F for the contributions of the initial condition and surface transient storage surface flux terms. (B) The total temperature, boundary condition term, and channel surface flux term predictions at 25 km. The spatially variable prediction (equation (4-9)) incorporates the 1-m hydraulic channel property estimates. The baseline prediction uses the averages of those estimates. (C) The absolute difference between the spatially variable and baseline predictions of total temperature and the boundary condition and channel surface flux terms. To investigate these differences over space, the range between the minimum and maximum differences for the last diel cycle are compared. This range contains positive and negative components.

slope) coincides with the greatest range of temperature differences. Conversely, locations with decreasing residence times (negative slope) coincide with the smallest range of differences. This pattern suggests that total temperature is most sensitive to spatially variable hydraulics that translate into relatively large residence times.

When the boundary condition contribution is large (> 80%), the differences in the channel surface flux term does not coincide with the differences in total temperature

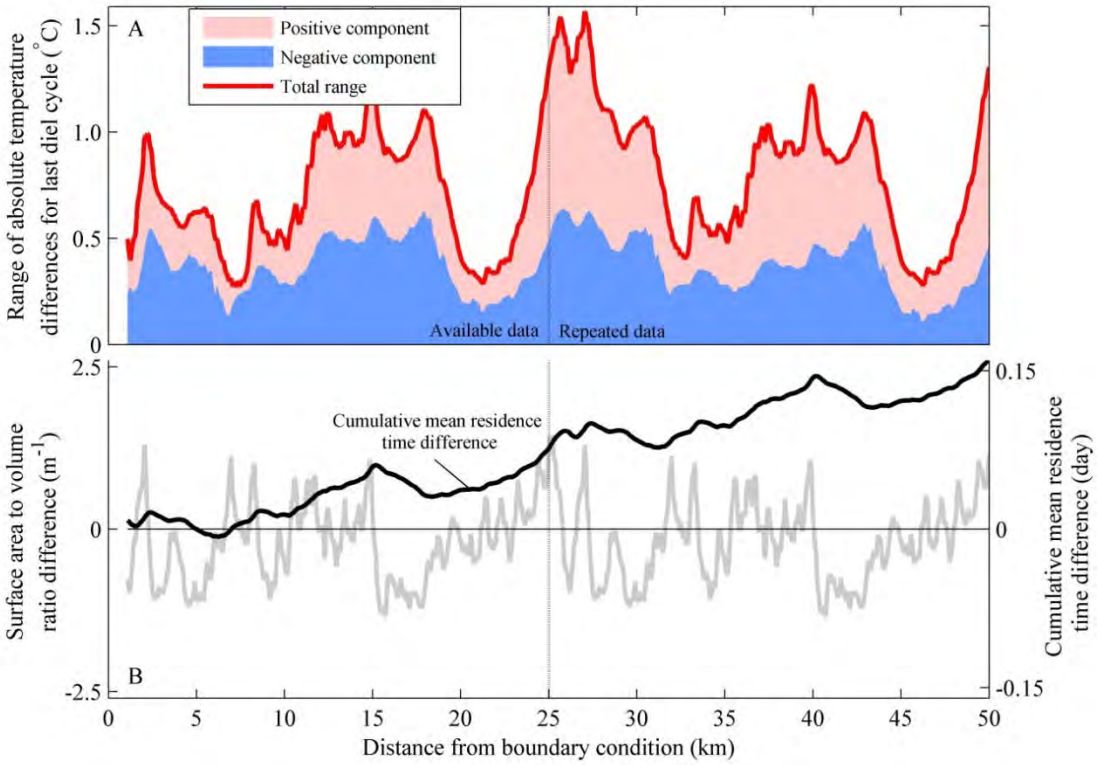

Figure 4-4. (A) The range of temperature differences for the last diel cycle between the spatially variable and baseline predictions through the study reach (25 km of available hydraulic data and repeated to 50 km). This range contains positive and negative components (see Figure 4-3C). For the hydraulic conditions of this study, the negative component represents a decrease in the temperature minima and the positive component represents an increase in the temperature maxima. (B) The difference between the spatially variable and baseline surface area to volume ratios and the cumulative mean residence time through the reach. The cumulative estimate incorporates all upstream spatial detail. Increasing (positive slope) residence times coincide with the highest ranges in temperature differences. Conversely, locations with decreasing residence times (negative slope) coincide with the smallest ranges. Incorporating spatial detail caused an overall increase in the cumulative mean residence time estimate. All lines shown here are the 500-m moving averages.

caused by incorporating spatially variable hydraulics (Figure 4-5). However, when the contribution decays to less than 80%, the difference in total temperature is clearly dictated by the difference surface flux term. Therefore, the sensitivity in total temperature due to spatial variability is caused primarily by the channel surface flux term. This agreement is even clearer once the boundary condition contribution decays to less than 10% (see Figure 4-3A).

Reach Segmentation Necessary to Capture Spatial Variability

Consistent with solute transport (see Chapter 3), the temperature prediction begins to converge with further segmentation (i.e., decreasing Δx) at scales coinciding with spatial correlation in the width observations (Figure 4-6). For example, considering the

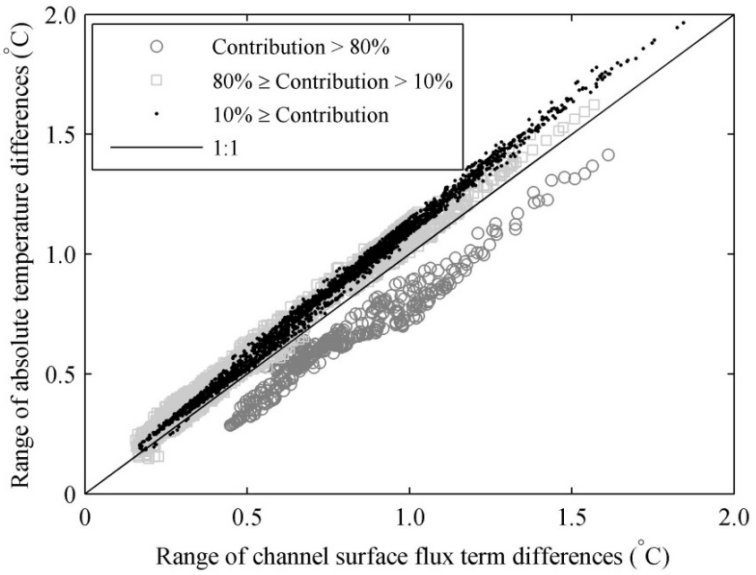

Figure 4-5. Range of absolute differences (spatially variable - baseline) for the last diel cycle of total temperature and the channel surface flux term. When the contribution of the boundary conditions is greater than 80%, it is not clear whether change in total temperature is driven by the channel surface flux term. However, once the contribution drops below 80%, the influence of spatial variability in the channel surface flux term starts to dictate the change in the total temperature. With less than 10% of the contribution remaining, the change in the total temperature amplitude is clearly due to the change in the channel surface flux term (also see Figure 4-3A).

prediction made at 25 km, width observations are spatially correlated at distances up to ~800 m (see Figure 4-1B). For Δx to be less than 800 m, $k = 30$ to represent the continuous 25 km reach. The difference in temperature predictions for $30 \geq k > 1$ from the baseline prediction ($k = 1$) appears random, but for $k > 30$, begins to overlay each other with further segmentation (Figure 4-6A). Consistently, the change in the negative

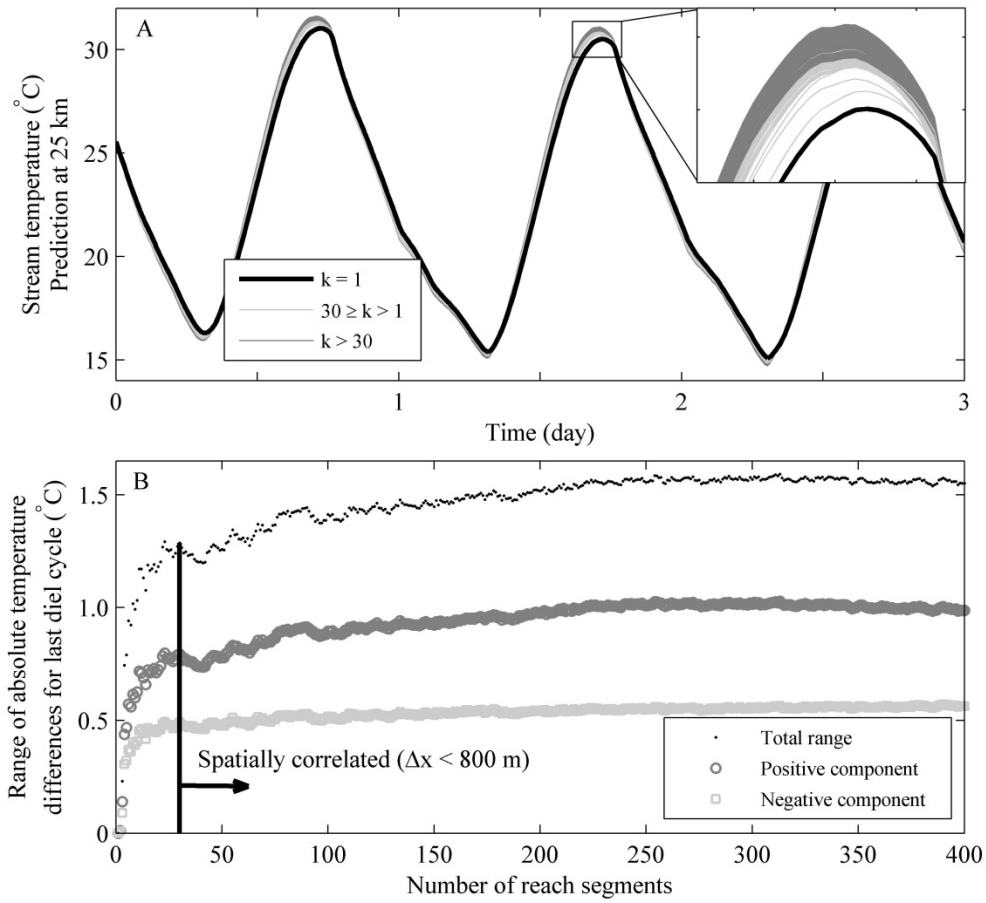

Figure 4-6. (A) Stream temperature prediction at the downstream end of the 25-km study reach for varying segmentation ($k = 1, 2, \ldots, N$). The black line is the prediction based on reach-averaged hydraulics (baseline prediction for $k = 1$) and the light grey lines represent the prediction for $30 \geq k > 1$. Note that at 25-km, the observed widths are spatially correlated at distances of ~800 m (see Figure 4-1B). Therefore, 30 segments results in a $\Delta x < 800$ m. The dark grey lines represent prediction for $k > 30$. (B) The range of absolute temperature differences for the last diel cycle for $k > 1$ from the baseline prediction ($k = 1$). This range contains positive and negative components that represent higher maxima and lower minima, respectively (see Figure 4-3C). The distance where widths are spatially correlated is shown by the vertical black line. The prediction begins to converge at reach segment lengths coinciding with spatial correlation.

and positive components of the range of absolute temperature differences begins to converge at reach segment lengths that coincide with distances of spatial correlation (vertical black line in Figure 4-6B). Therefore, this number of reach segments ($k > 30$) provides the segment lengths necessary ($\Delta x < 800$ m) to capture spatially variable hydraulics in the temperature prediction made at 25 km.

Discussion

Although some studies have indicated that the stream temperature amplitude is related to hydraulic characteristics [e.g., *Arscott et al.*, 2001; *Gu et al.*, 1998; *Gu and Li*, 2002], the influence of spatially variable hydraulics on a temperature model is still ambiguous. Typically, temperature model applications represent hydraulics with reach averages [e.g., *Bandaragoda and Neilson*, 2011; *Gooseff et al.*, 2005b; *Neilson et al.*, 2010a]. If a reach-average is used, we show that representing the true average is critical. For this study, misrepresentation can lead to over 4 °C uncertainty in the prediction (Figure 4-2). When spatial detail is considered, we found that temperature predictions are most sensitive to spatially variable hydraulics that translate into higher residence times (Figure 4-4). Consistent with *Gu et al*. [1998] and *Link et al*. [2013], we found that change in the amplitude was less sensitive under faster velocities and deeper depths that correspond with lower residence times. In all cases, we observed that incorporating spatial detail overall increased the estimate of residence time, which resulted in increased maximum and decreased minimum stream temperatures. For this study, the range of absolute temperature differences (change in the temperature extremes) varied from 0.2-1.6 °C (Figure 4-4). However, whether spatial detail is necessary or if a reach-average is

sufficient depends on modeling objectives. For example, spatial detail may be critical to predict stress on ecological health because the transition from optimal and lethal temperatures can be sensitive to only a few degrees [e.g., *Kelleher et al.*, 2012; *Poole and Berman*, 2001]. Conversely, if the objective is to provide coarser temporal (e.g., daily and seasonal trends) and spatial scale (e.g., network or watershed scales) stream temperatures, spatial detail may be less important [e.g., *Webb et al.*, 2008]. If spatial variability is considered, it can be represented by reach segmentation that produces segment lengths coinciding with spatial correlation in channel widths (Figure 4-6). This study does illustrate that high-resolution observations are necessary to determine the spatial correlation structure for a study reach.

In temperature modeling, the boundary condition is a continuous, dynamic signal influencing predictions and, therefore, can overwhelm the influences of the fluxes at the air-water and water-streambed interfaces (Figure 4-3). If these fluxes are overwhelmed, it is difficult to understand which components of the model are most sensitive to spatial variability. While numerical modeling techniques can provide the overall temperature response from the sum of individual fluxes [e.g., *Bandaragoda and Neilson*, 2011], they provide a limited understanding of the boundary condition influence [*Heavilin and Neilson*, 2012]. The semi-analytical solution developed in this chapter isolates the independent contributions of the boundary condition and fluxes at the stream interfaces (equations (4-8)-(4-9)). Because fluxes at the air-water interface are typically the dominant controls in streams, the term representing the surface fluxes was most sensitive to spatial variability. However, this could not be recognized at stream locations where the boundary condition contribution was large (Figure 4-5). Furthermore, knowledge of the

boundary condition contribution is necessary to ensure that data used for calibration techniques are collected at appropriate distances downstream [*Heavilin and Neilson*, 2012]. For example, if data are collected at a location where the boundary condition contribution is large, these data will be nearly analogous to the boundary condition and, therefore, not representative of fluxes controlling stream temperature. Although the individual terms and influence of spatial variability can be isolated, there are some limitations to this semi-analytical solution technique. While reasonable for the conditions of this study, a required assumption is that wind speed and flow are steady. If such dynamics are important, either a more complicated solution technique (i.e., through further transformations) similar to *Kumar et al*. [2010] or numerical modeling would be required.

Following an understanding of the influence of spatially variable hydraulics on stream temperature, other processes influenced by small scale hydraulic variations should be considered in future modeling work. For example, some factors relevant to stream temperature not addressed in our study include light attenuation, thermal stratification, and groundwater and tributary inputs. Similar to surface fluxes, light attenuation and thermal stratification depend on water depths and velocities [*Arscott et al.*, 2001; *Merck and Neilson*, 2012]. Additionally, changing discharge due to inputs (surface or subsurface) can also significantly affect stream temperature [*Briggs et al.*, 2012; *Cardenas et al.*, 2014; *Constantz*, 1998]. However, spatial estimates of hydraulic changes can be critical in capturing the associated stream temperature response. Even though bed conduction and STS and HTS processes were considered within this study, the influences on stream temperature are also known to be driven by the local hydraulic conditions

[*Sawyer et al.*, 2012; *Swanson and Cardenas*, 2010; *Wondzell*, 2011]. For example, although bed conduction influences are a function of streambed material, the water-streambed interface area is a function of local hydraulics (e.g., velocity, depth, and width) [*Hondzo and Stefan*, 1994]. Hyporheic exchange is also a function of streambed material, but is driven by the pressure gradients caused by stream hydraulics [e.g., *Buffington and Tonina*, 2009; *Stonedahl et al.*, 2010].

If the smaller scale influences of these processes are of interest in temperature modeling applications, estimating parameters that effectively represent these influences would require development of new approaches. Inverse tracer techniques are common for estimating parameters in transient storage modeling. The major concern with these techniques is that corresponding estimates often provide indirect physical meaning concerning transport processes [e.g., *Marion et al.*, 2003; *Ward et al.*, 2010]. Ambiguity in meaning casts doubt on the implications of transient storage on instream solute and temperature responses. Others have shown promise regarding better representation of STS and HTS residence times through scaling parameters with hydraulics [*Jackson et al.*, 2013; *O'Connor et al.*, 2010]. However, such scaling techniques have only been applied to solute transport and tested at small reach scales. The framework presented in this chapter to estimate and incorporate detailed hydraulic information may provide the foundation to expand parameter scaling techniques over longer reach scales and in the context of heat transfer. Applying such techniques along with other methods [e.g., *Bingham et al*., 2012] would allow for better parameter estimation. Furthermore, there are other approaches to narrow parameter space by using both temperature and solute as tracers in multiobjective calibration procedures [e.g., *Bandaragoda and Neilson*, 2011;

Naranjo et al., 2012]. Convolution approaches for semi-analytical solute (see Chapter 3) and temperature solutions may provide a way to incorporate necessary detail and apply such calibration techniques while avoiding numerical pitfalls such as instability or truncation error.

Through a combination of data collection, parameter estimation, and solution techniques, a more thorough understanding of key controlling factors for improving predictive capabilities of heat and solute transport is possible. This chapter provides a fundamental step to look at the influence of spatially variable hydraulics on a temperature prediction together with the individual contributions of different solution terms. This approach of incorporating spatial influences may allow for an enhanced understanding of the effects of proposed hydraulic alterations (e.g., stream restoration) on stream temperature because the model components most sensitive to such changes can be isolated.

Conclusions

In this chapter, we use a semi-analytical solution approach to determine the influence of spatially variable hydraulics on a temperature prediction while considering individual solution terms the represent transport of the initial conditions, boundary condition, channel surface fluxes, and ground conduction. In particular, with an understanding of the boundary condition contribution, it was clear that the term representing channel surface fluxes was most sensitive to spatially variable hydraulics. Hydraulic conditions that translated into larger residence times coincided with the largest effects on the temperature extremes. Conversely, the smallest influences on temperature

occurred under the lowest residence times. However, in all cases, incorporating spatial detail into the model increased the range between stream temperature extremes due to an overall increase in the residence time. Increased residence times reflected larger surface area to volume ratios of a wider, shallower channel. The importance of spatial variability depends on modeling objectives. If a reach-average is considered sufficient, we showed that misrepresenting this average can result in at least 4 °C uncertainty in the temperature prediction. If spatial detail is considered, the change in temperature was at most 1.6 °C due to spatially variable hydraulics. To incorporate spatially variable hydraulics into the model representation, only the number of reach segments that capture the spatial correlation in width estimates is necessary. With this approach, it is possible to determine whether spatial detail related to stream hydraulics is important to support accurate temperature predictions and how best to represent that detail.

CHAPTER 5

CONCLUSIONS

The common goal in transient storage model applications is to represent important solute and heat transport processes. Because these processes are heterogeneous and difficult to measure in stream systems, there is a need to assess and improve the representativeness of such models. Through the development and use of semi-analytical solutions, this dissertation examines how the parameters and model components represent a stream system and how best to establish reach segment lengths that capture the variability in hydraulics (as defined by the channel width, depth, and velocity) in the one-dimensional model representation. This work advances ways to ultimately better represent stream systems with transient storage models and improve solute and temperature predictions over long reach scales. This dissertation specifically provides an efficient parameter sensitivity analysis method (Chapter 2), an approach to capture variable hydraulics in solute predictions (Chapter 3), and a solution to isolate individual model terms and capture variable hydraulics in temperature predictions (Chapter 4).

In Chapter 2, the moment solutions combined with a fuzzy number sensitivity analysis were sufficient to determine the relative influence of each storage parameter. This is an efficient approach because model simulations are not required and fuzzy numbers provide a way to represent parameter uncertainty with limited prior knowledge. By holding the hydraulics constant, representing storage volumes was critical for accurate predictions. This sensitivity analysis method can also be used to determine whether a one-zone representation of transient storage is sufficient or if two zones are warranted.

It is well known that hydraulic conditions influence transient storage residence times. While other studies have inferred the effects of spatially variable hydraulics (e.g., longitudinal mean velocity) on solute transport modeling, Chapter 3 illustrated the smallest reach scales necessary to capture the effects of this variability on predictions. Starting with distributions of channel properties related to stream hydraulics (width, depth, velocity, and dispersion) derived from high-resolution imagery, changes in predictions were found to diminish at segment lengths equivalent to distances where channel properties were spatially correlated. Changes in the moment estimates also began to diminish at the same segment lengths. However, it is currently unclear if data structure and spatial correlation will always correspond to the same reach scales necessary for transient storage modeling.

In Chapter 4, the influence of spatially variable hydraulics on a temperature prediction was determined while considering individual solution terms that represent contributions of the initial conditions, boundary condition, channel surface fluxes, and ground conduction. With an understanding of the boundary condition contribution, it was clear that the term representing channel surface fluxes was most sensitive to spatially variable hydraulics. Hydraulic conditions that translated into larger residence times coincided with the largest effects on the temperature extremes. Conversely, the smallest influences on temperature occurred under the lowest residence times. However, incorporating spatial detail into the model caused an increase in range between temperature extremse due to an overall increase in the residence time. Consistent with solute transport, changes in stream temperature predictions were found to diminish at segment lengths equivalent to scales of spatial correlation.

CHAPTER 6

ENGINEERING SIGNIFICANCE

An understanding of how streams function in regards to the fate and transport of solutes and heat is necessary to inform policy and management of water resources. While field-based observations are critical in building this understanding, models are required to link together the mechanisms that theoretically represent the overall function. Therefore, through both data collection and modeling techniques, predicting how stream ecology and water quality will respond to change (e.g., restoration, pollutant loading, climate change, or water diversions) is potentially possible. However, common among all stream model applications, appropriately representing the dominant mechanisms is difficult primarily due to the inherent heterogeneity and dynamic nature of streams. Specific to transient storage models that are widely used to make reach scale predictions of one-dimensional solute and heat transport, it is still unclear whether retention processes should be represented by one or two storage zones. Although recent research has suggested that more realistic representation of these processes may be possible with more hydraulic information (e.g., measurements of stream depth and velocity), the role of spatially variable hydraulics in reach scale predictions was uncertain. For example, prior to this dissertation, it was not well understood how best to establish reach segments lengths in the model representation that capture the effects of that variability.

Through the development of semi-analytical solutions to transient storage models, this dissertation advances stream research by illustrating when a more complicated two-zone representation might be warranted. Furthermore, it shows when spatially variable hydraulic information may be important to consider and how to best represent that

information in the one-dimensional model. For example, spatially variable hydraulics that translate into lower stream residence times may significantly impact a temperature prediction. While the temperature solution allows for isolating the effects of spatial variability, is also allows for the isolation of the model components most sensitive to such variability. Therefore, use of this solution can provide an enhanced understanding of the effects of proposed hydraulic alterations (e.g., stream restoration) to stream temperature. This dissertation also provides information to incorporate the effects of spatially variable hydraulics into a transient storage model with the fewest measurements possible. For example, while reach segment lengths that capture spatial correlation are necessary to represent variability, only a very coarse number of segments are required to capture that correlation.

Although there are many other types of variability potentially important to consider in transient storage modeling that may require more detailed surface and subsurface two or three-dimensional modeling approaches, this dissertation provides a step towards improving the representation of stream function by incorporating longitudinally variable hydraulics over long reach scales. By appropriately accounting for some of the complexities in stream systems and reducing parameter uncertainty, water quality response to changes in channel geometry and flow can be more accurately anticipated at these spatial scales. This dissertation advances the understanding of what stream characteristics are most important to capture and how best to capture those characteristics in reach scale predictions of solute concentrations and stream temperature. These advancements allow for future efforts that focus on processes that control water quality and ecological health.

CHAPTER 7

RECOMMENDATIONS FOR FUTURE RESEARCH

Significant advancements in how best to represent the fate and transport of solute and heat in streams are presented in this dissertation. In Chapter 2, hydraulics were held constant to isolate the sensitivity of transient storage parameters and determine whether the moment solutions were sufficient to represent that sensitivity. Because these moment solutions were sufficient, the next step would be to apply the moment solutions presented in Chapter 3 that account for spatial variability to this approach. By representing the effects of variable hydraulics with these solutions, better isolation of the sensitivity of storage parameters may be possible.

Building on Chapter 3, where the effects of longitudinal, spatially variable hydraulics (i.e., channel width, depth, and velocity) are captured in a solute prediction, the next step would require consideration of other variability relevant to transient storage (e.g., stream permeability and geomorphic features). This step may be necessary to better scale transient storage parameters with stream hydraulics over longer reach and network scales. Furthermore, additional information such as surface storage widths and sinuosity could be extracted from the imagery to also support these techniques. By looking at the amount of detail required to represent the hydraulics, it was recognized that incorporating more detail into the prediction increased the variance or spread of the solute prediction. Because this result has been observed by others (e.g., including detail at a network scale), it is recommended that more research be focused towards investigating the mechanisms that produce variance. Although a connection between spatial correlation in observations and convergence in the solution was identified, this approach needs to be applied to other

systems with different channel structure to test if this connection is consistent across systems. If there is consistency, this could potentially simplify methods to capture variability in modeling approaches.

Based on an understanding of the role of longitudinal, spatially variable hydraulics in temperature modeling presented in Chapter 4, other processes influenced by hydraulics should be considered in future research. For example, if these techniques are applied to stream systems with turbid water or very high residence time pools, light attenuation and thermal stratification may be important in the model representation. It is also recommended that this temperature modeling approach be applied under different flow conditions and to other stream systems with large groundwater inputs. By applying this approach to other systems and flows, a more general understanding of the role of hydraulics might be identified. For example, if working in a system where groundwater inputs control stream temperature or if the hydraulic conditions translate into low residence times, spatial considerations may be less important or negligible. Because incorporating spatial detail in this study increased the range between temperature extremes, it is important to test if this pattern occurs for different systems and flows.

While the solute and heat transport approaches should be considered in other stream systems, it is recommended to collect solute and temperature data at more locations throughout the study reach. Because others have used both temperature and solute data to successfully calibrate model parameters, collecting these data at more locations would build on this dissertation by testing which data may be necessary to identify transient storage parameters spatially. To research methods of scaling transient storage parameters with hydraulics over long reach scales, more locations of tracer

observations would be necessary to corroborate model predictions. Furthermore, while modeling approaches of solute and heat transport need to consider the simplest representation sufficient to capture dominant processes, there is a need to test whether one-dimensional representations of spatial variable hydraulics are appropriate simplifications. Therefore, it is recommended that three-dimensional solute and heat transport models coupled with hydraulic routing should be compared to these one-dimensional representations. This comparison would further inform the spatial detail necessary to capture the hydraulics in predictions of solute concentrations and stream temperature. To support a three-dimensional model, high-resolution spatial data would be required. With advancements in remote sensing and topographic surveying, such data are attainable.

REFERENCES

Aris, R. (1958), On the dispersion of linear kinematic waves, *Proc. Royal Soc. London. Series A, Mathematical and Physical Sci.*, *245*(1241), 268-277.

Arscott, D. B., K. Tockner, and J. V. Ward (2001), Thermal heterogeneity along a braided floodplain river (Tagliamento River, northeastern Italy), *Can. J. Fish. Aquat. Sci.*, *58*, 2359-2373.

Bandaragoda, C., and B. T. Neilson (2011), Increasing parameter certainty and data utility through multi-objective calibration of a spatially distributed temperature and solute model, *Hydrol. Earth Syst. Sci.*, *15*(5), 1547-1561.

Bencala, K. E., and R. A. Walters (1983), Simulation of solute transport in a mountain pool-and-riffle stream: A transient storage model, *Water Resour. Res.*, *19*(3), 718-724.

Bencala, K. E., M. N. Gooseff, and B. A. Kimball (2011), Rethinking hyporheic flow and transient storage to advance understanding of stream-catchment connections, *Water Resour. Res.*, *47*(3), W00H03.

Bingham, Q. G., B. T. Neilson, C. M. U. Neale, and M. B. Cardenas (2012), Application of high-resolution, remotely sensed data for transient storage modeling parameter estimation, *Water Resour. Res.*, *48*(8), W08520.

Boano, F., J. W. Harvey, A. Marion, A. I. Packman, R. Revelli, L. Ridolfi, and A. Wörman (2014), Hyporheic flow and transport processes: Mechanisms, models, and biogeochemical implications, *Rev. Geophysics*, 2012RG000417.

Briggs, M. A., M. N. Gooseff, C. D. Arp, and M. A. Baker (2009), A method for estimating surface transient storage parameters for streams with concurrent hyporheic storage, *Water Resour. Res.*, *45*(4), W00D27.

Briggs, M. A., M. N. Gooseff, B. J. Peterson, K. Morkeski, W. M. Wollheim, and C. S. Hopkinson (2010), Surface and hyporheic transient storage dynamics throughout a coastal stream network, *Water Resour. Res.*, *46*(6), W06516.

Briggs, M. A., L. K. Lautz, and J. M. McKenzie (2012), A comparison of fibre-optic distributed temperature sensing to traditional methods of evaluating groundwater inflow to streams, *Hydrol. Processes*, *26*(9), 1277-1290.

Buffington, J. M., and D. Tonina (2009), Hyporheic exchange in mountain rivers II: Effects of channel morphology on mechanics, scales, and rates of exchange, *Geography Compass*, *3*(3), 1038-1062.

Caissie, D., N. El-Jabi, and M. G. Satish (2001), Modelling of maximum daily water temperatures in a small stream using air temperatures, *J. Hydrol.*, *251*(1–2), 14-28.

Caissie, D. (2006), The thermal regime of rivers: A review, *Freshwater Biol.*, *51*(8), 1389-1406.

Cardenas, M. B., M. Doering, D. S. Rivas, C. Galdeano, B. T. Neilson, and C. T. Robinson (2014), Analysis of the temperature dynamics of a proglacial river using time-lapse thermal imaging and energy balance modeling, *J. Hydrol.*, *519, Part B*(0), 1963-1973.

Chapra, S. C. (1997), *Surface Water-Quality Modeling*, McGraw-Hill Companies, Inc., Boston, MA.

Cheong, T. S., and I. W. Seo (2003), Parameter estimation of the transient storage model by a routing method for river mixing processes, *Water Resour. Res.*, *39*(4), 1074.

Choi, J., J. W. Harvey, and M. H. Conklin (2000), Characterizing multiple timescales of stream and storage zone interaction that affect solute fate and transport in streams, *Water Resour. Res.*, *36*(6), 1511-1518.

Constantz, J. (1998), Interaction between stream temperature, streamflow, and groundwater exchanges in alpine streams, *Water Resour. Res.*, *34*(7), 1609-1615.

De Hoog, F. R., J. H. Knight, and A. N. Stokes (1982), An improved method for numerical inversion of Laplace transforms, *J. Sci. Stat. Comput.*, *3*(3), 357-366.

De Smedt, F. (2006), Analytical solutions for transport of decaying solutes in rivers with transient storage, *J. Hydrol.*, *330*(3–4), 672-680.

Edinger, J. E., D. W. Duttweiler, and J. C. Geyer (1968), The response of water temperatures to meteorological conditions, *Water Resour. Res.*, *4*(5), 1137-1143.

Fischer, H. B. (1975), Discussion of "Simple method for predicting dispersion in streams" by R.S. McQuivey and T.N. Keefer, *J. Environ. Eng. Div. Am. Soc. Civ. Eng.*, *101*(3), 453-455.

Gomez, J. D., J. L. Wilson, and M. B. Cardenas (2012), Residence time distributions in sinuosity-driven hyporheic zones and their biogeochemical effects, *Water Resour. Res.*, *48*(9), W09533.

Gooseff, M., K. Strzepek, and S. Chapra (2005a), Modeling the potential effects of climate change on water temperature downstream of a shallow reservoir, lower madison river, MT, *Climatic Change*, *68*(3), 331-353.

Gooseff, M. N., K. E. Bencala, D. T. Scott, R. L. Runkel, and D. M. McKnight (2005b), Sensitivity analysis of conservative and reactive stream transient storage models applied to field data from multiple-reach experiments, *Adv. Water Resour.*, *28*(5), 479-492.

Gooseff, M. N., R. O. Hall, and J. L. Tank (2007), Relating transient storage to channel complexity in streams of varying land use in Jackson Hole, Wyoming, *Water Resour. Res.*, *43*(1), W01417.

Gu, R., S. Montgomery, and T. A. Austin (1998), Quantifying the effects of stream discharge on summer river temperature, *Hydrol. Sciences J.*, *43*(6), 885-904.

Gu, R. R., and Y. Li (2002), River temperature sensitivity to hydraulic and meteorological parameters, *J. Environ. Manage.*, *66*(1), 43-56.

Gupta, A., and V. Cvetkovic (2000), Temporal moment analysis of tracer discharge in streams: Combined effect of physicochemical mass transfer and morphology, *Water Resour. Res.*, *36*(10), 2985-2997.

Hannah, D. M., I. A. Malcolm, C. Soulsby, and A. F. Youngson (2004), Heat exchanges and temperatures within a salmon spawning stream in the Cairngorms, Scotland: Seasonal and sub-seasonal dynamics, *River Res. Applications*, *20*(6), 635-652.

Hannah, D. M., I. A. Malcolm, C. Soulsby, and A. F. Youngson (2008), A comparison of forest and moorland stream microclimate, heat exchanges and thermal dynamics, *Hydrol. Processes*, *22*(7), 919-940.

Hanss, M. (2002), The transformation method for the simulation and analysis of systems with uncertain parameters, *Fuzzy Sets and Systems*, *130*(3), 277-289.

Hanss, M. (2005), *Applied Fuzzy Arithmetic: An Introduction with Engineering Applications*, Springer-Verlag, Berlin Heidelberg.

Hanss, M., and S. Turrin (2010), A fuzzy-based approach to comprehensive modeling and analysis of systems with epistemic uncertainties, *Structural Safety*, *32*(6), 433-441.

Harvey, J. W., and K. E. Bencala (1993), The effect of streambed topography on surface-subsurface water exchange in mountain catchments, *Water Resour. Res.*, *29*(1), 89-98.

Harvey, J. W., B. J. Wagner, and K. E. Bencala (1996), Evaluating the reliability of the stream tracer approach to characterize stream-subsurface water exchange, *Water Resour. Res.*, *32*(8), 2441-2451.

Harvey, J. W., and B. J. Wagner (2000), Quantifying hydrologic interactions between streams and their subsurface zones, in *Streams and Ground Waters*, edited by J. B. Jones and P. J. Mulholland, pp. 3-44, Academic Press, San Diego, CA.

Harvey, J. W., E. S. James, and J. T. Newlin (2005), Solute transport and storage mechanisms in wetlands of the Everglades, south Florida, *Water Resour. Res.*, *41*(5).

Hays, J. R. (1966), Mass transport phenomena in open channel flow, PhD dissertation, Department of Chemical Engineering, Vanderbilt University, Nashville, TN.

Heavilin, J. E., and B. T. Neilson (2012), An analytical solution to main channel heat transport with surface heat flux, *Adv. Water Resour.*, *47*(0), 67-75.

Herbert, L. R. (1995), Seepage study of the Virgin River from Ash Creek to Harrisburg Dome, Washington County, *106*, 8, *U.S. Geol. Surv. Tech. Publ.*, Utah.

Hester, E. T., and M. W. Doyle (2011), Human impacts to river temperature and their effects on biological processes: A quantitative synthesis, *JAWRA J. Am. Water Resour. Assoc.*, *47*(3), 571-587.

Hollenbeck, K. J. (1998), INVLAP.M: A Matlab function for numerical inversion of laplace transforms by the De Hoog Algorithm. [Available at http://www.isva.dtu.dk/staff/karl/invlap.htm.]

Hondzo, M., and H. G. Stefan (1994), Riverbed heat conduction prediction, *Water Resour. Res.*, *30*(5), 1503-1513.

Jackson, T. R., R. Haggerty, S. V. Apte, A. Coleman, and K. J. Drost (2012), Defining and measuring the mean residence time of lateral surface transient storage zones in small streams, *Water Resour. Res.*, *48*(10), W10501.

Jackson, T. R., R. Haggerty, S. V. Apte, and B. L. O'Connor (2013), A mean residence time relationship for lateral cavities in gravel-bed rivers and streams: Incorporating streambed roughness and cavity shape, *Water Resour. Res.*, *49*(6), 3642-3650.

Johnson, S. L. (2004), Factors influencing stream temperatures in small streams: Substrate effects and a shading experiment, *Can. J. Fish. Aquat. Sci.*, *61*(6), 913-923.

Kazezyılmaz-Alhan, C. M. (2008), Analytical solutions for contaminant transport in streams, *J. Hydrol.*, *348*(3–4), 524-534.

Kelleher, C., T. Wagener, M. Gooseff, B. McGlynn, K. McGuire, and L. Marshall (2012), Investigating controls on the thermal sensitivity of Pennsylvania streams, *Hydrol. Processes*, *26*(5), 771-785.

Kelleher, C., T. Wagener, B. McGlynn, A. S. Ward, M. N. Gooseff, and R. A. Payn (2013), Identifiability of transient storage model parameters along a mountain stream, *Water Resour. Res.*, *49*(9), 5290-5306.

Kumar, A., D. K. Jaiswal, and N. Kumar (2010), Analytical solutions to one-dimensional advection–diffusion equation with variable coefficients in semi-infinite media, *J. Hydrol.*, *380*(3–4), 330-337.

Leube, P. C., W. Nowak, and G. Schneider (2012), Temporal moments revisited: Why there is no better way for physically based model reduction in time, *Water Resour. Res.*, *48*(11), W11527.

Li, S., and X. Zhou (1997), Stochastic theory for irregular stream modeling. II: Solute transport, *J. Hydraul. Eng.*, *123*(7), 610-616.

Link, O., A. Huerta, A. Stehr, A. Monsalve, C. Meier, and M. Aguayo (2013), The solar-to-stream power ratio: A dimensionless number explaining diel fluctuations of temperature in mesoscale rivers, *River Res. Applications*, *29*(6), 792-803.

Loheide, S. P., and S. M. Gorelick (2006), Quantifying stream−aquifer interactions through the analysis of remotely sensed thermographic profiles and in situ temperature histories, *Environ. Sci. Technol.*, *40*(10), 3336-3341.

Marion, A., M. Zaramella, and A. Packman (2003), Parameter estimation of the transient storage model for stream–subsurface sxchange, *J. Environ. Eng.*, *129*(5), 456-463.

Merck, M. F., and B. T. Neilson (2012), Modelling in-pool temperature variability in a beaded arctic stream, *Hydrol. Processes*, *26*(25), 3921-3933.

Mosley, M. P. (1983), Variability of water temperatures in the braided Ashley and Rakaia rivers, *N. Z. J. Marine and Freshwater Res.*, *17*(3), 331-342.

Naranjo, R. C., R. G. Niswonger, M. Stone, C. Davis, and A. McKay (2012), The use of multiobjective calibration and regional sensitivity analysis in simulating hyporheic exchange, *Water Resour. Res.*, *48*(1), W01538.

Neilson, B. T., D. K. Stevens, S. C. Chapra, and C. Bandaragoda (2009), Data collection methodology for dynamic temperature model testing and corroboration, *Hydrol. Processes*, *23*(20), 2902-2914.

Neilson, B. T., S. C. Chapra, D. K. Stevens, and C. Bandaragoda (2010a), Two-zone transient storage modeling using temperature and solute data with multiobjective calibration: 1. Temperature, *Water Resour. Res.*, *46*(12), W12520.

Neilson, B. T., D. K. Stevens, S. C. Chapra, and C. Bandaragoda (2010b), Two-zone transient storage modeling using temperature and solute data with multiobjective calibration: 2. Temperature and solute, *Water Resour. Res.*, *46*(12), W12521.

O'Connor, B., M. Hondzo, and J. Harvey (2010), Predictive modeling of transient storage and nutrient uptake: Implications for stream restoration, *J. Hydraul. Eng.*, *136*(12), 1018-1032.

Poole, G. C., and C. H. Berman (2001), An ecological perspective on in-stream temperature: Natural heat dynamics and mechanisms of human-caused thermal degradation, *Environ. Manage.*, *27*(6), 787-802.

Riml, J., and A. Wörman (2011), Response functions for in-stream solute transport in river networks, *Water Resour. Res.*, *47*(6), W06502.

Runkel, R. L., and S. C. Chapra (1993), An efficient numerical solution of the transient storage equations for solute transport in small streams, *Water Resour. Res.*, *29*(1), 211-215.

Runkel, R. L., K. E. Bencala, R. E. Broshears, and S. C. Chapra (1996), Reactive solute transport in streams: 1. Development of an equilibrium-based model, *Water Resour. Res.*, *32*(2), 409-418.

Runkel, R. L. (1998), One dimensional transport with inflow and storage (OTIS): A solute transport model for streams and rivers edited by U.S. Geological Survey Water-Resources Investigation Report, pp. 98-4018, U.S. Geological Survey, Denver.

Runkel, R. L. (2002), A new metric for determining the importance of transient storage, *J. N. Am. Benthol. Soc.*, *21*(4), 529-543.

Runkel, R. L. (2007), Toward a transport-based analysis of nutrient spiraling and uptake in streams, *Limnol. and Oceanogr. Methods*, *5*, 50-62.

Saco, P. M., and P. Kumar (2002), Kinematic dispersion in stream networks 1. Coupling hydraulic and network geometry, *Water Resour. Res.*, *38*(11), 1244.

Salehin, M., A. I. Packman, and M. Paradis (2004), Hyporheic exchange with heterogeneous streambeds: Laboratory experiments and modeling, *Water Resour. Res.*, *40*(11), W11504.

Sawyer, A. H., M. Bayani Cardenas, and J. Buttles (2012), Hyporheic temperature dynamics and heat exchange near channel-spanning logs, *Water Resour. Res.*, *48*(1), W01529.

Schmid, B. (2004), Simplification in longitudinal transport modeling: Case of instantaneous slug releases, *J. Hydrol. Eng.*, *9*(4), 319-324.

Schmid, B. H. (2003), Temporal moments routing in streams and rivers with transient storage, *Adv. Water Resour.*, *26*(9), 1021-1027.

Schmid, B. H., I. Innocenti, and U. Sanfilippo (2010), Characterizing solute transport with transient storage across a range of flow rates: The evidence of repeated tracer experiments in Austrian and Italian streams, *Adv. Water Resour.*, *33*(11), 1340-1346.

Stefan, H. G., and E. B. Preud'homme (1993), Stream temperature estimation from air temperature 1, *JAWRA J. Am. Water Resour. Assoc.*, *29*(1), 27-45.

Stewardson, M. J., and T. A. McMahon (2002), A stochastic model of hydraulic variations within stream channels, *Water Resour. Res.*, *38*(1), 8-1-8-.

Stewart, R. J., W. M. Wollheim, M. N. Gooseff, M. A. Briggs, J. M. Jacobs, B. J. Peterson, and C. S. Hopkinson (2011), Separation of river network–scale nitrogen removal among the main channel and two transient storage compartments, *Water Resour. Res.*, *47*(10), W00J10.

Stonedahl, S. H., J. W. Harvey, A. Wörman, M. Salehin, and A. I. Packman (2010), A multiscale model for integrating hyporheic exchange from ripples to meanders, *Water Resour. Res.*, *46*(12), W12539.

Stonedahl, S. H., J. W. Harvey, J. Detty, A. Aubeneau, and A. I. Packman (2012), Physical controls and predictability of stream hyporheic flow evaluated with a multiscale model, *Water Resour. Res.*, *48*(10), W10513.

Stonedahl, S. H., J. W. Harvey, and A. I. Packman (2013), Interactions between hyporheic flow produced by stream meanders, bars, and dunes, *Water Resour. Res.*, *49*(9), 5450-5461.

Stream Solute Workshop (1990), Concepts and methods for assessing solute dynamics in stream ecosystems, *J. N. Am. Benthol. Soc.*, *9*(2), 95-119.

Swanson, T. E., and M. B. Cardenas (2010), Diel heat transport within the hyporheic zone of a pool–riffle–pool sequence of a losing stream and evaluation of models for fluid flux estimation using heat, *Limnol. and Oceanography*, *55*(4), 1741-1754.

Tang, Y., P. Reed, T. Wagener, and K. van Werkhoven (2007), Comparing sensitivity analysis methods to advance lumped watershed model identification and evaluation, *Hydrol. Earth Syst. Sci.*, *11*(2), 793-817.

Theurer, F. D., K. A. Voos, and W. J. Miller (1984), Instream water temperature model. Instream flow information paper: No. 16, *U.S. Fish and Wildlife Service*, *FWS/OBS-85/15*.

Tonina, D., and J. M. Buffington (2009), A three-dimensional model for analyzing the effects of salmon redds on hyporheic exchange and egg pocket habitat, *Can. J. Fish. Aquat. Sci*., *66*, 2157-2173.

Toran, L., J. E. Nyquist, A. C. Fang, R. J. Rya./n, and D. O. Rosenberry (2013), Observing lingering hyporheic storage using electrical resistivity: Variations around stream restoration structures, Crabby Creek, PA, *Hydrol. Processes*, *27*(10), 1411-1425.

Valocchi, A. J. (1990), Use of temporal moment analysis to study reactive solute transport in aggregated porous media, *Geoderma*, *46*(1–3), 233-247.

Wagner, B. J., and J. W. Harvey (1997), Experimental design for estimating parameters of rate-limited mass transfer: Analysis of stream tracer studies, *Water Resour. Res.*, *33*(7), 1731-1741.

Ward, A. S., M. N. Gooseff, and K. Singha (2010), Imaging hyporheic zone solute transport using electrical resistivity, *Hydrol. Processes*, *24*(7), 948-953.

Ward, A. S., M. Fitzgerald, M. N. Gooseff, T. J. Voltz, A. M. Binley, and K. Singha (2012), Hydrologic and geomorphic controls on hyporheic exchange during base flow recession in a headwater mountain stream, *Water Resour. Res.*, *48*(4), W04513.

Ward, A. S., R. A. Payn, M. N. Gooseff, B. L. McGlynn, K. E. Bencala, C. A. Kelleher, S. M. Wondzell, and T. Wagener (2013), Variations in surface water-ground water interactions along a headwater mountain stream: Comparisons between transient storage and water balance analyses, *Water Resour. Res.*, *49*(6), 3359-3374.

Ward, A. S., M. N. Gooseff, M. Fitzgerald, T. J. Voltz, and K. Singha (2014), Spatially distributed characterization of hyporheic solute transport during baseflow recession in a headwater mountain stream using electrical geophysical imaging, *J. Hydrol.*, *517*(0), 362-377.

Webb, B. W., and Y. Zhang (1997), Spatial and seasonal variability in the components of the river heat budget, *Hydrol. Processes*, *11*(1), 79-101.

Webb, B. W., D. M. Hannah, R. D. Moore, L. E. Brown, and F. Nobilis (2008), Recent advances in stream and river temperature research, *Hydrol. Processes*, *22*(7), 902-918.

Williams, R. J., and D. B. Boorman (2012), Modelling in-stream temperature and dissolved oxygen at sub-daily time steps: An application to the River Kennet, UK, *Science of the Total Environ.*, *423*(0), 104-110.

Wondzell, S. M., and F. J. Swanson (1999), Floods, channel change, and the hyporheic zone, *Water Resour. Res.*, *35*(2), 555-567.

Wondzell, S. M. (2006), Effect of morphology and discharge on hyporheic exchange flows in two small streams in the Cascade Mountains of Oregon, USA, *Hydrol. Processes*, *20*(2), 267-287.

Wondzell, S. M. (2011), The role of the hyporheic zone across stream networks, *Hydrol. Processes*, *25*(22), 3525-3532.

Wondzell, S. M., and M. N. Gooseff (2013), 9.13 Geomorphic controls on hyporheic exchange across scales: Watersheds to particles, in *Treatise on Geomorphology*, edited by J. F. Shroder, pp. 203-218, Academic Press, San Diego.

Wörman, A. (1998), Analytical solution and timescale for transport of reacting solutes in rivers and streams, *Water Resour. Res.*, *34*(10), 2703-2716.

Wörman, A. (2000), Comparison of models for transient storage of solutes in small streams, *Water Resour. Res.*, *36*(2), 455-468.

Wörman, A., A. I. Packman, H. Johansson, and K. Jonsson (2002), Effect of flow-induced exchange in hyporheic zones on longitudinal transport of solutes in streams and rivers, *Water Resour. Res.*, *38*(1), 2-1-2-15.

Zarnetske, J. P., M. N. Gooseff, T. R. Brosten, J. H. Bradford, J. P. McNamara, and W. B. Bowden (2007), Transient storage as a function of geomorphology, discharge, and permafrost active layer conditions in Arctic tundra streams, *Water Resour. Res.*, *43*(7), W07410.

APPENDICES

Appendix A
Derivation of Solute Transport and Temporal Moment Solutions

The initial concentrations are, $C(x,t=0) = C_{STS}(x,t=0) = C_{HTS}(x,t=0) = 0$, with a time-dependent concentration type (Dirichlet) upper boundary condition, $C(x=0,t) = g(t)$, and solutions are bounded, $C(x \to \infty, t) = 0.$ Taking the Laplace transform, $\mathcal{L}\{f(x,t)\} = \int_0^\infty e^{-st} f(x,t)dt$, we arrive at the ordinary differential equation in *s* (Laplace variable),

$$s\overline{C}(x,s) - C(x,0) = D\frac{d^2}{dx^2}\overline{C} - U\frac{d}{dx}\overline{C} + \kappa_1\left(\overline{C}_{STS} - \overline{C}\right) + \kappa_2\left(\overline{C}_{HTS} - \overline{C}\right), \qquad \text{(A-1)}$$

and similarly for the associated equations for the transient storage zones (equations (2-2) and (2-3)) yields

$$s\overline{C}_{STS}(x,s) - C_{STS}(x,0) = \kappa_3\left(\overline{C} - \overline{C}_{STS}\right), \qquad \text{(A-2)}$$

$$s\overline{C}_{HTS}(x,s) - C_{HTS}(x,0) = \kappa_4\left(\overline{C} - \overline{C}_{HTS}\right), \qquad \text{(A-3)}$$

where $\overline{C}(x,s) = \mathcal{L}\{C(x,t)\}$. Refer to Chapter 2 for κ_1, κ_2, κ_3, and κ_4. Rearranging equations (A-2) and (A-3) for $\overline{C}_{STS}$ and $\overline{C}_{HTS}$ in terms of $\overline{C}$ and applying the initial conditions (equation (2-4)) we have

$$\overline{C}_{STS} = \frac{\kappa_3}{(s+\kappa_3)}\overline{C}, \qquad \text{(A-4)}$$

$$\overline{C}_{HTS} = \frac{\kappa_4}{(s+\kappa_4)}\overline{C}. \qquad \text{(A-5)}$$

By substitution we arrive at a second-order, linear, homogeneous ordinary differential equation,

$$D\frac{d^2}{dx^2}\overline{C} - U\frac{d}{dx}\overline{C} - \psi(s)\overline{C} = 0, \qquad \text{(A-6)}$$

where $\psi(s) = \left(s + \kappa_1 + \kappa_2 - \frac{\kappa_1 \kappa_3}{(s+\kappa_3)} - \frac{\kappa_2 \kappa_4}{(s+\kappa_4)} \right)$. The general solution is

$$\overline{C} = ¢ \exp\left[\frac{x}{2D} \left(U - \sqrt{U^2 + 4D\psi(s)} \right) \right]. \tag{A-7}$$

Using the Laplace transformed boundary condition, $\overline{g}(s)$, to solve for $¢$, the solution to the solute component of the TZTS model (equation (2-1)) is

$$\overline{C} = \overline{g}(s) \exp\left[\frac{x}{2D} \left(U - \sqrt{U^2 + 4D\psi(s)} \right) \right]. \tag{A-8}$$

The governing equations to the 2-SZ model can be written as [*Choi et al*., 2000; *Briggs et al.*, 2009]

$$\frac{\partial C}{\partial t} = D \frac{\partial^2 C}{\partial x^2} - \frac{Q}{A} \frac{\partial C}{\partial x} + \alpha_{STS,2-SZ} (C_{STS} - C) + \alpha_{HTS,2-SZ} (C_{HTS} - C), \tag{A-9}$$

$$\frac{dC_{STS}}{dt} = \alpha_{STS,2-SZ} \frac{A}{A_{STS}} (C - C_{STS}), \tag{A-10}$$

$$\frac{dC_{HTS}}{dt} = \alpha_{HTS,2-SZ} \frac{A}{A_{HTS}} (C - C_{HTS}). \tag{A-11}$$

where $\alpha_{STS,2-SZ}$ is the exchange rate coefficient between the MC and the STS zone (T^{-1}); $\alpha_{HTS,2-SZ}$ is the exchange rate coefficient between the MC and HTS zone (T^{-1}); and A, A_{STS}, and A_{HTS} are the MC, STS, and HTS cross-sectional areas (L^2), respectively (see Figure A-1 for conceptual formulations of the 2-SZ and TZTS models).

By similar method, the solutions in the Laplace domain to the 2-SZ model are

$$\overline{C} = \overline{g}(s) \exp\left[\frac{x}{2D} \left(U - \sqrt{U^2 + 4D\phi(s)} \right) \right], \tag{A-12}$$

$$\overline{C}_{STS} = \frac{\eta_1}{(s+\eta_1)} \overline{C}, \tag{A-13}$$

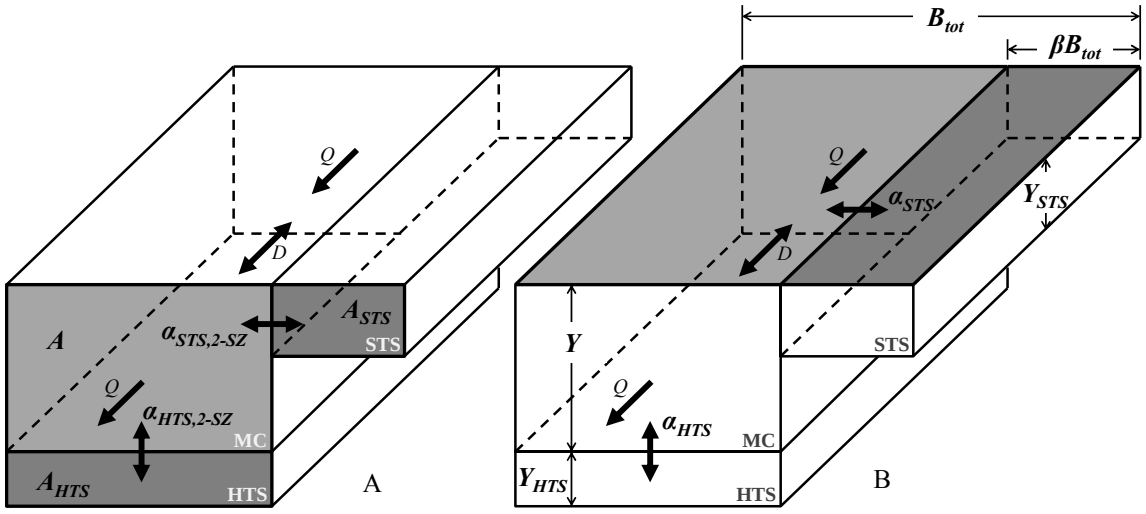

Figure A-1. Conceptual formulation of (A) the 2-SZ solute transport model based on cross-sectional areas of the MC, STS, and HTS zones (modified from *Briggs et al.* [2009]); and of (B) the TZTS transport model based on zonal widths and depths (modified from *Neilson et al.* [2010a, 2010b]). The gray shading highlights the conceptual differences between the 2-SZ and TZTS transport models.

$$\overline{C}_{HTS} = \frac{\eta_2}{(s+\eta_2)}\overline{C}\,, \tag{A-14}$$

where $\phi(s) = \left(s + \alpha_{STS,2-SZ} + \alpha_{HTS,2-SZ} - \frac{\alpha_{STS,2-SZ}\eta_1}{(s+\eta_1)} - \frac{\alpha_{HTS,2-SZ}\eta_2}{(s+\eta_2)} \right)$, $\eta_1 = \alpha_{STS,2-SZ}\frac{A}{A_{STS}}$,

and $\eta_2 = \alpha_{HTS,2-SZ}\frac{A}{A_{HTS}}$.

Because the 2-SZ and TZTS models are derived from the same concepts, we relate the parameters through equations (A-15) and (A-16) to provide a means for direct comparison. Assuming each zone is rectangular, the zonal cross-sectional areas perpendicular to main stream flow of the MC, STS, and HTS zones are

$$A = B_{tot}(1-\beta)Y = BY\,,$$

$$A_{STS} = \beta B_{tot} Y_{STS} = B_{STS} Y_{STS}\text{, and}$$

$$A_{HTS} = B_{tot}(1-\beta)Y_{HTS} = BY_{HTS}\,. \tag{A-15}$$

The relationships between the exchange coefficients are [*Neilson et al.*, 2010a]

$$\alpha_{STS,2-SZ} = \frac{\alpha_{STS} Y_{STS}}{B_{STS} YB},$$

and

$$\alpha_{HTS,2-SZ} = \frac{\alpha_{HTS}}{Y_{HTS} Y}. \tag{A-16}$$

The *k*th temporal moment can be expressed as higher order derivatives of the normalized solution in the Laplace domain evaluated at $s = 0$ [*Aris*, 1958],

$$n_k = (-1)^k \left. \frac{\partial^k \overline{c}(x,s)}{\partial s^k} \right|_{s=0} = E[t^k] = \int_0^\infty c(x,t) t^k dt, \tag{A-17}$$

where $\overline{c}(x,s) = \overline{C}(s,x)/n_{0,\overline{C}}$, $n_{0,\overline{C}} = \overline{C}(x,s=0) = \overline{g}(s=0)$ is the zeroth temporal moment of $\overline{C}(x,s)$ and area under the inflow solute breakthrough curve, $E[\ldots]$ denotes the expected value of random variable t representing residence times, $\mathcal{L}^1\{\overline{c}(x,s)\} = c(x,t)$, $c(x,t) = C(x,t)/\int_0^\infty C(x,t)dt$ is the solute residence time probability density function denoted by a lower case c, and $\int_0^\infty c(x,t)dt = 1$. This normalization is necessary because temporal moments are based on concepts from probability theory [e.g., *Schmid*, 2003; *Wörman*, 2000]. The only requirements to equation (A-17) are that the governing equations be linear with time invariant coefficients [e.g., *Leube et al.*, 2012].

The temporal moments were derived using equation (A-17) for the MC (equation (A-8)), STS (equation (A-4)), and HTS (equation (A-5)) solutions normalized by $n_{0,\overline{C}}$ to ultimately arrive at the closed form solutions of the mean, μ_t (T), variance, σ_t^2 (T^2), third central moment, S_t (T^3), and fourth central moment, K_t (T^4). The mean is the

centroid of the solute residence time probability density function and provides an estimate of mean residence time from an Eulerian perspective. The variance describes the temporal spread of that distribution about the mean. The third and fourth central moments are related to the formal statistical definitions of skewness, S_t / σ_t^3 (dimensionless), and kurtosis, K_t / σ_t^4 (dimensionless), respectively. Skewness is a measure of symmetry about the mean where increasing values indicate decreasing symmetry and a heavier weighted tail (falling limb). Increasing values of kurtosis suggest an increasing tendency (probability) for extreme values from the mean.

The μ_t, σ_t^2, S_t, and K_t were derived as [e.g., *Riml and Wörman*, 2011; *Schmid*, 2003]

$$\mu_t = n_1, \tag{A-18}$$

$$\sigma_t^2 = m_2 = n_2 - n_1^2 = n_2 - \mu_t^2, \tag{A-19}$$

$$S_t = m_3 = n_3 - 3\left(n_2 - n_1^2\right)n_1 - n_1^3 = n_3 - 3\sigma_t^2\mu_t - \mu_t^3, \tag{A-20}$$

$$\begin{aligned} K_t = m_4 &= n_4 - 6\left(n_2 - n_1^2\right)n_1^2 - 4\left[n_3 - 3\left(n_2 - n_1^2\right)n_1 - n_1^3\right]\left(n_1\right) - n_1^4, \\ &= n_4 - 6\sigma_t^2\mu_t^2 - 4S_t\mu_t - \mu_t^4 \end{aligned} \tag{A-21}$$

where $m_k = E[(t-\mu_t)^k] = \int_0^\infty c(x,t)(t-\mu_t)^k\,dt$ is the *k*th temporal moment centered about the mean (i.e., central moment). To arrive at these central moments, we derive closed form solutions to the temporal moments.

The *zeroth temporal moments* (n_0) are unity due to the normalization,

$$n_0 = \bar{c}\big|_{s=0} = \bar{c}_{STS}\big|_{s=0} = \bar{c}_{HTS}\big|_{s=0} = 1, \tag{A-22}$$

which are equivalent to the integral of a solute probability density function in the original state space, $n_0 = \int_0^\infty c(x,t)t^0 dt = 1$. The *first temporal moments* (n_1) are

$$n_1 = n_1(x=0) + \frac{x}{U}\Psi, \tag{A-23}$$

$$n_{1,STS} = n_1 + \frac{1}{\kappa_3}, \tag{A-24}$$

$$n_{1,HTS} = n_1 + \frac{1}{\kappa_4}, \tag{A-25}$$

where $n_1(x=0)$ is the first temporal moment originating from the boundary condition and $\Psi = 1 + \frac{\kappa_1}{\kappa_3} + \frac{\kappa_2}{\kappa_4} = 1 + \frac{Y_{STS}B_{STS}}{YB} + \frac{Y_{HTS}}{Y}$. The *second temporal moments* (n_2) are

$$n_2 = \sigma_t^{\,2}(x=0) + 2\frac{x}{U}\left(\Theta + \frac{D}{U^2}\Psi^2\right) + n_1^{\,2}, \tag{A-26}$$

$$n_{2,STS} = n_2 + \frac{2}{\kappa_3}n_{1,STS}, \tag{A-27}$$

$$n_{2,HTS} = n_2 + \frac{2}{\kappa_4}n_{1,HTS}, \tag{A-28}$$

where $\sigma_t^{\,2}(x=0) = n_2(x=0) - [n_1(x=0)]^2$ is the variance originating from the boundary condition and $\Theta = \frac{\kappa_1}{\kappa_3^{\,2}} + \frac{\kappa_2}{\kappa_4^{\,2}} = \frac{Y_{STS}B_{STS}^{\,3}}{YB\alpha_{STS}} + \frac{Y_{HTS}^{\,3}}{Y\alpha_{HTS}}$. The *third temporal moments* (n_3) are

$$n_3 = S_t(x=0) + 6\frac{x}{U}\left(\Phi + \frac{2D}{U^2}\Theta\Psi + \frac{2D^2}{U^4}\Psi^3\right) + 3\left(n_2 - n_1^{\,2}\right)\left(n_1\right) + n_1^{\,3}, \tag{A-29}$$

$$n_{3,STS} = n_3 + \frac{3}{\kappa_3}n_{2,STS}, \tag{A-30}$$

$$n_{3,HTS} = n_3 + \frac{3}{\kappa_4} n_{2,HTS}, \tag{A-31}$$

where $S_t(x=0) = n_3(x=0) - 3n_1(x=0)\sigma_t^{\,2}(x=0) - \left[n_1(x=0)\right]^3$ is the third central moment originating from the boundary condition and

$\Phi = \frac{\kappa_1}{\kappa_3^{\,3}} + \frac{\kappa_2}{\kappa_4^{\,3}} = \frac{Y_{STS} B_{STS}^{\,5}}{YB\alpha_{STS}^{\,2}} + \frac{Y_{HTS}^{\,5}}{Y\alpha_{HTS}^{\,2}}$. The *fourth temporal moments* (n_4) are

$$\begin{aligned} n_4 = {} & K_t(x=0) + 2\frac{x}{U}\left(6\sigma_t^{\,2}(x=0)\Theta + 66\sigma_t^{\,2}(x=0)\frac{D}{U^2}\Psi^2\right) \\ & + \frac{x}{U}\left(24\Omega + \frac{24D\Theta^2 + 48D\Phi\Psi}{U^2} + \frac{144D^2}{U^4}\Theta\Psi^2 + \frac{120D^3}{U^6}\Psi^4\right), \\ & + \frac{x^2}{U^2}\left(12\Theta^2 + \frac{24D}{U^2}\Theta\Psi^2 + \frac{12D^2}{U^4}\Psi^4\right) \\ & + 6\left(n_2 - n_1^{\,2}\right)n_1^{\,2} + 4\left[n_3 - 3\left(n_2 - n_1^{\,2}\right)n_1 - n_1^{\,3}\right]n_1 + n_1^{\,4} \end{aligned} \tag{A-32}$$

$$n_{4,STS} = n_4 + \frac{4}{\kappa_3} n_{3,STS}, \tag{A-33}$$

$$n_{4,HTS} = n_4 + \frac{4}{\kappa_4} n_{3,HTS}, \tag{A-34}$$

where $K_t(x=0) = n_4(x=0) - 6\sigma_t^{\,2}(x=0)\left[n_1(x=0)\right]^2 - 4S_t(x=0)n_1(x=0) - \left[n_1(x=0)\right]^4$ is the fourth central moment originating from the boundary condition and

$\Omega = \frac{\kappa_1}{\kappa_3^{\,4}} + \frac{\kappa_2}{\kappa_4^{\,4}} = \frac{Y_{STS} B_{STS}^{\,7}}{YB\alpha_{STS}^{\,3}} + \frac{Y_{HTS}^{\,7}}{Y\alpha_{HTS}^{\,3}}$.

Appendix B
Constraints and Model Parameter Ranges for Sensitivity Analyses

Choi et al. [2000] describe solute residence time in a transient storage compartment relative to the main channel (MC) by

$$t_s = \frac{A_S}{\alpha A}, \tag{B-1}$$

where A_S is the cross-sectional area of a storage compartment (m^2), α is the first-order exchange coefficient (s^{-1}), A is the cross-sectional area of the MC stream flow (m^2), and the subscript S designates a storage zone. This residence time has two components referred to as the storage capacity, A_S, and the exchange flux [*Harvey et al.*, 1996],

$$q_s = \alpha A. \tag{B-2}$$

Using these relationships for a typical stream system, *Choi et al.* discriminated between cases when a one-zone transient storage model (TSM) effectively characterizes dominant storage processes and when a two-zone TSM is the more suitable option. This was done by examining the residence time (R_t) and exchange flux ratios (R_q) between the two storage compartments. We use a similar approach to highlight the utility of the closed form moment solutions to estimate the relative influence of parameters contributing to transient storage.

While *Choi et al.* based their analysis on two arbitrary storage compartments, we start by designating these as STS and HTS zones because a distinction between STS and HTS parameters is important as evidenced by differing fates of solutes [*Stewart et al.*, 2011] and heat in each zone [*Neilson et al.*, 2010a, 2010b]. Residence times of the STS and HTS zones are estimated using the TZTS model parameterization,

$$t_{STS} = \frac{B_{STS}{}^2}{\alpha_{STS}}, \tag{B-3}$$

$$t_{HTS} = \frac{Y_{HTS}^{\ 2}}{\alpha_{HTS}}. \tag{B-4}$$

The corresponding STS and HTS exchange fluxes are

$$q_{STS} = \alpha_{STS} \frac{Y_{STS}}{B_{STS}}, \tag{B-5}$$

$$q_{HTS} = \alpha_{HTS} \frac{B}{Y_{HTS}}. \tag{B-6}$$

Residence time ratios are calculated to indicate the relative proportion of STS and HTS influences. When $t_{HTS} \le t_{STS}$ and $q_{STS} \le q_{HTS}$, the residence time ratio is defined by equation (2-9) in Chapter 2. Conversely, when $t_{HTS} > t_{STS}$ and $q_{STS} > q_{HTS}$, the residence time ratio is defined,

$$R_{t_{HTS}} = \frac{t_{HTS}}{t_{STS}} = \frac{Y_{HTS}B}{B_{STS}Y_{STS}} \frac{q_{STS}}{q_{HTS}} = \frac{Y_{HTS}B}{B_{STS}Y_{STS}} R_{q_{HTS}}. \tag{B-7}$$

where $R_{q_{HTS}}$ is the associated exchange flux ratio.

Choi et al. [2000] observed that parameter combinations resulting in $R_t < 5$ implied comparable exchange fluxes and storage capacities between the two storage zones. These conditions are considered *additive* (Case I). They further observed that a resulting $R_t > 5$ implied either *competing* (Case II) or *dominant* (Case III) storage conditions. Under competing conditions between the two zones, the proportions of exchange flux and storage capacity driving transient storage were essentially reciprocals of one another. Under dominant conditions, transient storage was driven by both the exchange flux and storage capacity of a single zone. Based on these findings, we can

generalize STS and HTS conditions for each case. For storage conditions where $t_{HTS} \le t_{STS}$ (equation (2-9)), these generalizations are:

1) Case I (*additive*) as $R_{t_{STS}} < 5$,

2) Case II (*competitive*) as $R_{t_{STS}} > 5$, $q_{STS} << q_{HTS}$, and $Y_{HTS}B >> B_{STS}Y_{STS}$, and

3) Case III (*dominant*) as $R_{t_{STS}} > 5$, $q_{STS} << q_{HTS}$, and $Y_{HTS}B << B_{STS}Y_{STS}$.

For storage conditions where $t_{HTS} > t_{STS}$ (equation (B-7)), these generalizations are:

1) Case I (*additive*) as $R_{t_{HTS}} < 5$,

2) Case II (*competitive*) as $R_{t_{HTS}} > 5$, $q_{STS} >> q_{HTS}$, and $Y_{HTS}B << B_{STS}Y_{STS}$, and

3) Case III (*dominant*) as $R_{t_{HTS}} > 5$, $q_{STS} >> q_{HTS}$, and $Y_{HTS}B >> B_{STS}Y_{STS}$.

Although both Case II and III correspond to conditions where the residence time ratio is greater than 5, *Choi et al.* found that for all parameter combinations satisfying Case II, the proportionality of the exchange flux ratio to the residence time ratio was greater than 3/5.

To provide an example of the utility of central moment solutions to reflect the relative influence of each storage parameter on the transport solution, we use the constraints established for Case I and set arbitrary constraints for a reasonable illustration of Case III. For $t_{HTS} \le t_{STS}$, these Case III constraints are:

1) $R_{t_{STS}} > 50$, and

2) $\frac{R_{q_{STS}}}{R_{t_{STS}}} < \frac{3}{5}$.

For $t_{HTS} > t_{STS}$, these Case III constraints are:

1) $R_{t_{HTS}} > 50$, and

2) $\frac{R_{q_{HTS}}}{R_{t_{HTS}}} < \frac{3}{5}$.

We establish TZTS model storage parameter ranges that are comparable to *Choi et al*. [2000] and use these ranges as bounds in Latin hypercube sampling. Because there can be many combinations of widths and depths that correspond to the same cross-sectional area (Figure B-1A), we start with assuming the MC width, *B*, is 2 m. We base this on values presented in *Wagner and Harvey* [1997] for a typical stream similar to *Choi et al*. Assuming that both $\alpha_{STS,2-SZ}$ and $\alpha_{HTS,2-SZ}$ and both A_{STS} and A_{HTS} of the 2-SZ model have the same ranges of 1E-5 to 1E-3 and 0.1 to 2.0, respectively, the ranges of the HTS depth and exchange coefficient are determined,

$$Y_{HTS} = \frac{A_{HTS}}{B} \text{ and } \alpha_{HTS} = \alpha_{HTS,2-SZ} Y_{HTS} Y . \quad \text{(B-8)}$$

The total channel width is assumed less than 5 m [*Wagner and Harvey*, 1997] making maximum B_{STS} equal to 3 m. Based on this assumption, ranges of Y_{STS} that satisfy the two possible combinations of A_{STS} = 0.1 or 2.0 m^2 are established (Figure B-1B). This provides estimates of α_{STS} using equation (B-8) because the $\alpha_{STS,2-SZ}$ range is defined. With these overall parameter ranges and applying constraints for Case I and Case III, we arrive at the TZTS model storage parameter ranges that are related to the 2-SZ model storage parameters (Table B-1).

With these ranges (Table B-1), triangular fuzzy numbers are constructed to represent distributions of each storage parameter. Here, nine levels of membership (i.e.,

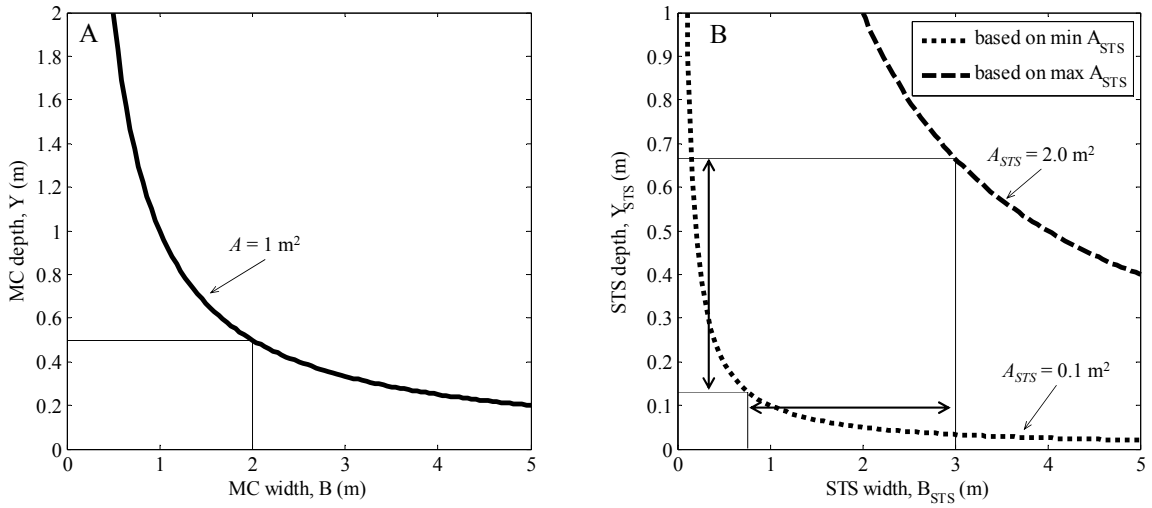

Figure B-1. (A) Combinations of main channel (MC) widths, B, and depths, Y, that equate to a cross-sectional area of 1 m^2. The B was set at an arbitrary 2 m that results in a MC depth of 0.5 m. (B) Combinations of surface transient storage (STS) widths, B_{STS}, and depths, Y_{STS}, that satisfy the STS cross-sectional area $0.1 < A_{STS} < 2.0$ m^2 and $B_{STS} < 3$ m. The maximum B_{STS} was set by assuming the total channel width does not exceed 5 m, which provides an estimate of maximum Y_{STS}. The minimum B_{STS} and Y_{STS} were set arbitrarily that satisfy a A_{STS} of 0.1 m^2. These bounds are used within Latin hypercube sampling to generate possible parameter combinations.

plausibility) are used. Figure B-2A shows an example of the parameter triangular fuzzy numbers used in Case I. With the general transformation method proposed by *Hanss* [2002; 2005], we arrive at relative influences of each parameter on the central moment solutions by essentially normalizing the resulting fuzzy numbers for the central moments by the parameter fuzzy numbers. An example of these resulting central moment fuzzy numbers is shown in Figure B-2B.

The 2-SZ model parameter ranges were derived from the TZTS parameter ranges (equations (A-15) and (A-16)) and were also used with the fuzzy number sensitivity analysis. Under both additive case conditions ($t_{HTS} \le t_{STS}$ and $t_{HTS} > t_{STS}$), each parameter has nearly equal influence on the σ_t^2, S_t, and K_t (Figures B-3A and B-3C). These results are attributed to comparable exchange fluxes and storage capacities between the

Table B-1. TZTS and 2-SZ parameter ranges comparable to values presented in *Choi et al.* [2000] for a typical stream used to estimate parameter ranges for cases where two storage zone processes are additive (Case I) and dominant (Case III). These cases are separated into conditions where either HTS residence time is greater than STS residence time ($t_{HTS} > t_{STS}$) or STS residence time is greater than HTS residence time ($t_{HTS} \leq t_{STS}$). These ranges are then used to construct fuzzy numbers for the sensitivity analysis.

	2-SZ and TZTS Parameter	Range and values from or comparable to *Choi et al.*	$t_{HTS} > t_{STS}$		$t_{HTS} \leq t_{STS}$	
			I Additive	III Dominant	I Additive	III Dominant
Fuzzy numbers	α_{STS} (m^2 s^{-1})	(5.9-450)E-5	(1.4-45)E-4	(7.1-41)E-4	(1.8-45)E-4	(2.9-42)E-4
	α_{HTS} (m^2 s^{-1})	(2.5-5000)E-7	(5.5-498)E-6	(5.2-26)E-6	(4.7-500)E-6	(1.1-4.9)E-4
	Y_{STS} (m)	0.13-0.67	0.13-0.67	0.19-0.41	0.15-0.67	0.32-0.67
	Y_{HTS} (m)	0.05-1.0	0.14-1.0	0.75-0.97	0.07-1.0	0.05-0.18
	B_{STS} (m)	0.77-3.0	0.77-3.0	0.79-1.4	0.77-3.0	1.4-3.0
	$\alpha_{STS,2\text{-}SZ}$ (s^{-1})	(1.0-100)E-5	(2.4-100)E-5	(1.8-14)E-4	(3.6-98)E-5	(6.6-94)E-5
	$\alpha_{HTS,2\text{-}SZ}$ (s^{-1})	(1.0-100)E-5	(7.9-99)E-5	(1.4-5.4)E-5	(1.3-10)E-4	(4.4-5.4)E-3
	A_{STS} (m^2)	0.1-2.0	0.1-1.99	0.15-0.70	0.12-1.99	0.58-1.89
	A_{HTS} (m^2)	0.1-2.0	0.28-2.0	1.50-1.94	0.14-1.99	0.11-0.34
Set Parameters	A (m^2)	1.0				
	Q (m^3 s^{-1})	0.08				
	D (m^2 s^{-1})	0.4				
	x (m)	150				
	B (m)	2.0				
	Y (m)	0.5				

STS and HTS zones. When exchange flux and storage capacity of a single zone drive transient storage, the cross-sectional area has the highest measure of sensitivity on the σ_t^2, S_t, and K_t (Figures B-3B and B-3D). These results of the dominant case examples are similar to those found by *Wagner and Harvey* [1997] where the storage capacity (represented by the cross-sectional area) of a one-zone TSM had the highest sensitivity on an instream solute prediction. These results on the moments are not consistent with the influence on the solute prediction.

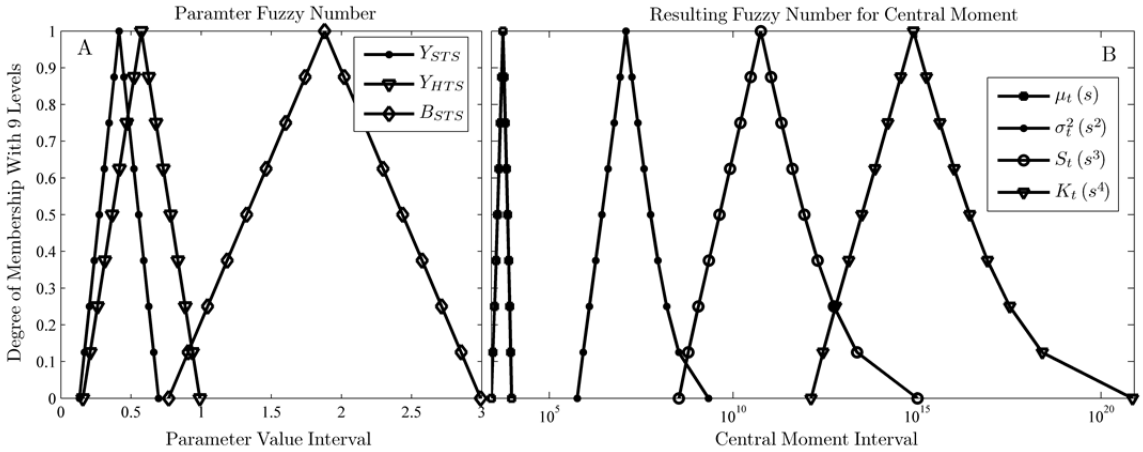

Figure B-2. (A) An example of triangular fuzzy numbers representing the TZTS storage parameters (Y_{STS}, Y_{HTS}, and B_{STS} in m) used in the *additive* case with nine levels of membership. Central tendency within these intervals is assumed. (B) An example of the resulting fuzzy numbers for the moment solutions (mean (μ_t), variance (σ_t^2), third central moment (S_t), and fourth central moment (K_t)).

Given a set of reasonable parameter combinations used to describe transient storage conditions in a stream system of interest, this fuzzy number approach can add clarity to the relative influence of each parameter on the central moment solutions and key parameters related to solute predictions. This also can help determine when to use a one-zone or two-zone TSM because additive or dominant storage conditions (such as those illustrated in Figures B-3 and 2-1) can rely on a one-zone approach while other circumstances will likely require a two-zone approach. Additionally, by comparing sensitivity results of two different two-zone TSM parameterizations, we can see that parameterization influences the importance of various parameters.

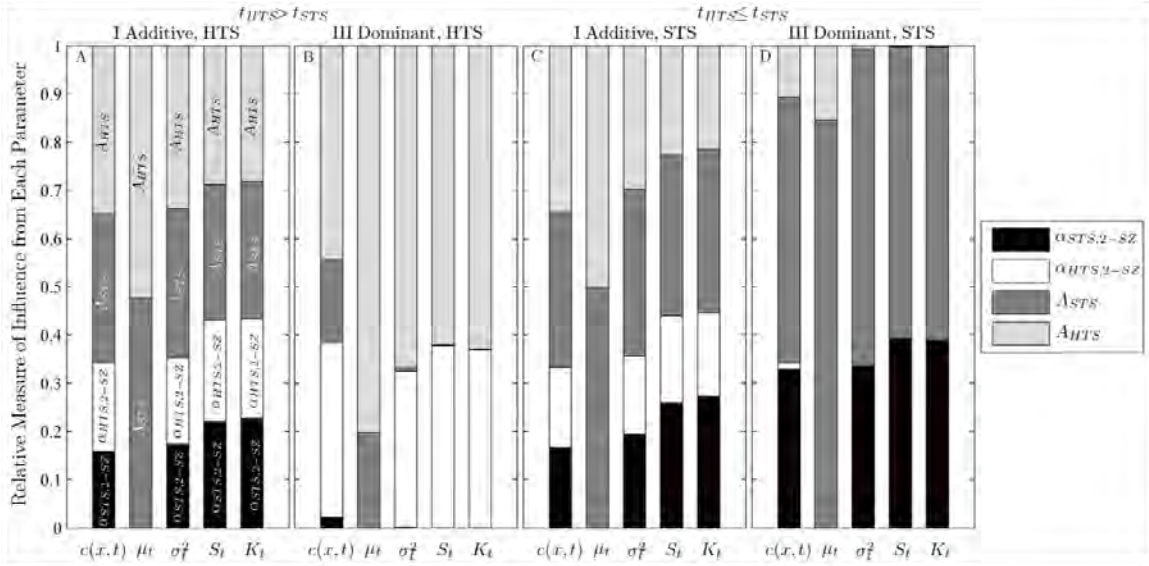

Figure B-3. A fuzzy number sensitivity analysis to estimate the relative influence of each 2-SZ model storage parameter on the solute residence time probability density function ($c(x,t)$) and the moment solutions (mean (μ_t), variance (σ_t^2), third central moment (S_t), and fourth central moment (K_t)). These results illustrate *additive* (Case I) and *dominant* (Case III) storage conditions. These two cases are illustrated separately for when HTS residence time is greater than STS residence time ($t_{HTS} > t_{STS}$) and when STS residence time is greater than HTS residence time ($t_{HTS} \leq t_{STS}$). When $t_{HTS} > t_{STS}$, each parameter has a significant influence on $c(x,t)$, σ_t^2, S_t, and K_t for the (A) additive case. The mean, μ_t, is insensitive the exchange rate coefficients, indicating that an estimate of mean residence time in the stream is influenced by storage capacities (A_{STS} and A_{HTS}). When $t_{HTS} \leq t_{STS}$ for the additive case (C), the results are nearly identical because storage timescales are comparable. For the dominant case, there are fewer parameters significantly influencing the central moments. In (B) the HTS exchange coefficient, $\alpha_{HTS,2-SZ}$, has a relative influence of less than 45% and the storage capacity, A_{HTS}, has more than 55% influence on σ_t^2, S_t, and K_t. Conversely, in (D) we see $\alpha_{STS,2-SZ}$ has a relative influence of less than 45% and the storage capacity, A_{STS}, has an influence of more than 55%.

Appendix C
Other Channel Properties Derived from Width Estimates

Total channel width, B_{tot}(m), was delineated every 5 m to arrive at $B_{tot}(x)$ where x is the streamwise distance from 0 m (upper reach limit) to 6.96 km (downstream reach limit) at 5-m intervals. Mean depth, $Y(x)$ (m), mean velocity, $U(x)$ (m s^{-1}), and the longitudinal dispersion coefficient, $D(x)$ (m^2 s^{-1}), were estimated spatially through hydraulic principles of open channel flow (i.e., momentum and continuity). Specifically, using the $B_{tot}(x)$ estimates and flow (Q (m^3 s^{-1})) measured at x = 0 m, $Y(x) = f(Q, B_{tot}(x), S_o, S_f(x))$ and was estimated through iteration of the momentum equation for steady, non-uniform flow (the sum of forces equals the change in momentum) in an assumed rectangular channel as

$$\begin{aligned}\rho\frac{Q^2}{B_{tot}(x-\Delta x)Y(x-\Delta x)} = \rho\frac{Q^2}{B_{tot}(x)Y(x)} &+ \rho g B_{tot}(x)Y(x)\left(\frac{Y(x)}{2}\right)\\ &- \rho g B_{tot}(x-\Delta x)Y(x-\Delta x)\left(\frac{Y(x-\Delta x)}{2}\right)\\ &+ \rho g \Delta x S_0\left(\frac{B_{tot}(x)Y(x)+B_{tot}(x-\Delta x)Y(x-\Delta x)}{2}\right)\\ &- \rho g \Delta x S_f(x)\left(\frac{B_{tot}(x)Y(x)+B_{tot}(x-\Delta x)Y(x-\Delta x)}{2}\right)\end{aligned}, \quad \text{(C-1)}$$

where S_o is the mean streambed slope, S_f is the slope of friction, ρ is the density of water (kg m^{-3}), and g is the gravitational acceleration (m s^{-2}). Friction losses (defined by $S_f(x)$ averaged over each 5-m interval) were estimated using Manning's equation,

$$\begin{aligned}S_f(x) = \frac{n^2Q^2}{2}\Bigg[&(B_{tot}(x)Y(x))^{-2}\left(\frac{B_{tot}(x)Y(x)}{2Y(x)+B_{tot}(x)}\right)^{(-4/3)}\\ &+(B_{tot}(x-\Delta x)Y(x-\Delta x))^{-2}\left(\frac{B_{tot}(x-\Delta x)Y(x-\Delta x)}{2Y(x-\Delta x)+B_{tot}(x-\Delta x)}\right)^{(-4/3)}\Bigg]\end{aligned}, \quad \text{(C-2)}$$

where n is the reach-averaged Manning's roughness coefficient and S_o was assumed constant over the study reach and estimated from a 10-m digital elevation model. In this iteration, a starting estimate of $Y(x = X)$ at the downstream study reach limit (X) was used

to estimate the next upstream $Y(x = X - 5\text{ m})$ because normal depth is greater than critical depth; this $Y(x = X - 5\text{ m})$ estimate was used to estimate the next upstream $Y(x = X - 10\text{ m})$ and repeated to estimate all $Y(x)$. With Q, $B_{tot}(x)$, and $Y(x)$ estimated, $U(x) = f(Q, B_{tot}(x), Y(x))$ and was estimated from continuity. Note that external forces due to expansion or contraction between sequential reach segments were not accounted for in equation (C-1). Although neglecting these forces can introduce bias towards lower variability in $Y(x)$, these forces are assumed negligible relative to frictional forces. Lastly, $D(x)$ was estimated using an empirical relationship [*Fischer*, 1975],

$$D(x) = 0.011 \frac{U(x)^2 B_{tot}(x)^2}{Y(x) u^*(x)}, \tag{C-3}$$

where $u^*(x) = \sqrt{gR(x)S_E(x)}$ is the shear stress velocity (m s^{-1}), R is the hydraulic radius (m), and S_E is the slope of the energy grade line (assumed to be S_f). In summary, $B_{tot}(x)$, Q, and S_o were estimated independently for the study reach; $Y(x)$ is negatively correlated to $B_{tot}(x)$ where increasing $B_{tot}(x)$ generally results in decreasing $Y(x)$; $U(x)$ is positively correlated to $Y(x)$ where increasing $Y(x)$ generally results in increasing $U(x)$; and $D(x)$ is negatively correlated to $U(x)$ where increasing $U(x)$ generally results in decreasing $D(x)$.

Appendix D
Derivation of Closed Form Moment Solutions with Spatial Variability Factors

The *j*th-order temporal moment (n_j) of a solute residence time PDF ($c(x,t)$ (T^{-1})) is defined as [*Aris*, 1958]

$$n_j = (-1)^j \left. \frac{\partial^j \bar{c}(x,s)}{\partial s^j} \right|_{s=0} = E[t^j] = \int_0^\infty t^j c(x,t)dt, \tag{D-1}$$

where $\mathcal{L}^{-1}\{\bar{c}(x,s)\} = c(x,t)$, $c(x,t) = C(x,t)/\int_0^\infty C(x,t)dt$, $\int_0^\infty c(x,t)dt = 1$, $C(x,t)$ is the solute concentration (M L^{-3}), the residence time t is the random variable, s is the Laplace variable, and $E[\ldots]$ denotes the expected value. Centering equation (D-1) about the first temporal moment (n_1) provides the *j*th central moment (m_j),

$$m_j = \int_0^\infty (t - n_1)^j c(x,t)dt = E[(t - n_1)^j] \text{ for } j > 1. \tag{D-2}$$

Substituting the Laplace-domain solution (see equation (3-6)) normalized by the zeroth temporal moment into equation (D-2)—assuming the governing equations are linear with time invariant coefficients [*Leube et al*., 2012]—yields the first through third temporal moments,

$$n_1 = \mu_t = \mu_t(x=0) + \frac{x}{U}(1+\Lambda), \tag{D-3}$$

$$n_2 = \sigma_t{}^2(x=0) + 2\frac{x}{U}\Theta + 2\frac{xD}{U^3}(1+\Lambda)^2 + n_1{}^2, \tag{D-4}$$

$$n_3 = S_t(x=0) + 6\frac{x}{U}\Phi + 12\frac{xD}{U^3}\Theta(1+\Lambda) + 12\frac{xD^2}{U^5}(1+\Lambda)^3 + 3(n_2 - n_1{}^2)(n_1) + n_1{}^3, \tag{D-5}$$

where $\mu_t(x=0)$, $\sigma_t{}^2(x=0) = n_2(x=0) - [n_1(x=0)]^2$, and $S_t(x=0) = n_3(x=0) - 3n_1(x=0)\sigma_t{}^2(x=0) - [n_1(x=0)]^3$ are the mean (T), variance (T^2), and third central moment (T^3) originating from the boundary condition, respectively;

$\Lambda = \frac{Y_{STS}\beta}{Y(1-\beta)} + \frac{Y_{HTS}}{Y}$; $\Theta = \frac{(B_{tot}\beta)^2}{\alpha_{STS}} \frac{Y_{STS}\beta}{Y(1-\beta)} + \frac{{Y_{HTS}}^2}{\alpha_{HTS}} \frac{Y_{HTS}}{Y}$;

$\Phi = \frac{(B_{tot}\beta)^4}{{\alpha_{STS}}^2} \frac{Y_{STS}\beta}{Y(1-\beta)} + \frac{{Y_{HTS}}^4}{{\alpha_{HTS}}^2} \frac{Y_{HTS}}{Y}$; the subscripts STS and HTS represent surface transient storage and hyporheic transient storage, respectively; α_{STS} is the exchange rate coefficient between the main portion of the stream and the STS zone ($L^2\ T^{-1}$); α_{HTS} is the exchange rate coefficient between the main portion of the stream and the HTS zone ($L^2\ T^{-1}$); Y_{STS} and Y_{HTS} are the STS and HTS mean depths (L), respectively; and β is the STS fraction of the total channel width.

When the continuous study reach is segmented into spatially distinct reach segments, the reach averaged temporal moments can be expressed as the summation of reach segment specific temporal moments,

$$\langle n_1 \rangle_k = \langle \mu_t \rangle_k = n_1(x=0) + \sum_{i=1}^{k} \frac{\langle \Delta x_k \rangle}{E[\mathbf{U}_{ki}]} (1 + \Lambda_{ki}), \tag{D-6}$$

$$\langle n_2 \rangle_k = {\sigma_t}^2(x=0) + 2\sum_{i=1}^{k} \frac{\langle \Delta x_k \rangle}{E[\mathbf{U}_{ki}]} \Theta_{ki} + 2\sum_{i=1}^{k} \frac{\langle \Delta x_k \rangle E[\mathbf{D}_{ki}]}{E[\mathbf{U}_{ki}]^3} (1 + \Lambda_{ki})^2 + \langle {n_{1,k}}^2 \rangle, \tag{D-7}$$

$$\begin{aligned} \langle n_3 \rangle_k = {} & S_t(x=0) + 6\sum_{i=1}^{k} \frac{\langle \Delta x_k \rangle}{E[\mathbf{U}_{ki}]} \Phi_{ki} + 12\sum_{i=1}^{k} \frac{\langle \Delta x_k \rangle E[\mathbf{D}_{ki}]}{E[\mathbf{U}_{ki}]^3} \Theta_{ki} (1 + \Lambda_{ki}) \\ & + 12\sum_{i=1}^{k} \frac{\langle \Delta x_k \rangle E[\mathbf{D}_{ki}]^2}{E[\mathbf{U}_{ki}]^5} (1 + \Lambda_{ki})^3 + 3\langle n_{2,k} \cdot n_{1,k} \rangle - 2\langle {n_{1,k}}^3 \rangle \end{aligned}, \tag{D-8}$$

where segmentation ranges from $k = 1, 2, \ldots, N$; i is the reach segment index; N is the total number of reach segments, $\Delta x_k = X/k$ is the segment length; X is the total study reach length; $\langle ... \rangle$ denotes the study reach averaged value for each k;

$$\Lambda_{ki} = \frac{Y_{STS}\beta}{E[\mathbf{Y}_{ki}](1-\beta)} + \frac{Y_{HTS}}{E[\mathbf{Y}_{ki}]};\ \Theta_{ki} = \frac{\left(E[\mathbf{B}_{tot,ki}]\beta\right)^2}{\alpha_{STS}} \frac{Y_{STS}\beta}{E[\mathbf{Y}_{ki}](1-\beta)} + \frac{{Y_{HTS}}^2}{\alpha_{HTS}} \frac{Y_{HTS}}{E[\mathbf{Y}_{ki}]};$$

$$\Phi_{ki} = \frac{\left(E[\mathbf{B}_{tot,ki}]\beta\right)^4}{{\alpha_{STS}}^2} \frac{Y_{STS}\beta}{E[\mathbf{Y}_{ki}](1-\beta)} + \frac{{Y_{HTS}}^4}{{\alpha_{HTS}}^2} \frac{Y_{HTS}}{E[\mathbf{Y}_{ki}]};$$ and $\mathbf{B}_{tot,ki}$, $\mathbf{Y}_{ki}$, $\mathbf{U}_{ki}$, and $\mathbf{D}_{ki}$ are the resulting vectors of depth, velocity, and dispersion estimates that fall within the *i*th reach segment, respectively.

The reach averaged second and third central moments are (after *Riml and Wörman* [2011])

$$\left\langle \sigma_t^{\,2} \right\rangle = \left\langle n_2 \right\rangle - \left\langle n_1 \right\rangle^2 = \left\langle n_2 \right\rangle - \left\langle n_1^{\,2} \right\rangle + \left\langle n_1^{\,2} \right\rangle - \left\langle n_1 \right\rangle^2, \tag{D-9}$$

$$\begin{aligned} \left\langle S_t \right\rangle &= \left\langle n_3 \right\rangle - 3\left\langle n_2 \right\rangle\left\langle n_1 \right\rangle + 2\left\langle n_1 \right\rangle^3 \\ &= \left\langle n_3 \right\rangle - 3\left\langle n_2 \cdot n_1 \right\rangle + 2\left\langle n_1^{\,3} \right\rangle + 3\left\langle n_2 \cdot n_1 \right\rangle - 2\left\langle n_1^{\,3} \right\rangle - 3\left\langle n_2 \right\rangle\left\langle n_1 \right\rangle + 2\left\langle n_1 \right\rangle^3. \end{aligned} \tag{D-10}$$

Evaluating terms in equations (D-9) and (D-10), the mean residence time of $c_k(X,t)$ for segmentation varying from $k = 1, 2, \ldots, N$ is

$$\left\langle n_1 \right\rangle_k = \left\langle \mu_t \right\rangle_k = \mu_t(x=0) + \frac{X}{\left\langle U \right\rangle}\left(1 + \left\langle \Lambda \right\rangle\right)\lambda_{1,k}, \tag{D-11}$$

where $\left\langle \Lambda \right\rangle = \frac{Y_{STS}\beta}{\left\langle Y \right\rangle(1-\beta)} + \frac{Y_{HTS}}{\left\langle Y \right\rangle}$; $\left\langle U \right\rangle = E[\mathbf{U}_{11}]$ and $\left\langle Y \right\rangle = E[\mathbf{Y}_{11}]$ are the expected values of the corresponding reference distributions (i.e., for $k = 1$); and $\lambda_{1,k}$ is the spatial variability factor (shown below in equation (D-14)). The variance about the mean is

$$\left\langle \sigma_t^2 \right\rangle_k = \sigma_t^2(x=0) + \frac{2X}{\left\langle U \right\rangle^3}\left[\left\langle U \right\rangle^2\left\langle \Theta \right\rangle\lambda_{2,k} + \left\langle D \right\rangle\left(1 + \left\langle \Lambda \right\rangle\right)^2\lambda_{3,k} + X\left\langle U \right\rangle\left(1 + \left\langle \Lambda \right\rangle\right)^2\lambda_{4,k}\right], \tag{D-12}$$

where $\langle\Theta\rangle = \frac{\left(\langle B_{tot}\rangle\beta\right)^2}{\alpha_{STS}}\frac{Y_{STS}\beta}{\langle Y\rangle(1-\beta)} + \frac{{Y_{HTS}}^2}{\alpha_{HTS}}\frac{Y_{HTS}}{\langle Y\rangle}$, $\langle D\rangle = E[\mathbf{D}_{11}]$, and $\langle B_{tot}\rangle = E[\mathbf{B}_{tot,11}]$. The third central moment is

$$\begin{aligned}\langle S_t\rangle_k = {} & S_t(x=0) + 6\frac{X}{\langle U\rangle}\langle\Phi\rangle\lambda_{5,k} + 12\frac{X\langle D\rangle}{\langle U\rangle^3}\langle\Theta\rangle\left(1+\langle\Lambda\rangle\right)\lambda_{6,k} \\ & + 12\frac{X\langle D\rangle^2}{\langle U\rangle^5}\left(1+\langle\Lambda\rangle\right)^3\lambda_{7,k} \\ & + X^2\left[\frac{3\mu_t(x=0)\left(1+\langle\Lambda\rangle\right)^2}{\langle U\rangle^2}\lambda_{4,k} + \frac{6\langle\Theta\rangle\left(1+\langle\Lambda\rangle\right)}{\langle U\rangle^2}\lambda_{8,k} + \frac{6\left(1+\langle\Lambda\rangle\right)^3}{\langle U\rangle^4}\lambda_{9,k}\right] \\ & + X^3\frac{6\left(1+\langle\Lambda\rangle\right)^3}{\langle U\rangle^3}\lambda_{10,k}\end{aligned}, \quad \text{(D-13)}$$

where $\langle\Phi\rangle = \frac{\left(\langle B_{tot}\rangle\beta\right)^4}{{\alpha_{STS}}^2}\frac{Y_{STS}\beta}{\langle Y\rangle(1-\beta)} + \frac{{Y_{HTS}}^4}{{\alpha_{HTS}}^2}\frac{Y_{HTS}}{\langle Y\rangle}$.

The spatial variability factor of the mean (equation (D-11)) is

$$\lambda_{1,k} = \sum_{i=1}^{k}\frac{\eta_k}{\gamma_{U,ki}}\left[\frac{\left(1+\langle\Lambda\rangle\gamma_{\Lambda,ki}\right)}{\left(1+\langle\Lambda\rangle\right)}\right], \quad \text{(D-14)}$$

where $\eta_k = \frac{\Delta x_k}{X}$; $\gamma_{U,ki} = \frac{U_{ki}}{\langle U\rangle}$ and $\gamma_{\Lambda,ki} = \frac{\Lambda_{ki}}{\langle\Lambda\rangle}$. The spatial variability factors of the variance about the mean (equation (D-12)) are

$$\lambda_{2,k} = \sum_{i=1}^{k}\eta_k\frac{\gamma_{\Theta,ki}}{\gamma_{U,ki}}, \quad \text{(D-15)}$$

$$\lambda_{3,k} = \sum_{i=1}^{k}\eta_k\frac{\gamma_{D,ki}}{{\gamma_{U,ki}}^3}\left[\frac{\left(1+\langle\Lambda\rangle\gamma_{\Lambda,ki}\right)}{\left(1+\langle\Lambda\rangle\right)}\right]^2, \quad \text{(D-16)}$$

$$\lambda_{4,k} = \sum_{i=1}^{k}\frac{{\sigma_{\eta,k}}^2}{{\gamma_{U,ki}}^2}\left[\frac{\left(1+\langle\Lambda\rangle\gamma_{\Lambda,ki}\right)}{\left(1+\langle\Lambda\rangle\right)}\right]^2, \quad \text{(D-17)}$$

where $\gamma_{D,ki} = \frac{D_{ki}}{\langle D \rangle}$; $\gamma_{\Theta,ki} = \frac{\Theta_{ki}}{\langle \Theta \rangle}$; $\sigma_{\eta,k}{}^2 = \frac{\langle \Delta x_k{}^2 \rangle - \langle \Delta x_k \rangle^2}{X^2} = \frac{\sigma_{x,k}{}^2}{X^2}$; and

$\sigma_{x,k}{}^2 = E[\Delta x_k{}^2] - E[\Delta x_k]^2 = \langle \Delta x_k{}^2 \rangle - \langle \Delta x_k \rangle^2$ is the spatial variance. The spatial variability factors of the third central moment (equation (D-13)) are

$$\lambda_{5,k} = \sum_{i=1}^{k} \eta_k \frac{\gamma_{\Phi,ki}}{\gamma_{U,ki}}, \tag{D-18}$$

$$\lambda_{6,k} = \sum_{i=1}^{k} \eta_k \frac{\gamma_{D,ki}\gamma_{\Theta,ki}}{\gamma_{U,ki}{}^3} \left[\frac{\left(1 + \langle \Lambda \rangle \gamma_{\Lambda,ki}\right)}{\left(1 + \langle \Lambda \rangle\right)} \right], \tag{D-19}$$

$$\lambda_{7,k} = \sum_{i=1}^{k} \eta_k \frac{\gamma_{D,ki}{}^2}{\gamma_{U,ki}{}^5} \left[\frac{\left(1 + \langle \Lambda \rangle \gamma_{\Lambda,ki}\right)}{\left(1 + \langle \Lambda \rangle\right)} \right]^3, \tag{D-20}$$

$$\lambda_{8,k} = \sum_{i=1}^{k} \frac{\sigma_{\eta,k}{}^2 \gamma_{\Theta,ki}}{\gamma_{U,ki}{}^2} \left[\frac{\left(1 + \langle \Lambda \rangle \gamma_{\Lambda,ki}\right)}{\left(1 + \langle \Lambda \rangle\right)} \right]^2, \tag{D-21}$$

$$\lambda_{9,k} = \sum_{i=1}^{k} \frac{\sigma_{\eta,k}{}^2}{\gamma_{U,ki}{}^4} \left[\frac{\left(1 + \langle \Lambda \rangle \gamma_{\Lambda,ki}\right)}{\left(1 + \langle \Lambda \rangle\right)} \right]^3, \tag{D-22}$$

$$\lambda_{10,k} = \sum_{i=1}^{k} \frac{\sigma_{\eta,k}{}^3}{\gamma_{U,ki}{}^3} \left[\frac{\left(1 + \langle \Lambda \rangle \gamma_{\Lambda,ki}\right)}{\left(1 + \langle \Lambda \rangle\right)} \right]^3, \tag{D-23}$$

where $\gamma_{\Phi,ki} = \frac{\Phi_{ki}}{\langle \Phi \rangle}$; $\sigma_{\eta,k}{}^3 = \frac{\langle \Delta x_k{}^3 \rangle - \langle \Delta x_k \rangle^3}{X^3} = \frac{\sigma_{x,k}{}^3}{X^3}$; and $\sigma_{x,k}{}^3 = \langle \Delta x_k{}^3 \rangle - \langle \Delta x_k \rangle^3$ is the spatial skewness. The spatial variability factors $\lambda_{1,k}$, $\lambda_{2,k}$, $\lambda_{3,k}$, $\lambda_{5,k}$, $\lambda_{6,k}$, and $\lambda_{7,k}$ take the value of unity if channel properties are constant. When Δx_k is constant, $\sigma_{\eta,k}{}^2 = 0$, $\sigma_{\eta,k}{}^3 = 0$, and, therefore, $\lambda_{4,k}$ and $\lambda_{8,k}$ through $\lambda_{10,k}$ are zero.

Appendix E
Repeat of Comparisons Using Randomized Channel Widths

A pseudorandom number generator was used to generate random width estimates from a lognormal distribution with a similar expected value and variance as observed over the entire study reach. These randomized width estimates were generated at the same number of observed widths that correspond to 5-m streamwise intervals. Mean depth, mean velocity, and the dispersion coefficient were estimated again at 5-m intervals using the same procedure described in SI 1. Because these properties are derived from the width estimates, they are also randomized. For illustrative purposes, we show a portion of the randomized widths relative to the observed widths (Figure E-1A). The probability density function (PDF) of the randomized widths has a similar expected value and variance as observed (Figures E-1B and E-1C). The semivariance of the randomized width estimates indicates that estimates are not spatially correlated at any distance because the semivariance is similar to the overall variance at every lag distance (Figure E-1C). The observed semivariance indicates that estimates are spatially correlated at distances up to 150 m (also see Figure 3-3B).

Repeating the comparison of channel property distributions using the Kolmogorov-Smirnov (K-S) test indicates that when the number of reach segments, k, is 50, the k-distribution based on randomized widths clearly does not represent the reference distribution (Figure E-2A). The reference distributions of the randomized and observed widths are nearly identical. The maximum differences (K-S statistic) based on randomized widths are larger and do not decrease as quickly with further segmentation as do the maximum differences based on observed widths (Figure E-2B). The maximum difference also approaches zero and the p-value approaches 1 at a distinctly higher number of reach segments (Figure E-2C). From these results, it takes roughly an order of

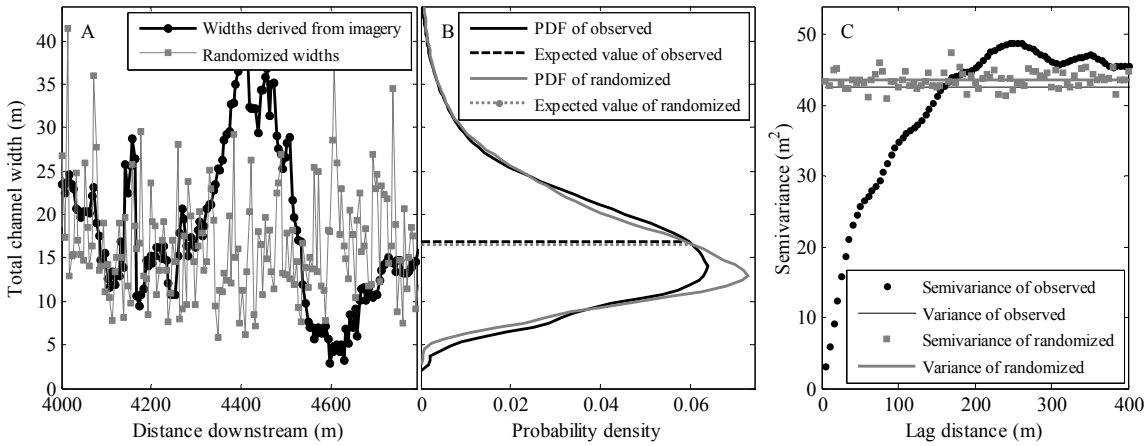

Figure E-1. (A) Total channel width estimates ($B_{tot}(x)$) derived every 5 meters from the imagery shown in Figure 3-1 and randomized width estimates. (B) Probability density functions and expected values of observed $B_{tot}(x)$ estimates and randomized estimates. The randomized estimates follow an assumed lognormal distribution with a similar expected value and variance as observed. (C) The semivariance and variance of $B_{tot}(x)$ derived from the imagery and randomized width estimates at different separation distances (lag distance). The randomized widths are not spatially correlated at any distance because semivariance is similar to the overall variance at every lag distance.

magnitude more segments to represent the reference distribution if width estimates are random. A repeat of the comparison of solute predictions indicates that a solution containing random, spatially variable channel properties does not converge at any number of reach segments (Figures E-3A and E-3D). The root mean square error (RMSE) of predictions for $k > 1$ relative to the prediction for $k = 1$ confirms that the change in the prediction steadily increases with further segmentation and does not converge if widths are random (Figures E-3B and E-3E). The rate of change in RMSE with respect to a change in k further indicates that a solution containing randomized widths does not converge (Figures E-3C and E-3F).

A repeat of the comparison of statistical moments provides similar results as the solute predictions. If width estimates are random, a moment solution (mean, variance, or third central moment of the solute residence time PDF) does not converge to one solution

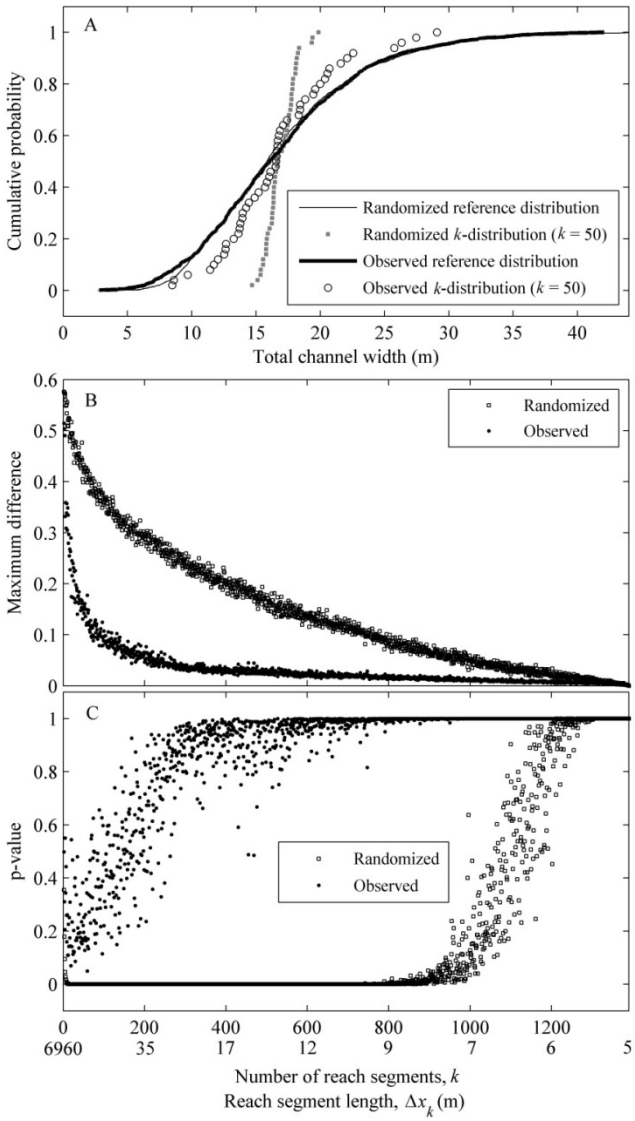

Figure E-2. (A) Example nonparametric cumulative distribution functions (CDF) for k = 50 relative to the reference distribution of both observed and randomized width estimates. (B) The resulting Kolmogorov-Smirnov (K-S) statistic (maximum difference) for varying k = 1, 2, …, N reach segments based on both observed and randomized width estimates. (C) The accompanying p-value that represents the probability that the maximum difference is equal to or larger than all possible differences between the k-distribution and the reference distribution.

containing the significant effects of spatial variability (Figures E-4A, E-4B, and E-4C). The rate of percent change with respect to a change in k again indicates that there is not a distinct change in slope of the percent change if widths are random (Figures E-4D, E-4E, and E-4F).

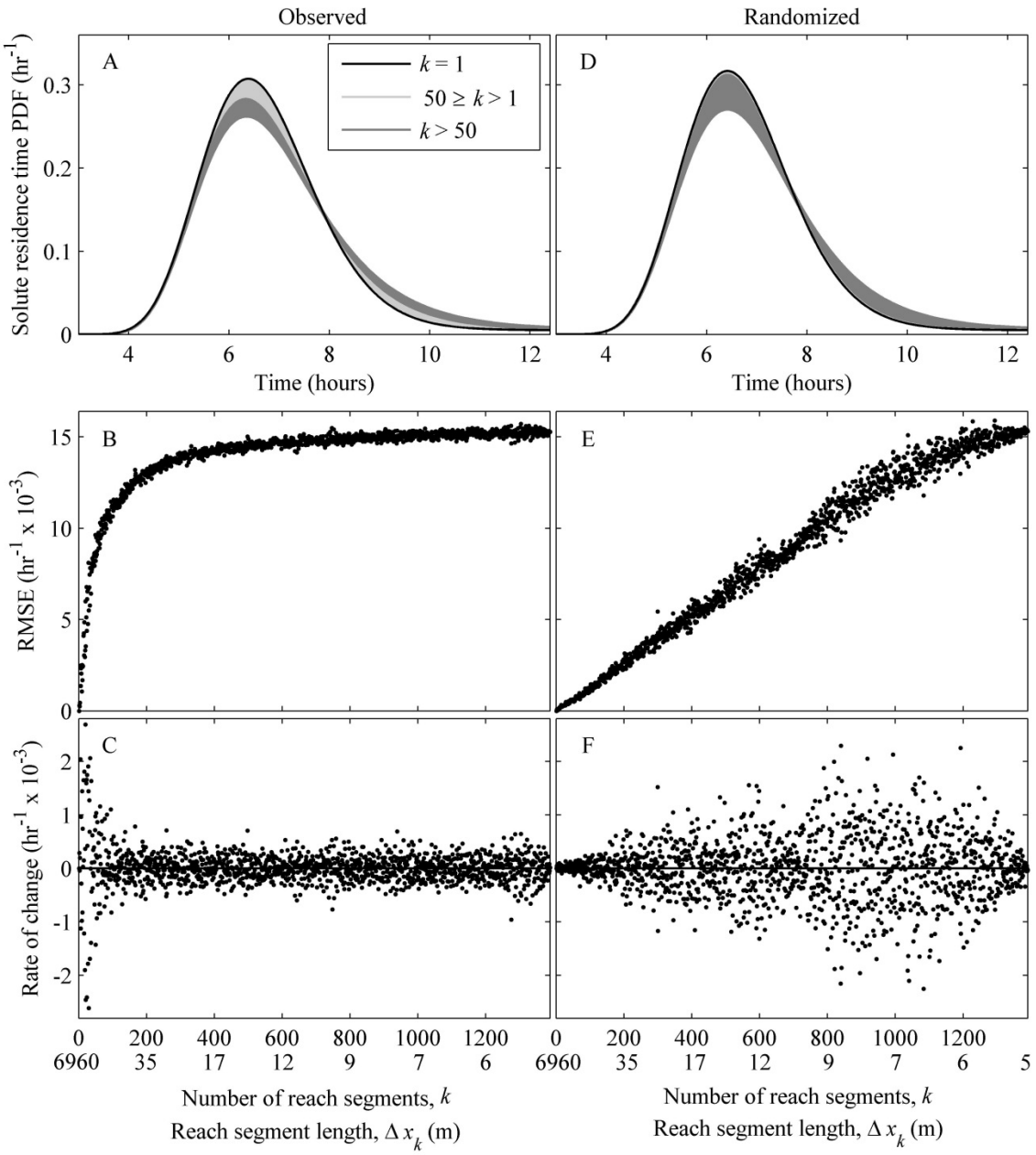

Figure E-3. Solute residence time probability density function (PDF) predictions at the downstream reach limit for varying $k = 1, 2, \ldots, N$ reach segments based on both (A) observed and (D) randomized channel widths. The root mean square error (RMSE) as a measure of change of the predictions for $k > 1$ from the prediction for $k = 1$ based on both (B) observed and (E) randomized channel widths. The rate of change in RMSE with respect to a change in k based on both (C) observed and (F) randomized channel widths. The differences between predictions based on observed and random estimates are distinct. If channel widths are random, a solution containing the effects of spatially variable channel properties does not converge.

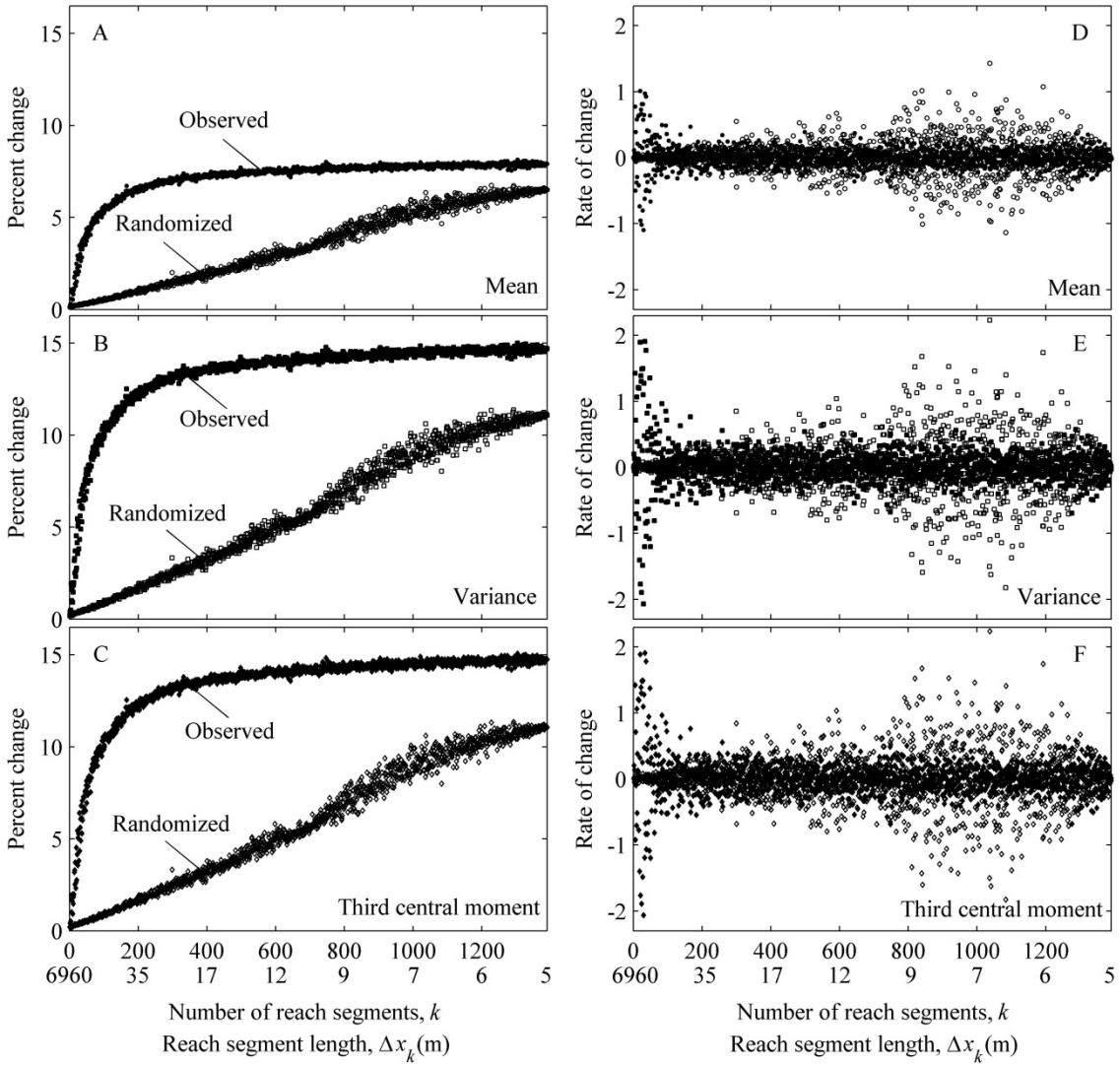

Figure E-4. The percent change of the (A) mean, (B) variance, and (C) third central moment estimates for more than one reach segment, $k > 1$, relative to the estimates for $k = 1$ based on both observed and random width estimates. If widths are random, a moment solution containing the significant effects of spatially variable channel properties does not converge with further segmentation, but does if widths are observed. The rate of percent change with respect to a change in k of the (D) mean, (E) variance, and (F) third central moment indicates that a distinct change in slope of the percent change does not occur if widths are random.

Appendix F
Derivation of the Semi-Analytical Temperature Solution

Recall that the channel surface heat flux term in equation (4-1) is defined as

$$h(t,T) = \frac{A_S}{V\rho C_p} J_{atm} = \frac{A_S}{V\rho C_p}\left[J_{sn} + J_{an} - \left(J_{br} + J_c + J_e\right)\right], \tag{F-1}$$

where A_S is the stream water surface area at the air-water interface (cm^2), V is the water volume in the channel (cm^3), and J_{atm} is the total surface heat flux (cal cm^{-2} d^{-1}). Note that because we assume the channel is rectangular, the surface area to volume ratio is $A_S/V = 1/Y$. Modification of the Stefan-Boltzmann law provides the semi-empirical relationships [*Chapra*, 1997],

$$J_{an}(t,T_{air}) = \sigma\left(T_{air} + 273\right)^4\left(A + 0.031\sqrt{e_{air}}\right)\left(1 - R_L\right), \tag{F-2}$$

$$J_{br}(t,T) = \varepsilon\sigma\left(T + 273\right)^4, \tag{F-3}$$

$$J_c(t,T) = c_1 f(U_w)\left(T - T_{air}\right), \tag{F-4}$$

$$J_e(t,T) = f(U_w)\left(e_{sat} - e_{air}\right), \tag{F-5}$$

where

$$f(U_w) = 19.0 + 0.95{U_w}^2, \tag{F-6}$$

$$e_{sat} = 4.596\exp\left(\frac{17.27T}{237.3 + T}\right), \tag{F-7}$$

$$e_{air} = \frac{R_h}{100}4.596\exp\left(\frac{17.27T_{air}}{237.3 + T_{air}}\right), \tag{F-8}$$

U_w is the wind speed (m s^{-1}); e_{sat} is the water saturation pressure; e_{air} is the air saturation pressure; T is the water temperature (°C); T_{air} is the air temperature (°C); R_h is the relative humidity; σ is the Stefan-Boltzmann constant (11.7 x 10^{-8} cal cm^{-2} d^{-1} K^{-4}); A is a coefficient (0.5 to 0.7); R_L is the reflection coefficient (0.03); and ε is the emissivity of water (0.97). Using Laplace transforms to solve partial differential equations requires the

surface heat flux term to be linearized. Because J_{br} and J_e are nonlinear in T, a first-order Taylor series expansion about the initial temperature, T_o, was employed,

$$J_{br}(t,T) \approx \varepsilon\sigma 4\left(T_o + 273\right)^3 T + \varepsilon\sigma\left(T_o + 273\right)^3\left(273 - 3T_o\right), \tag{F-9}$$

$$\begin{aligned} e_{sat} \approx\ & 4.596 \exp\left(\frac{17.27T_o}{237.3 + T_o}\right)\left(\frac{17.27 \cdot 237.3}{\left(237.3 + T_o\right)^2}\right)T \\ & + 4.596 \exp\left(\frac{17.27T_o}{237.3 + T_o}\right)\left(1 - \frac{17.27 \cdot 237.3}{\left(237.3 + T_o\right)^2}T_o\right) \end{aligned}, \tag{F-10}$$

$$\begin{aligned} J_e(t,T) \approx\ & f(U_w)4.596 \exp\left(\frac{17.27T_o}{237.3 + T_o}\right)\left(\frac{17.27 \cdot 237.3}{\left(237.3 + T_o\right)^2}\right)T \\ & + f(U_w)\left[4.596 \exp\left(\frac{17.27T_o}{237.3 + T_o}\right)\left(1 - \frac{17.27 \cdot 237.3}{\left(237.3 + T_o\right)^2}T_o\right) - e_{air}\right] \end{aligned}. \tag{F-11}$$

Collecting terms,

$$\begin{aligned} h(t,T) \approx -\frac{T}{\rho C_p Y}\Big[& \varepsilon\sigma 4\left(T_o + 273\right)^3 + f(U_w)c_1 \\ & + f(U_w)4.596 \exp\left(\frac{17.27T_o}{237.3 + T_o}\right)\left(\frac{17.27 \cdot 237.3}{\left(237.3 + T_o\right)^2}\right)\Big] \\ & + \frac{1}{\rho C_p Y}\Big[J_{sn} + \sigma\left(T_{air} + 273\right)^4\left(A + 0.031\sqrt{e_{air}}\right)\left(1 - R_L\right) \\ & - \varepsilon\sigma\left(T_o + 273\right)^3\left(273 - 3T_o\right) \\ & - f(U_w)4.596 \exp\left(\frac{17.27T_o}{237.3 + T_o}\right)\left(1 - \frac{17.27 \cdot 237.3}{\left(237.3 + T_o\right)^2}T_o\right) \\ & + f(U_w)\left(c_1 T_{air} - e_{air}\right)\Big] \end{aligned}, \tag{F-12}$$

which simplifies to

$$h(t,T) \approx \frac{\phi(t)}{Y}T + \frac{\theta(t)}{Y}, \tag{F-13}$$

where

$$\phi(t) = \frac{-1}{\rho C_p}\left[\varepsilon\sigma 4\left(T_o + 273\right)^3 + f(U_w)c_1 + f(U_w)4.596 \exp\left(\frac{17.27T_o}{237.3 + T_o}\right)\left(\frac{17.27 \cdot 237.3}{\left(237.3 + T_o\right)^2}\right)\right]$$

and varies only upon wind speed(cm d^{-1}); and

$$\theta(t) = \frac{1}{\rho C_p}\left[J_{sn} + \sigma(T_{air} + 273)^4\left(A + 0.031\sqrt{e_{air}}\right)(1 - R_L) - \varepsilon\sigma(T_o + 273)^3(273 - 3T_o)\right.$$
$$\left. - f(U_w)4.596\exp\left(\frac{17.27T_o}{237.3 + T_o}\right)\left(1 - \frac{17.27 \cdot 237.3}{(237.3 + T_o)^2}T_o\right) + f(U_w)(c_1 T_{air} - e_{air})\right]$$

varies upon wind speed, air temperature, relative humidity, and net shortwave radiation (^{o}C cm d^{-1}). See Figure F-1 for the surface heat fluxes and linearized surface heat flux term (equation (F-13)) for the meteorological conditions of the three day study period (assuming wind speed is constant and estimated as the three day average).

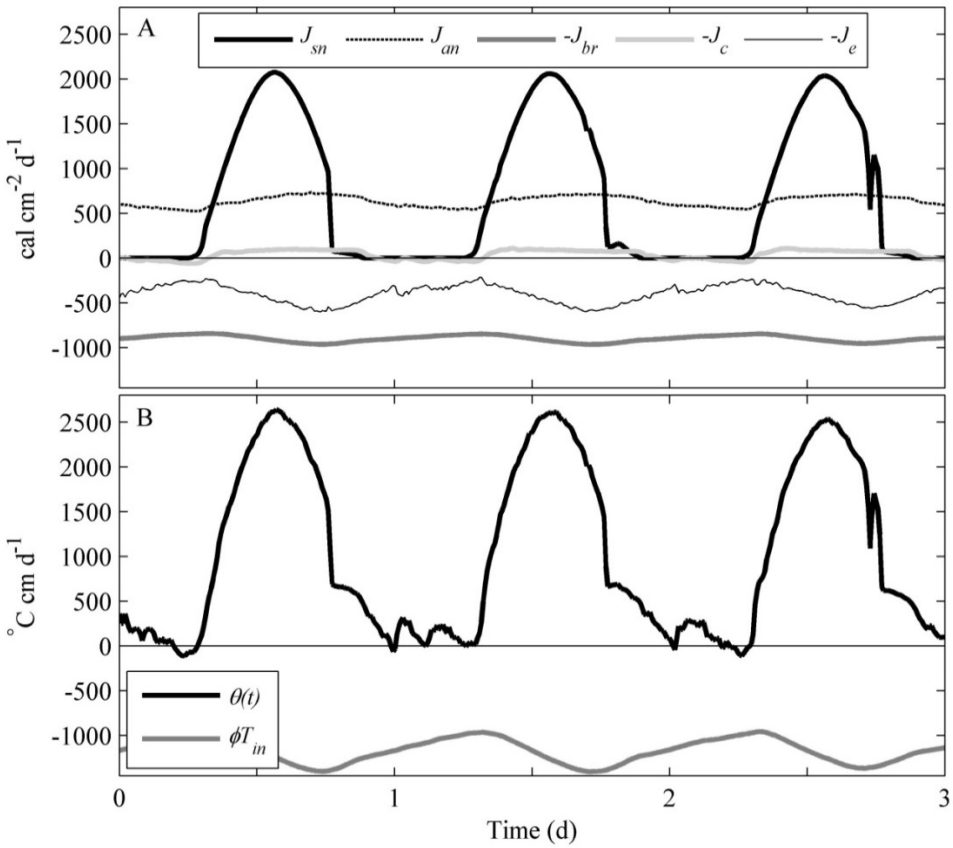

Figure F-1. (A) The observed net solar shortwave radiation (J_{sn}), the net atmospheric longwave radiation (J_{an}), the longwave back radiation from the water (J_{br}), the conduction and convection based on constant wind speed (J_c), and evaporation and condensation based on constant wind speed (J_e). (B) The $\theta(t)$ (°C m d^{-1}) and ϕT_{in} (°C m d^{-1}) terms of equation (F-13) that represent the linearized form the channel surface heat flux term. Note wind speed is set to the three day study period average.

The STS surface heat flux term is

$$h_{STS}(t,T) \approx \frac{\phi(t)_{STS}}{Y_{STS}} T_{STS} + \frac{\theta_{STS}(t)}{Y_{STS}}, \tag{F-14}$$

where

$$\phi_{STS}(t) = \frac{-1}{\rho C_p}\Big[\varepsilon\sigma 4\left(T_{o,STS} + 273\right)^3 + f(U_w)c_1 + f(U_w)4.596\exp\left(\frac{17.27T_{o,STS}}{237.3 + T_{o,STS}}\right)\left(\frac{17.27 \cdot 237.3}{\left(237.3 + T_{o,STS}\right)^2}\right)\Big]$$

and

$$\theta_{STS}(t) = \frac{1}{\rho C_p}\Big[J_{sn} + \sigma\left(T_{air} + 273\right)^4\left(A + 0.031\sqrt{e_{air}}\right)\left(1 - R_L\right) - \varepsilon\sigma\left(T_{o,STS} + 273\right)^3\left(273 - 3T_{o,STS}\right) - f(U_w)4.596\exp\left(\frac{17.27T_{o,STS}}{237.3 + T_{o,STS}}\right)\left(1 - \frac{17.27 \cdot 237.3}{\left(237.3 + T_{o,STS}\right)^2}T_{o,STS}\right) + f(U_w)\left(c_1 T_{air} - e_{air}\right)\Big].$$

Using the linearized forms of the surface heat flux terms (equations (F-13) and (F-14)), assuming are $\phi(t)$ and $\phi_{STS}(t)$ are constant over the three day study period [*Heavilin and Neilson,* 2012], and taking the Laplace transform, $\mathcal{L}\{f(x,t)\} = \int_0^\infty e^{-st} f(x,t)dt$, of equations (4-1)-(4-4) in the Chapter 4 yields

$$s\overline{T} - T_o = D\overline{T}_{xx} - U\overline{T}_x + \kappa_1\left(\overline{T}_{STS} - \overline{T}\right) + \kappa_2\left(\overline{T}_{HTS} - \overline{T}\right) + \varepsilon\kappa_5\left(\overline{T}_{HTS} - \overline{T}\right) + \frac{\phi}{Y}\overline{T} + \frac{\mathcal{L}\{\theta(t)\}}{Y}, \tag{F-15}$$

$$s\overline{T}_{STS} - T_{STS}(x,0) = \kappa_3\left(\overline{T} - \overline{T}_{STS}\right) + \varepsilon\kappa_6\left(\overline{T}_{STS,sed} - \overline{T}_{STS}\right) + \frac{\phi_{STS}}{Y_{STS}}\overline{T}_{STS} + \frac{\mathcal{L}\{\theta_{STS}(t)\}}{Y_{STS}}, \tag{F-16}$$

$$s\overline{T}_{HTS} - T_{HTS}(x,0) = \frac{\kappa_4}{\varepsilon}\left(\overline{T} - \overline{T}_{HTS}\right) + \kappa_7\left(\overline{T} - \overline{T}_{HTS}\right) + \kappa_8\left(\mathcal{L}\{T_{gr}(t)\} - \overline{T}_{HTS}\right), \tag{F-17}$$

$$s\overline{T}_{STS,sed} - T_{STS,sed}(x,0) = \kappa_7\left(\overline{T}_{STS} - \overline{T}_{STS,sed}\right) + \kappa_8\left(\mathcal{L}\{T_{gr}(t)\} - \overline{T}_{STS,sed}\right) \tag{F-18}$$

where $\overline{T}(x,s) = \mathcal{L}\{T(x,t)\}$; s is the Laplace variable; $U = \dfrac{Q}{B_{tot}(1-\beta)Y}$ is the velocity (m s^{-1}); $\kappa_1 = \dfrac{\alpha_{STS}Y_{STS}}{Y(1-\beta)\beta B_{tot}^{\ 2}}$; $\kappa_2 = \dfrac{\alpha_{HTS}}{Y_{HTS}Y}$; $\kappa_3 = \dfrac{\alpha_{STS}}{(\beta B_{tot})^2}$; $\kappa_4 = \dfrac{\alpha_{HTS}}{Y_{HTS}^{\ 2}}$; $\kappa_5 = \dfrac{\alpha_{sed}}{Y_{HTS}Y}$; $\kappa_6 = \dfrac{\alpha_{sed}}{Y_{HTS}Y_{STS}}$; $\kappa_7 = \dfrac{\alpha_{sed}}{Y_{HTS}^{\ 2}}$; $\kappa_8 = \dfrac{\alpha_{sed}}{Y_{HTS}Y_{gr}}$; and $\varepsilon = \dfrac{\rho_{sed}C_{p,sed}}{\rho C_p}$. Through substitution and applying the initial conditions, $T(x,0) = T_o$, $T_{STS}(x,0) = T_{STS,o}$, $T_{HTS}(x,0) = T_{HTS,o}$, and $T_{STS,sed}(x,0) = T_{STS,sed,o}$, yields the linear, nonhomogeneous ordinary differential equation,

$$\begin{aligned} -D\overline{T}_{xx} + U\overline{T}_x + \psi(s)\overline{T} = {} & \frac{\mathcal{L}\{\theta(t)\}}{Y} + \frac{\kappa_1\mathcal{L}\{\theta_{STS}(t)\}}{\gamma_{STS}(s)Y_{STS}} + \gamma_{gr}(s)\mathcal{L}\{T_{gr}(t)\} \\ & + T_o + \frac{\kappa_1 T_{STS,o}}{\gamma_{STS}(s)} + \frac{(\kappa_2 + \varepsilon\kappa_5)T_{HTS,o}}{\gamma_{HTS}(s)} \\ & + \frac{\varepsilon\kappa_1\kappa_6 T_{STS,sed,o}}{\gamma_{STS}(s)\gamma_{STS,sed}(s)} \end{aligned} \quad . \qquad \text{(F-19)}$$

See equation (4-8) in Chapter 4 for definitions of $\psi(s)$, $\gamma_{STS}(s)$, $\gamma_{HTS}(s)$, $\gamma_{STS,sed}(s)$, and $\gamma_{gr}(s)$. Applying the boundary condition, $T(0,t) = T_{in}(t)$, yields the general solution,

$$\begin{aligned} \overline{T} = {} & \left[\mathcal{L}\{T_{in}(t)\} - \frac{1}{\psi(s)}\left(\frac{\mathcal{L}\{\theta(t)\}}{Y} + \frac{\kappa_1\mathcal{L}\{\theta_{STS}(t)\}}{\gamma_{STS}(s)Y_{STS}} + \gamma_{gr}(s)\mathcal{L}\{T_{gr}(t)\} + T_o + \frac{\kappa_1 T_{STS,o}}{\gamma_{STS}(s)}\right.\right. \\ & \left.\left. + \frac{\varepsilon\kappa_1\kappa_6 T_{STS,sed,o}}{\gamma_{STS}(s)\gamma_{STS,sed}(s)} + \frac{(\kappa_2 + \varepsilon\kappa_5)T_{HTS,o}}{\gamma_{HTS}(s)}\right)\right]\exp\left[\frac{x}{2D}\left(U - \sqrt{U^2 + 4D\psi(s)}\right)\right] \\ & + \frac{1}{\psi(s)}\left(\frac{\mathcal{L}\{\theta(t)\}}{Y} + \frac{\kappa_1\mathcal{L}\{\theta_{STS}(t)\}}{\gamma_{STS}(s)Y_{STS}} + \gamma_{gr}(s)\mathcal{L}\{T_{gr}(t)\} + T_o + \frac{\kappa_1 T_{STS,o}}{\gamma_{STS}(s)} + \right. \\ & \left. \frac{\varepsilon\kappa_1\kappa_6 T_{STS,sed,o}}{\gamma_{STS}(s)\gamma_{STS,sed}(s)} + \frac{(\kappa_2 + \varepsilon\kappa_5)T_{HTS,o}}{\gamma_{HTS}(s)}\right) \end{aligned} \quad , \qquad \text{(F-20)}$$

Separating terms and inverting term-by-term into the original state space yields,

$$
\begin{aligned}
T(x,t) = {} & T_{IN}(t) * \mathcal{L}^{-1}\{f(x,s)\} \\
& + \theta(t) * \mathcal{L}^{-1}\left\{\frac{1-f(x,s)}{\psi(s)Y}\right\} \\
& + \theta_{STS}(t) * \mathcal{L}^{-1}\left\{\frac{\kappa_1 - \kappa_1 f(x,s)}{\psi(s)\gamma_{STS}(s)Y_{STS}}\right\} \\
& + T_{gr}(t) * \mathcal{L}^{-1}\left\{\frac{\gamma_{gr}(s) - \gamma_{gr}(s)\cdot f(x,s)}{\psi(s)}\right\} \\
& + T_o \mathcal{L}^{-1}\left\{\frac{1-f(x,s)}{\psi(s)}\right\} \\
& + T_{STS,o} \mathcal{L}^{-1}\left\{\frac{\kappa_1 - \kappa_1 f(x,s)}{\psi(s)\gamma_{STS}(s)}\right\} \\
& + T_{HTS,o} \mathcal{L}^{-1}\left\{\frac{(\kappa_2 + \varepsilon\kappa_5) - (\kappa_2 + \varepsilon\kappa_5) f(x,s)}{\psi(s)\gamma_{HTS}(s)}\right\} \\
& + T_{STS,sed,o} \mathcal{L}^{-1}\left\{\frac{\varepsilon\kappa_1\kappa_6 - \varepsilon\kappa_1\kappa_6 \cdot f(x,s)}{\psi(s)\gamma_{STS}(s)\gamma_{STS,sed}(s)}\right\} \quad , \qquad \text{(F-21)}
\end{aligned}
$$

where $f(x,s) = \exp\left(\frac{x}{2D}\left(U - \sqrt{U^2 + 4D\psi(s)}\right)\right)$ and $f * g = \int_0^t f(\tau)g(t-\tau)d\tau$ is the convolution. The inversions from the Laplace-domain to the time-domain were performed using the *Hollenbeck* [1998] function based on the *De Hoog et al*. [1982] algorithm. For the purpose of this study, we assume a constant T_{gr}. Using the three days of surface flux estimates (Figure F-1), we apply equation (F-21) and investigate how the contribution each term to total temperature at the end of three days changes over space (Figure F-2A). Note that the initial conditions are not shown in Figure F-2A because their contributions are fully decayed at the end of three days. As an example, the total temperature and each solution term over time are shown at 10 km (Figures F-2B and F-2C) and 25 km (Figures F-2D and F-2E) from the boundary condition.

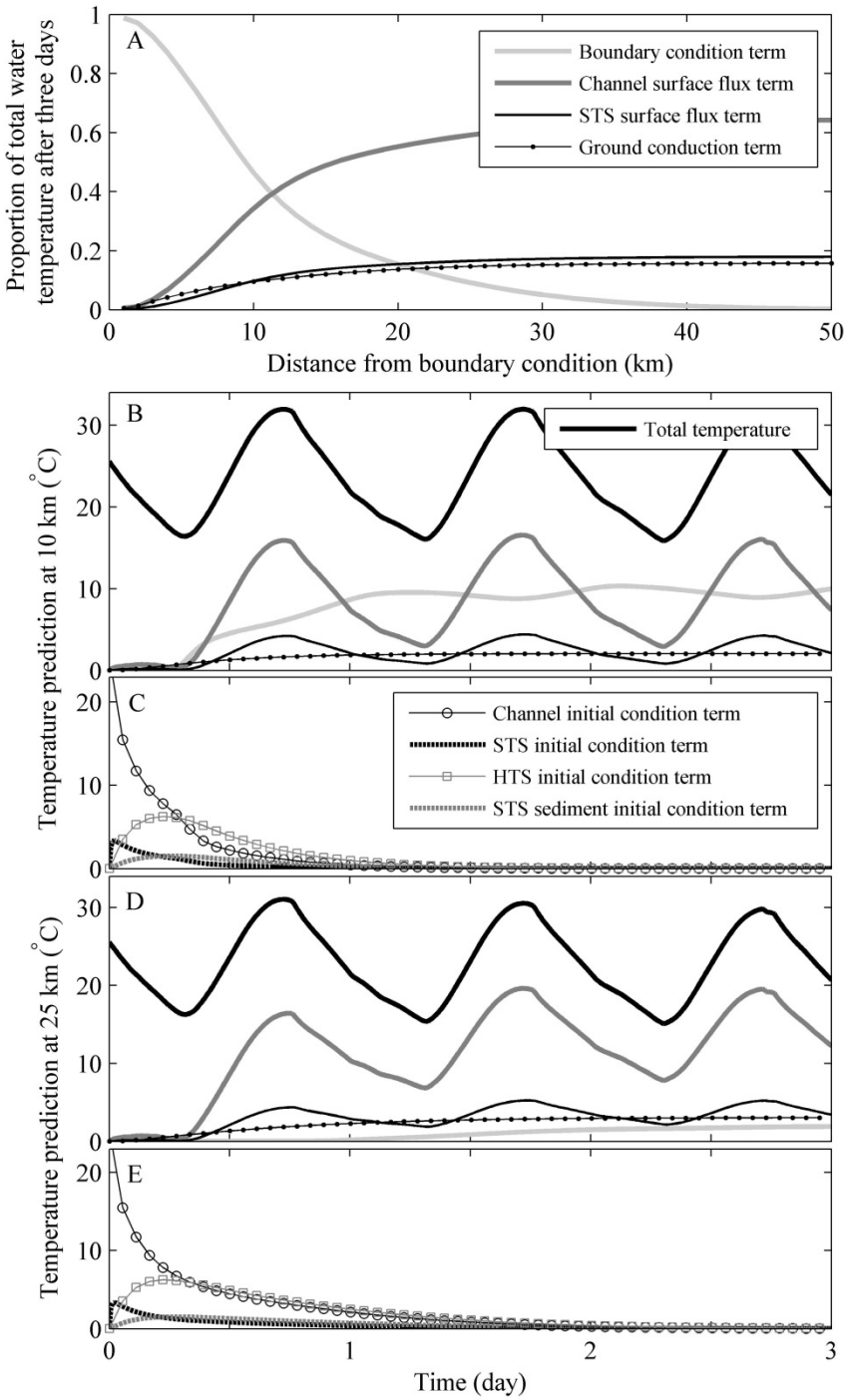

Figure F-2. (A) The proportion of total water temperature after three days over space of the boundary condition term, channel surface flux term, surface transient storage (STS) surface flux term, and ground conduction term. The predictions of the total water temperature, boundary condition term, channel surface flux term, STS surface flux term, and ground conduction term over time at (B) 10 km and (D) 25 km from the boundary condition. The corresponding predictions of the channel, STS, hyporheic transient storage (HTS), and STS sediment initial condition terms over time at (C) 10 km and (E) 25 km from the boundary condition.

To incorporate spatially variable hydraulic channel properties into the model representation, we employ a convolution of the Laplace domain solution (equation (4-9)). For simplicity, we illustrate this convolution in the Laplace-domain with three reach segments that represent a continuous reach with the boundary condition term only. At the end of reach segment 1, $\bar{g}(x_1,s) = \mathcal{L}\{T_{IN}(t)\} f_1(\Delta x, s)$; at the end of reach segment 2, $\bar{h}(x_2,s) = \bar{g}(x_1,s) f_2(\Delta x, s)$; lastly, at the end of reach segment 3, $\bar{m}(x_3,s) = \bar{m}(x_2,s) f_3(\Delta x, s)$. The final downstream prediction at the end of reach segment 3 can also be written as $\bar{m}(x_3,s) = \mathcal{L}\{T_{in}(t)\} \cdot \prod_{i=1}^{3} f_i(\Delta x, s)$ where *i* is the reach segment index. Accounting for the remaining solution terms, the convolution of *k* reach segments is represented as equation (4-9).

To have an understanding of how spatially variable hydraulic channel properties alters residence time in the channel, we estimated the cumulative mean residence time through the reach. The cumulative mean residence time was estimated using the closed form first temporal moment solution presented in Chapter 3,

$$\langle \mu_t \rangle = \frac{X}{\langle U \rangle}\left(1 + \langle \Lambda \rangle\right)\lambda, \tag{F-22}$$

where $\langle \Lambda \rangle = \frac{Y_{STS}\beta}{\langle Y \rangle(1-\beta)} + \frac{Y_{HTS}}{\langle Y \rangle}$; $\langle ... \rangle$ denotes the reach average; $\lambda = \sum_{i=1}^{k} \frac{\eta}{\gamma_{U,i}}\left[\frac{\left(1 + \langle \Lambda \rangle \gamma_{\Lambda,i}\right)}{\left(1 + \langle \Lambda \rangle\right)}\right]$ represents the influence of spatial variability, *k* is the number of spatial observations; $\eta = \frac{\Delta x}{X}$; $\gamma_{U,i} = \frac{U_i}{\langle U \rangle}$; and $\gamma_{\Lambda,i} = \frac{\Lambda_i}{\langle \Lambda \rangle}$. This moment is represents the mean residence time of a conservative solute.

Appendix G
Hydraulics Estimated Spatially from Imagery

Following methods from Chapter 3 and building on *Bingham et al*. [2012], total channel width ($B_{tot}(x)$) was estimated every 1 streamwise meter where x is the streamwise distance from 0 km to 25 km using all available thermal imagery. In this estimation method, transects were set (assumed perpendicular to main stream flow) along a centerline bisecting the clipped raster of only water temperature (Figure G-1A). To prevent crossing transects and misrepresenting channel width, this centerline was smoothed using Bézier interpolation. Each transect was the clipped to the outline of the raster that represents the edge of water (see Figure G-1B for example).

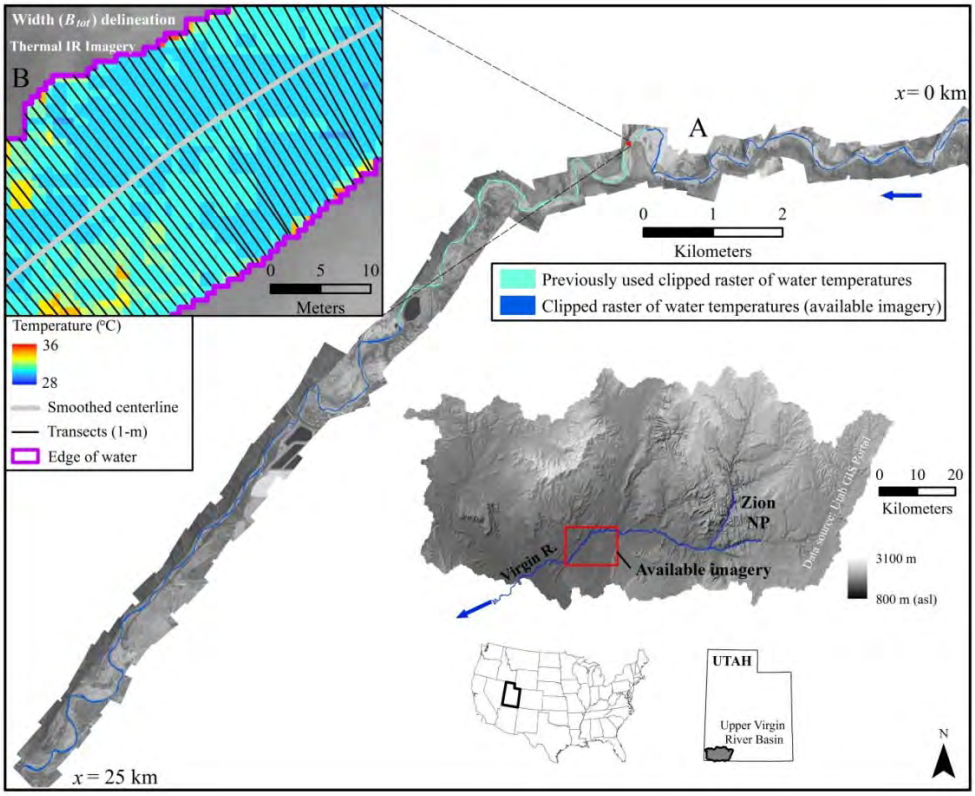

Figure G-1. Virgin River study reach located in southwestern Utah. (A) The clipped raster of only water temperature pixels from *Bingham et al*. [2012] used to delineate total channel width ($B_{tot}(x)$ in m) every 1 streamwise meter. The raster from Chapter 3 is shown relative the raster clipped from the full available imagery. (B) Similar to the procedure from Chapter 3, a streamwise centerline bisecting this clipped raster was approximated to set transects every 1 m. To prevent crossing transects, this centerline was smoothed using Bézier interpolation. To arrive at representative width estimates, these transects were clipped by the outline of the raster that represents the edge of water.

We estimated the distance where width estimates are spatially correlated through the reach to better understand the natural channel structure. This distance consisted of quantifying the squared differences of pairs of width estimates at different separation distances. This produced the semivariance at each separation distance. For example, based on the width estimates from 0-10 km (Figure G-2A), the semivariance increases when the distances between width observations (separation distances) increase (Figure G-2B). When using the full dataset from 0-25 km (Figure G-2C), there is a similar pattern in the semivariance at different increasing separation distances (Figure G-2D). The distances where width estimates are considered spatially correlated though the 25 km study reach were determined by where the semivariance approach the corresponding overall variance in width estimates (gray shading in Figures G-2B and G-2D).

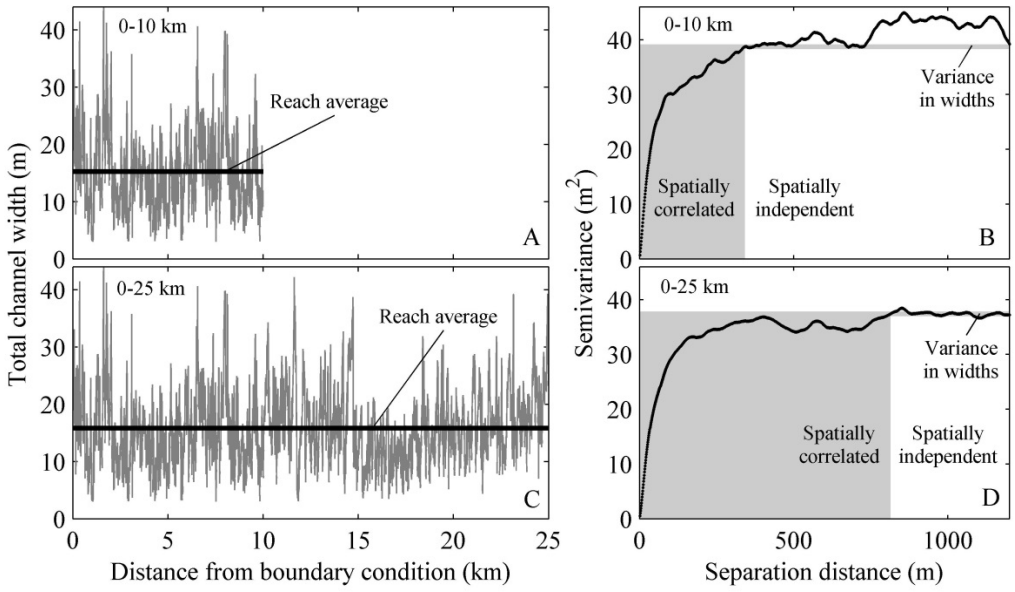

Figure G-2. (A) Total channel width estimated every 1 streamwise meter from 0-10 km and the overall reach average. Using these estimates, (B) the semivariance at increasing separation distances relative to the overall variance. The gray shading represents the separation distances where the semivariance is less than the overall variance and, therefore considered spatially correlated. (C) All available total channel widths from 0-25 km and the overall reach average. Using these estimates, (D) separation distances where the semivariance is less that and the overall variance are considered spatially correlated and shown by the gray shading.

See Chapter 3 for a site description of the Virgin River study reach. Regarding values and parameters used in the Chapter 4 modeling example, the streambed slope (S_o) was set of 0.0039 m m^{-1}. Flow (Q) was set to 1.06 m^3 s^{-1} and assumed steady. The transient storage parameters, α_{STS}, α_{HTS}, Y_{STS}, Y_{HTS}, and β, were set to values within the narrowed bounds presented in *Bandaragoda and Neilson* [2011] and held constant over the entire study reach. Specifically, α_{STS} = 0.5 m^2 s; α_{HTS}, =6 x 10^{-7} m^2 s, Y_{STS}, = 0.15 m, Y_{HTS}, = 0.10 m, β = 0.21, Y_{gr} = 1 m. Additionally, $C_{p,sed}$ = 0.7 cal g^{-1} °C^{-1}, and ρ_{sed} = 1.97 g cm^{-3}, and α_{sed} = 9.12 x 10^{-3} cm^2 s^{-1} were taken from *Bingham et al*. [2012].

Appendix H
License Agreement

JOHN WILEY AND SONS LICENSE TERMS AND CONDITIONS
Dec 11, 2014

This is a License Agreement between Noah M Schmadel ("You") and John Wiley and Sons ("John Wiley and Sons") provided by Copyright Clearance Center ("CCC"). The license consists of your order details, the terms and conditions provided byJohn Wiley and Sons, and the payment terms and conditions.

All payments must be made in full to CCC. For payment instructions, please see information listed at the bottom of this form.

License Number	3526060695503
License date	Dec 11, 2014
Order Content Publisher	John Wiley and Sons
Order Content Publication	Water Resources Research
Order Content Title	The influence of spatially variable stream hydraulics on reach scale solute transport modeling (used in Chapter 3 of this dissertation)
Licensed copyright line	© 2014. American Geophysical Union. All Rights Reserved.
Order Content Author	Noah M. Schmadel, Bethany T. Neilson, Justin E. Heavilin, David K. Stevens, Anders Wörman
Order Content Date	Dec 9, 2014
Start page	n/a
End page	n/a
Type of use	Dissertation/Thesis
Requestor type	Author of this Wiley article
Format	Print and electronic
Portion	Full article
Will you be translating?	No
Title of your thesis /dissertation	Use of Semi-Analytical Solutions to Examine Parameter Sensitivity and the Role of Spatially Variable Stream Hydraulics in Transient Storage Modeling
Expected completion date	Jan 2015
Expected size (number of pages)	140
Total	0.00 USD

TERMS AND CONDITIONS

This copyrighted material is owned by or exclusively licensed to John Wiley & Sons, Inc. or one of its group companies (each a"Wiley Company") or handled on behalf of a society with which a Wiley Company has exclusive publishing rights in relation to a particular work (collectively "WILEY"). By clicking “accept” in connection with completing this licensing transaction, you agree that the following terms and conditions apply to this transaction (along with the billing and payment terms and conditions established by the Copyright Clearance Center Inc., ("CCC's Billing and Payment terms

and conditions"), at the time that you opened your Rightslink account (these are available at any time at http://myaccount.copyright.com).

Terms and Conditions

- The materials you have requested permission to reproduce or reuse (the "Wiley Materials") are protected by copyright.
- You are hereby granted a personal, nonexclusive, non-sub licensable (on a standalone basis), nontransferable, worldwide, limited license to reproduce the Wiley Materials for the purpose specified in the licensing process. This license is for a onetime use only and limited to any maximum distribution number specified in the license. The first instance of republication or reuse granted by this licence must be completed within two years of the date of the grant of this licence (although copies prepared before the end date may be distributed thereafter). The Wiley Materials shall not be used in any other manner or for any other purpose, beyond what is granted in the license. Permission is granted subject to an appropriate acknowledgement given to the author, title of the material/book/journal and the publisher. You shall also duplicate the copyright notice that appears in the Wiley
- publication in your use of the Wiley Material. Permission is also granted on the understanding that nowhere in the text is a previously published source acknowledged for all or part of this Wiley Material. Any third party content is expressly excluded from this permission.
- With respect to the Wiley Materials, all rights are reserved. Except as expressly granted by the terms of the license, no part of the Wiley Materials may be copied, modified, adapted (except for minor reformatting required by the new Publication), translated, reproduced, transferred or distributed, in any form or by any means, and no derivative works may be made based on the Wiley Materials without the prior permission of the respective copyright owner. You may not alter, remove or suppress in any manner any copyright, trademark or other notices displayed by the Wiley Materials. You may not license, rent, sell, loan, lease, pledge, offer as security, transfer or assign the Wiley Materials on a standalone basis, or any of the rights granted to you hereunder to any other person.
- The Wiley Materials and all of the intellectual property rights therein shall at all times remain the exclusive property of John Wiley & Sons Inc, the Wiley Companies, or their respective licensors, and your interest therein is only that of having possession of and the right to reproduce the Wiley Materials pursuant to Section 2 herein during the continuance of this Agreement. You agree that you own no right, title or interest in or to the Wiley Materials or any of the intellectual property rights therein. You shall have no rights hereunder other than the license as provided for above in Section 2. No right, license or interest to any trademark, trade name, service mark or other branding ("Marks") of WILEY or its licensors is granted hereunder, and you agree that you shall not assert any such right, license or interest with respect thereto.
- NEITHER WILEY NOR ITS LICENSORS MAKES ANY WARRANTY OR REPRESENTATION OF ANY KIND TO YOU OR ANY THIRD PARTY, EXPRESS, IMPLIED OR STATUTORY, WITH RESPECT TO THE MATERIALS OR THE ACCURACY OF ANY INFORMATION CONTAINED IN THE MATERIALS, INCLUDING, WITHOUT LIMITATION, ANY IMPLIED

WARRANTY OF MERCHANTABILITY, ACCURACY, SATISFACTORY QUALITY, FITNESS FOR A PARTICULAR PURPOSE, USABILITY, INTEGRATION OR NONINFRINGEMENT AND ALL SUCH WARRANTIES ARE HEREBY EXCLUDED BY WILEY AND ITS LICENSORS AND WAIVED BY YOU

- WILEY shall have the right to terminate this Agreement immediately upon breach of this Agreement by you.
- You shall indemnify, defend and hold harmless WILEY, its Licensors and their respective directors, officers, agents and employees, from and against any actual or threatened claims, demands, causes of action or proceedings arising from any breach of this Agreement by you.
- IN NO EVENT SHALL WILEY OR ITS LICENSORS BE LIABLE TO YOU OR ANY OTHER PARTY OR ANY OTHER PERSON OR ENTITY FOR ANY SPECIAL, CONSEQUENTIAL, INCIDENTAL, INDIRECT, EXEMPLARY OR PUNITIVE DAMAGES, HOWEVER CAUSED, ARISING OUT OF OR IN CONNECTION WITH THE DOWNLOADING, PROVISIONING, VIEWING OR USE OF THE MATERIALS REGARDLESS OF THE FORM OF ACTION, WHETHER FOR BREACH OF CONTRACT, BREACH OF WARRANTY, TORT, NEGLIGENCE, INFRINGEMENT OR OTHERWISE (INCLUDING, WITHOUT LIMITATION, DAMAGES BASED ON LOSS OF PROFITS, DATA, FILES, USE, BUSINESS OPPORTUNITY OR CLAIMS OF THIRD PARTIES), AND WHETHER OR NOT THE PARTY HAS BEEN ADVISED OF THE POSSIBILITY OF SUCH DAMAGES. THIS LIMITATION SHALL APPLY NOTWITHSTANDING ANY FAILURE OF ESSENTIAL PURPOSE OF ANY LIMITED REMEDY PROVIDED HEREIN.
- Should any provision of this Agreement be held by a court of competent jurisdiction to be illegal, invalid, or unenforceable, that provision shall be deemed amended to achieve as nearly as possible the same economic effect as the original provision, and the legality, validity and enforceability of the remaining provisions of this Agreement shall not be affected or impaired thereby.
- The failure of either party to enforce any term or condition of this Agreement shall not constitute a waiver of either party's right to enforce each and every term and condition of this Agreement. No breach under this agreement shall be deemed waived or excused by either party unless such waiver or consent is in writing signed by the party granting such waiver or consent. The waiver by or consent of a party to a breach of any provision of this Agreement shall not operate or be construed as a waiver of or consent to any other or subsequent breach by such other party.
- This Agreement may not be assigned (including by operation of law or otherwise) by you without WILEY's prior written consent.
- Any fee required for this permission shall be nonrefundable after thirty (30) days from receipt by the CCC.
- These terms and conditions together with CCC’s Billing and Payment terms and conditions (which are incorporated herein) form the entire agreement between you and WILEY concerning this licensing transaction and (in the absence of fraud) supersedes all prior agreements and representations of the parties, oral or written. This Agreement may not be amended except in writing signed by both parties. This

Agreement shall be binding upon and inure to the benefit of the parties' successors, legal representatives, and authorized assigns.

- In the event of any conflict between your obligations established by these terms and conditions and those established by CCC's Billing and Payment terms and conditions, these terms and conditions shall prevail.
- WILEY expressly reserves all rights not specifically granted in the combination of (i) the license details provided by you and accepted in the course of this licensing transaction, (ii) these terms and conditions and (iii) CCC's Billing and Payment terms and conditions.
- This Agreement will be void if the Type of Use, Format, Circulation, or Requestor Type was misrepresented during the licensing process.
- This Agreement shall be governed by and construed in accordance with the laws of the State of New York, USA, without regards to such state's conflict of law rules. Any legal action, suit or proceeding arising out of or relating to these Terms and Conditions or the breach thereof shall be instituted in a court of competent jurisdiction in New York County in the State of New York in the United States of America and each party hereby consents and submits to the personal jurisdiction of such court, waives any objection to venue in such court and consents to service of process by registered or certified mail, return receipt requested, at the last known address of such party.

WILEY OPEN ACCESS TERMS AND CONDITIONS

Wiley Publishes Open Access Articles in fully Open Access Journals and in Subscription journals offering Online Open. Although most of the fully Open Access journals publish open access articles under the terms of the Creative Commons Attribution (CC BY) License only, the subscription journals and a few of the Open Access Journals offer a choice of Creative Commons Licenses:: Creative Commons Attribution (CCBY) license Creative Commons Attribution NonCommercial (CCBYNC) license and Creative Commons Attribution NonCommercialNoDerivs (CCBYNCND) License. The license type is clearly identified on the article. Copyright in any research article in a journal published as Open Access under a Creative Commons License is retained by the author(s). Authors grant Wiley a license to publish the article and identify itself as the original publisher. Authors also grant any third party the right to use the article freely as long as its integrity is maintained and its original authors, citation details and publisher are identified as follows: [Title of Article/Author/Journal Title and Volume/Issue. Copyright (c) [year] [copyright owner as specified in the Journal]. Links to the final article on Wiley's website are encouraged where applicable.

The Creative Commons Attribution License

The Creative Commons Attribution License (CCBY) allows users to copy, distribute and transmit an article, adapt the article and make commercial use of the article. The CCBY license permits commercial and noncommercial reuse of an open access article, as long as the author is properly attributed. The Creative Commons Attribution License does not affect the moral rights of authors, including without limitation the right not to have their work subjected to derogatory treatment. It also does not affect any other rights held by authors or third parties in the article, including without limitation the rights of privacy

Use by commercial "for-profit" organisations

Use of Wiley Open Access articles for commercial, promotional, or marketing purposes requires further explicit permission from Wiley and will be subject to a fee. Commercial purposes include:

- Copying or downloading of articles, or linking to such articles for further redistribution, sale or licensing;
- Copying, downloading or posting by a site or service that incorporates advertising with such content;
- The inclusion or incorporation of article content in other works or services (other than normal quotations with an appropriate citation) that is then available for sale or licensing, for a fee (for example, a compilation produced for marketing purposes, inclusion in a sales pack)
- Use of article content (other than normal quotations with appropriate citation) by for-profit organisations for promotional purposes
- Linking to article content in emails redistributed for promotional, marketing or educational purposes;
- Use for the purposes of monetary reward by means of sale, resale, licence, loan, transfer or other form of commercial exploitation such as marketing products

VITA

Noah M. Schmadel

Graduate Research Assistant, PhD Candidate
Department of Civil and Environmental Engineering
Utah Water Research Laboratory, Utah State University
Email: nschmadel@gmail.com

Education

Doctor of Philosophy, Civil and Environmental Engineering, *expected* December 2014
Utah State University, Logan, Utah

Master of Science, Civil and Environmental Engineering, December 2009
Utah State University, Logan, Utah

Bachelor of Science, Environmental Engineering, May 2006
Northern Arizona University, Flagstaff, Arizona

Fundamentals of Engineering Examination, Passed May 2006

Professional Experience

Graduate Research Assistant, June 2007-Current, Department of Civil and Environmental Engineering, Utah Water Research Laboratory, Utah State University, Logan, Utah.

Graduate Teaching Assistant, Spring 2011, Department of Civil and Environmental Engineering, Utah State University, Logan, Utah.

Research Aide (Laboratory Technician), September 2005-May 2006, Department of Civil and Environmental Engineering, Northern Arizona University, Flagstaff, Arizona.

Forestry Technician (Fire Engine Operator), Seasonal 2003-2006, USDA Forest Service, Sedona, Arizona.

Research Interests

Pollutant fate and transport modeling and supporting data collection

- Data collection strategies for quantifying mass and heat transport in rivers and streams.
- Developing, testing, and implementing mass and heat stream transport models.
- Analytical and numerical solution techniques to transport models.
- Parameter sensitivity analysis methods.
- The role of spatially variable parameters in downstream predictions.

Surface water-groundwater interactions

- Data collection strategies over various spatiotemporal scales for quantifying groundwater exchange in rivers and streams.
- Statistical techniques for quantifying confidence in groundwater exchange estimates.
- The role of surface water-groundwater interactions in stream transport.

Refereed Publications

Published

1. **Schmadel, N.M.**, B.T. Neilson, D.K. Stevens, 2010. Approaches to estimate uncertainty in longitudinal channel water balances. *Journal of Hydrology*, 394: 357-369, doi:10.1016/j.jhydrol.2010.09.011.

2. Wörman, A., J. Riml, **N. Schmadel**, B.T. Neilson, A. Bottacin-Busolin, J.E. Heavilin, 2012. Spectral scaling of heat fluxes in streambed sediments. *Geophysical Research Letters*, 39, L23402, doi:10.1029/2012GL053922.

3. **Schmadel, N.M.**, B.T. Neilson, T. Kasahara, 2014. Deducing the spatial variability of exchange within a longitudinal water balance. *Hydrological Processes*, doi:10.1002/hyp.9854.

In Review, Revision, or Press

4. **Schmadel, N.M.**, B.T. Neilson, J.E. Heavilin, D.K. Stevens, A. Wörman. The influence of spatially variable stream hydraulics on reach scale solute transport modeling. *Water Resources Research*, In Press.

In Preparation

5. **Schmadel, N.M.**, B.T. Neilson, J.E. Heavilin. The influence of spatially variable stream hydraulics on reach scale heat transport modeling.

6. **Schmadel, N.M.**, B.T. Neilson, J.E. Heavilin, A. Wörman. Isolating the sensitivity of key transient storage model parameters.

7. Majerova, M., B.T. Neilson, **N.M. Schmadel**, J.M. Wheaton, C.J. Snow. Impact of beaver dams on hydrologic and temperature regimes considering various spatial and temporal scales.

Professional Presentations

1. **Schmadel, N.M.**, J.D. Bingham, B.T. Neilson, A.J. Hobson. Methods for quantifying groundwater and surface water interactions in Curtis Creek. March 2008. Utah State University Spring Runoff Conference, Logan, UT (poster).

2. **Schmadel, N.M.**, B.T. Neilson, T. Kasahara. Comparison of approaches used to characterize stream water-groundwater exchange. December 2008. American Geophysical Union Fall Meeting, San Francisco, CA. Abstract H33F-1083 (poster).

3. **Schmadel, N.M.** and B.T. Neilson. Estimating uncertainty in approaches used to quantify surface water-ground water exchange. March 2009. Lessons from Continuity and Change in the Fourth International Polar Year Symposium, Fairbanks, AK (poster including synopsis paper).

4. **Schmadel, N.M.** and B.T. Neilson. Reliability of approaches used to characterize surface water-groundwater exchange. April 2009. Utah State University Spring Runoff Conference, Logan, UT (Awarded 1st place in student oral presentation competition).

5. Ghabayen, S., **N.M. Schmadel**, B.T. Neilson. Characterization of groundwater-surface water interactions using GMS and differential gauging approaches. September 2009. AWRA Fall Annual Conference, Seattle, WA (talk).

6. **Schmadel, N.M.**, B.T. Neilson, D.K. Stevens. Reliability of approaches used to quantify surface water-groundwater interactions. December 2009. American Geophysical Union Fall Meeting, San Francisco, CA. Abstract H51I-0902 (poster).

7. Lyman, C., B.T. Neilson, **N.M. Schmadel**. Effects of beaver dams on Curtis Creek temperature and flow. April 2010. Utah State University Spring Runoff Conference, Logan, UT (poster).

8. **Schmadel, N.M.**, J.E. Heavilin, B.T. Neilson, A. Wörman. Incorporating channel spatial variability into two-zone transient storage modeling. March 2011. Utah State University Spring Runoff Conference, Logan, UT (talk).

9. Marquina, O.A., B.T. Neilson, **N.M. Schmadel**. Seasonal fluctuations of stream water-groundwater interactions. March 2011. Utah State University Spring Runoff Conference, Logan, UT (poster).

10. Heavilin, J.E, B.T. Neilson, **N.M. Schmadel**, A. Wörman. Advancing solutions of the two-zone temperature and solute transport model by solving a simplified temperature transport component. April 2011. European Geosciences Union General Assembly, Vienna, Austria. EGU2011-3914 (poster).

11. **Schmadel, N.M.**, J. Heavilin, B.T. Neilson, A. Wörman. Investigating the effects of channel spatial variability on two-zone transient storage modeling. April 2011. European Geosciences Union General Assembly, Vienna, Austria. EGU2011-3749 (talk).

12. Neilson, B.T., C. Bandaragoda, S.C. Chapra, D.K. Stevens, **N.M. Schmadel**, Q.G. Bingham, C.M.U. Neale, and M.B. Cardenas. Use of instream heat budgets and supporting data for predicting surface and subsurface transient storage influences. October 2011. Geological Society of America Annual Meeting, Minneapolis, MN (invited talk).

13. Riml, J., A.Wörman, **N.M. Schmadel**, B.T. Neilson. Temperature: a natural tracer to define residence time distributions in transient storage zones. December 2011. American Geophysical Union Fall Meeting, San Francisco, CA. Abstract H33I-01 (talk).

14. **Schmadel, N.M.**, B.T. Neilson, T. Kasahara. Combining conventional data collection techniques to identify surface-subsurface exchange components. March 2012. Utah State University Spring Runoff Conference, Logan, UT (talk).

15. Wörman, A., J. Riml, **N. Schmadel**, B. Neilson, A. Bottacin-Busolin, and J. Heavilin. Evaluating thermal diffusivity in stream-beds from temperature spectra. April 2012. European Geoscience Union General Assembly, Vienna, Austria. Vol. 14, EGU2012-6318-4 (talk).

16. Riml, J., A. Wörman, **N. Schmadel**, and B. Neilson. Estimating residence time distributions in the hyporheic zone using heat. April 2012. European Geosciences Union General Assembly, Vienna, Austria. Vol. 14, EGU2012-7283 (talk).

17. **Schmadel, N.M.**, B.T. Neilson, J.E. Heavilin, A. Wörman. Analysis of two-zone transient storage parameters using analytical transport solutions, moment statistics, and a convolution of solutions. December 2012. American Geophysical Union Fall Meeting, San Francisco, CA. Abstract H14B-08 (talk).

18. **Schmadel, N.M.**, B.T. Neilson, J.E. Heavilin, A. Wörman. Investigating the impact of higher spatial resolution parameter information on stream solute transport predictions. April 2013. Utah State University Spring Runoff Conference, Logan, UT (talk).

19. **Schmadel, N.M.**, B.T. Neilson, J.E. Heavilin, A. Wörman. The role of spatially variable stream hydraulics in reach scale, one-dimensional solute predictions. December 2013. American Geophysical Union Fall Meeting, San Francisco, CA. Abstract H32C-08 (talk, winner of Outstanding Student Paper Award).

Professional Development

Emergency Medical Technician Basic Training, Bridgerland Applied Technology College, Logan, UT, September-December 2009.

DTS Down to Earth: Principles, Applications, Operational Factors, and Demonstrations for Environmental Sensing, Fiber Optic Distributed Temperature Sensing Workshop, UC Berkeley, CA, December 12, 2009.

Getting Started as a Successful Proposal Writer and Academician Workshop, Logan, UT, April 17, 2012.

National Science Foundation Arctic Field Training, Logan, UT, February 2013.

Professional Activities

Reviewer:

Journal of Hydrology
Hydrology and Earth Systems Science
Journal of Water Resources Planning and Management

Professional Affiliations

American Geophysical Union (2007-Present)
Geological Society of America (2012-Present)

Awards

- American Water Works Association Intermountain Water Quality Student Section Linda Moss Scholarship, April 2008
- Utah State University Engineering Scholarship, Tuition Waiver, Fall 2008
- First Place in Student Oral Presentation Competition, Utah State University Spring Runoff Conference, April 2009
- Outstanding Student Paper, American Geophysical Union Fall Meeting, Hydrology Section, Abstract H32C-08, December 2013
- Utah State University Graduate Research Assistantship, 2006-2014

Research Projects and Involvement

Key projects

1. Virgin River in southwestern Utah (desert river)
   - Participated in a one week data collection campaign summer 2007. The purpose was to design a data collection scheme to support solute and heat transport modeling.
   - Supporting team member role.
   - Produced one paper currently in review in Water Resources Research (lead author) and one paper in preparation (lead author).

2. Curtis Creek in northern Utah (mountain headwater stream)
   - Participated in an extensive data collection campaign from 2007 to 2013. The purpose was to investigate surface water-groundwater interactions over various spatiotemporal scales.
   - Supporting to lead role. Led teams of two to five and mentored two MS students regarding field-based data collection techniques.
   - Produced one paper published in Journal of Hydrology (lead author) and one paper published in Hydrological Processes (lead author).

3. Säva Brook in southeastern Sweden (coastal stream)
   - Led a six week data collection campaign spring 2011. The purpose was to design a data collection scheme to support solute and heat transport modeling.
   - Lead role. Designed and implemented the study and mentored a PhD student regarding field-based data collection techniques.
   - Produced one paper published in Geophysical Research Letters (third author).

Additional involvement

1. Imnavait Creek in northern Alaska (arctic headwater stream)
   - Participated in a two week data collection campaign summer 2009. The purpose was to develop data collection and modeling strategies for arctic headwater streams.
   - Involved to provide knowledge of data collection strategies and accomplish project goals.

2. Silver Creek in northern Utah (wastewater dominated stream)
   - Participated in a one week data collection campaign summer 2012. The purpose was to quantify a channel water balance.
   - Involved to mentor a MS student regarding field-based data collection techniques.

3. Kuparuk River in northern Alaska (arctic river)
   - Participated in data collection campaign summer 2013. The purpose was to develop data collection and modeling strategies for arctic rivers.
   - Involved for two weeks to mentor a new PhD student and help start the project.

4. iUtah Summer Research Institute, Logan River in northern Utah (mountain river)
   - Participated in a one week training workshop summer 2014.
   - Taught basic data collection and analysis strategies to high school and undergraduate students.

5. Red Butte Creek in northern Utah (mountain headwater stream)
   - Participated in a data collection campaign summer 2014. The purpose was to investigate surface water-groundwater interactions at a watershed scale using tracer techniques.
   - Involved for one week to mentor a new undergraduate, MS, and PhD student regarding field-based data collection techniques.